ABSTRACT

Title: MODELING THE INTEGRATION OF THERMOELECTRICS IN ANODE EXHAUST COMBUSTORS FOR WASTE HEAT RECOVERY IN FUEL CELL SYSTEMS.

Anita Maghdouri Moghaddam, Master of Science, 2011

Directed By: Professor Gregory Jackson

Department of Mechanical Engineering

Recently developed small-scale hydrocarbon-fueled fuel cell systems for portable power under 1 kW have overall system efficiencies typically no higher than 30-35%. This study explores the possibility of using of thermoelectric waste heat recovery in anode exhaust combustors to improve the fuel cell system efficiencies by as much as 4-5% points and further to reduce required battery power during system start-up. An integrated SOFC system with simplified catalytic combustor model and integrated TEs between the air preheating channels as well as a transient model of a TE-integrated catalytic combustor were developed to explore the additional amount of power generation during SOFC operation, and to investigate the performance of the TEs during transient start-up of the combustor respectively. Results for the SOFC system indicate that while the TEs may recover as much as 4% of the total fuel energy into the system, their benefit is reduced in part because they reduce the waste heat transferred back to the incoming air stream and thereby lower the SOFC operating temperatures and operating efficiencies. The TE-integrated catalytic combustor model incorporated more detailed catalytic combustion chemistry, active TE modeling and enhanced cooling air fin heat transfer to show the dynamic heating of the integrated combustor. This detailed model provided a basis for exploring combustor designs and showed the importance of adequate reactant preheating when burning exhaust from a reformer during start-up for the TEs to produce significant power to reduce the size of system batteries for start-up.

MODELING THE INTEGRATION OF THERMOELECTRICS IN ANODE EXHAUST COMBUSTORS FOR WASTE HEAT RECOVERY IN FUEL CELL SYSTEMS.

By

Anita Maghdouri Moghaddam

Thesis submitted to the Faculty of the Graduate School of the

University of Maryland, College Park, in partial fulfillment

of the requirements for the degree of

Master of Science

2011

Advisory Committee:

Professor Gregory Jackson, Chair

Associate Professor Bao Yang

Associate Professor Chandrasekhar Thamire

Table of Content

List of Figures

List of Tables

Nomenclature

α_{TE}	thermoelectric Seebeck coefficient ($V \cdot K^{-1}$)
α_{diff}	thermal diffusivity ($m^2 \cdot s^{-1}$)
a_{cat}	surface areas of catalyst per volume of washcoat volume ratio ($m^2 \cdot m^{-3}$)
ε	porosity
θ_k	catalyst surface species site fraction
Φ	equivalence ratio
d_{hydr}	hydraulic diameter (m)
I	current (A)
V	voltage (V)
v	volume (m^3)
P	pressure (Pa)
$P_{t=0}$	initial pressure (Pa)
Q	heat flux ($W.m^{-2}$)
R_c	electrical contact resistance between TE junction contacting area (Ω)
R_{TE}	thermoelectric electrical resistance (Ω)
R_{load}	electrical load resistance (Ω)
Re	Reynolds number
Pr	Prandtl number
ρ_{TE}	thermoelectric resistivity ($\Omega \cdot m$)
$\rho_{TE,m}$	thermoelectric density ($kg \cdot .m^{-3}$)
K_{TE}	thermoelectric conductance ($W \cdot K^{-1}$)
K_T	thermoelectric conductivity ($W \cdot K^{-1} \cdot m^{-1}$)
ρ_{wash}	washcoat density ($kg \cdot m^{-3}$)

k_c	mass transfer coefficient ($m \cdot s^{-1}$)
y_{TE}	height of TE element (m)
$n_{TE,j}$	number of TE couple per discretization
$\rho_{comb,f}$	combustion flow density ($kg \cdot m^{-3}$)
t	time (s)
$T_{comb,wall}$	combustor wall temperature (K)
$T_{comb,f}$	combustor flow temperature (K)
$T_{air,f}$	air flow temperature (K)
$T_{air,wall}$	air wall Temperature (K)
T_{TE}	thermoelectric temperature (K)
$W_{TE,elec}$	electric work of TE (W)
Nu	Nusselt number
$\dot{m}$	mass flow rate ($kg \cdot s^{-1}$)
μ_k	kinematic viscosity ($m^2 \cdot s^{-1}$)
μ_d	dynamic viscosity ($kg \cdot m^{-1} \cdot s^{-1}$)
$\dot{m}_y$ ($kg \cdot s^{-1}$)	surface gas phase species mass flow rate through catalytic washcoat
$\dot{m}_{YVk,int,j}$	mass flow of diffused species rate through catalytic wash coat ($kg \cdot s^{-1}$)
$YV_{k,int,j}$	mass weighted diffusion velocity of species k ($m \cdot s^{-1}$)
$\frac{\partial}{\partial t}$	time derivative
C_p	specific heat capacity at constant pressure ($J \cdot kg^{-1} \cdot K^{-1}$)
C_v	specific heat capacity at constant volume ($J \cdot kg^{-1} \cdot K^{-1}$)
h_T	convective heat transfer coefficient ($W \cdot m^{-2} \cdot K^{-1}$)
$k_{T,comb,f}$	combustor flow conductive heat transfer coefficient ($W \cdot m^{-2} \cdot K^{-1}$)
$A_{wash,int}$	area of the washcoat and channel flow interface (m^2)

$A_{\text{wash,cross}}$	cross sectional area of washcoat (m^2)
$\dot{s}_k$	molar production rate of k species per unit surface area ($gmol \cdot m^{-2} \cdot s^{-1}$)
Sh_{k}	Sherwood number of k species
$D_{k,m}$	mixture-averaged diffusion coefficient ($m^2 \cdot s^{-1}$)
$W_{\text{k\_gas}}$	molar mass of washcoat species ($g \cdot gmol^{-1}$)
$W_{\text{k\_flow}}$	molar mass of combustor flow species ($g \cdot gmol^{-1}$)
Γ_{l_surf}	surface site density of the catalyst ($gmol \cdot m^{-2}$)
θ_{l_surf,k_surf}	surface site fraction of the k^{th} species
η_{ht}	waste heat fraction efficiency
η_{TE}	thermoelectric efficiency

1 Introduction

1.1 Combustors and Potential for Waste Heat Recovery in Fuel Cell Systems

Fuel cells convert chemical bond energy directly to electrical work through electrochemical oxidation of fuel, but integrated fuel cell systems, particularly with hydrocarbon fuels, often include some form of combustor due to the fact that the fuel cell anode cannot consume all of the fuel. The fuel remaining in the anode exhaust is consumed in a downstream combustor, either as a conventional or catalytic combustor. For high-temperature solid oxide fuel cells (SOFCs) or for fuel cell systems with high-temperature fuel reformers, the combustor thermal energy release can be recovered to preheat reactants. In addition, the combustor provides heating during start-up to get the high-temperature fuel cell and/or fuel reformer must be heated. Even for small fuel cell systems, start-up times for preheating can be long, on the order of several tens of minutes and during start-up power is required to run the balance of plant as the high-temperature reactors and flows increase in temperature. Batteries typically provide the power for running the balance of plant components during the start-up period and their size will depend on the time required before the fuel cell can begin producing power [1]. If the battery storage requirements become large relative to the fuel cell plant, the advantages of fuel cell systems operating on energy dense fuels, particularly for portable applications, is greatly reduced or lost altogether. Thus, any technology that can reduce the need for battery power during portable fuel cell system start-up may increase the value and marketability of fuel cell systems for mobile/portable power applications.

This thesis explores the possibility of reducing hybrid electrical energy storage by integration of thermoelectric (TE) modules into fuel cell anode exhaust combustors for conversion of waste-heat to electrical power. By recuperating the combustor waste heat through thermoelectric modules some fraction of the waste heat is converted to electrical power. This electrical power can be generated rapidly during combustor operation start-up and can be generated during fuel cell system operation in order to increases the overall efficiency. The current study focuses on small-scale SOFC systems being developed for new portable power supplies. These systems are often designed to operate on hydrocarbons with power outputs ranging from 10 W to 1 kW [1]. However, the principles for waste heat recovery using thermoelectric generation may be applied to other fuel cell systems involving anode exhaust combustors.

SOFCs, in particular, are high temperature electrochemical cells with operating temperatures typically above 925 K, These high temperatures allow operation on hydrocarbon fuels or reformed syngas (H_2/CO rich mixtures from fuel processors), but the systems require some preheating either through fuel combustion or some other means [2]. If waste heat from the SOFC and anode exhaust combustor can be recovered either chemically through endothermic reforming or through reactant preheating, the SOFC power plant can achieve high or overall system efficiencies, approaching 50% depending on the size and fuel of the system [3]. However, smaller portable SOFC-based systems do not achieve such high efficiencies due to increased thermal losses and work lost to balance of plant components [3]. Thus, the performance and overall efficiency of the small scale portable SOFC power units are affected by system architecture. In order to better understand the potential

for thermal heat recovery in SOFC power unit and its effect on the overall system efficiency, critical aspects of the SOFC in small scale portable power systems must be further explored.

The study by Zhu and Kee shows that fuel utilization in fuel cell's anode highly affects the efficiency of the SOFCs. SOFC produce electric power when the fuel is oxidized at the anode and the reversible cell potential is higher than the cell operating potential [3]. As fuel is utilized along the length of the anode flow path, the local reversible potential of the cell decreases which reduces the current and electrical power densities (in terms of Amps and Watts per area of fuel cell membrane respectively). To maintain a steady, reliable condition for SOFCs and power generation, no more than 85% of the fuel entering the anode side [1]. The excess fuel exiting the anode must be fed to a downstream combustor where it is mixed and burned, typically with cathode exhaust. The research in this study explores whether the heat release in the anode exhaust combustor can be utilized to make additional electric power both during fuel cell operation as well as during start-up before the fuel cell has reached operating conditions.

Numerous studies on integrated meso-scale SOFC systems have illustrated that at power scales below 1.0 kW, integrated hydrocarbon fueled SOFC systems with their balance of plant and anode exhaust combustor have overall thermal efficiencies below 35% [1]. Kattke and Braun have achieved an efficiency of about 21% for a 60 tubular SOFC stack system model with 637 W power [4]. Examples of the manufactured portable SOFC-based power units include the 3.7 kW power units by Delphi operating on natural gas with thermal efficiency of 38% [5] and the 75W

Protonex power unit operating on propane with thermal efficiency of 30% [6]. Low system efficiency of small scale fuel cell systems for portable applications is thus one of the challenges amongst the researchers and the industry. Effective waste heat recovery from combustion of the anode exhaust as one of the ways of improving system efficiency and operability.

In addition to improving steady-state efficiencies, reducing the startup time increase the effective time-integrated system efficiency by reducing the amount of electric power from the fuel cell which must recharge the start-up batteries. The anode exhaust combustor often doubles as a start-up burner for heating up reactants to high-temperature fuel reformers and/or the SOFC itself. Using TE module to recover some of the high temperature combustor waste heat as electric power can reduce the need to charge batteries for start-up and thus reduce system fuel consumption.

1.2 Thermoelectric Power Generation in Combustors

Thermoelectric (TE) modules have recently been implemented with combustors for direct thermal to electric power generation (TEG). Minimal balance of plant and TE module reliability make these modules an attractive option for power generation from wasted heat or combustion process. TEs involve solid state energy conversion by directly converting heat transfer across a temperature difference into electric current across a voltage gradient. TE materials such as Lead Telluride (PbTe), Bismuth Telluride (Bi_2Te_3) and others are semiconductors which rely on the Seebeck effect. The Seebeck effect causes an electrical potential across two dissimilar conductors (i.e., a couple) when a temperature gradient is applied [7].

Figure 1-1 presents a graphical configuration of a thermoelectric couple which consists of two dissimilar n-type and p-type legs that are electrically connected in series through a semiconductor material and also separated from the heat source through electrically insulated material such as ceramics. The temperature gradient across the TE couple drives a heat flux through the couple which causes a flow of electrons in the n-type material and positively charged holes in the p-type material away from the hot heat source to the cold heat sink [7]. This results in a current flow along with a voltage difference across the base of each leg [8] which implies electric power if connected to an external circuit. Equation 1-1 represents the over potential or TE voltage generation term as function of temperature based on Seebeck phenomenon;

$$V = \int_{T_{cold}}^{T_{hot}} \alpha_p(T) - \alpha_n(T) \, . \, dT \qquad \text{(Eq. 1-1)}$$

or

$$V_{TE} = \Delta V_{OC} = \alpha_{TE} \, (T_{hot} - T_{cold})$$

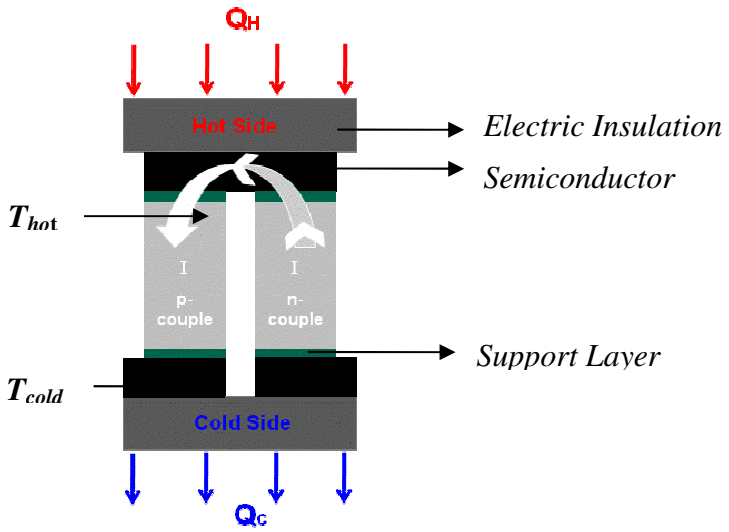

Figure 1-1: Heat Transfer and current flow through TE couple

$$\dot{Q}_H = K_{TE}(T_H - T_C) + \alpha_{TE} T_H I - \frac{1}{2} I^2 R_{TE} - I^2 R_c \qquad \text{(Eq. 1-2)}$$

$$\dot{Q}_C = K_{TE}(T_H - T_C) + \alpha_{TE} T_C I + \frac{1}{2} I^2 R_{TE} + I^2 R_c \qquad \text{(Eq. 1-3)}$$

α represents the Seebeck coefficient of the n-or p-type thermoelectric material at a specific temperature. The rate of heat transfer to the hot and cold conjunction of a TE couple can be mathematically expressed as in equation 1-2, 3. T_H represents the temperature of the hot side of TE and T_C represents the cold side temperature. R_{TE} is the thermoelectric material resistance whereas R_c is the contact resistance at the point of contact between TE legs and the semiconductor layer. K_{TE} is the TE thermal conductance and I is the total current through the TE couple [7].

The electric conversion efficiency of a TE module is the fraction of Q_H converted to electric power. The conversion efficiency η_{TE} depends on the T_H and T_C as well as the thermoelectric material used as well as the external load resistance R_{load} as expressed in equations 1-4, 1-5.

$$W_{elec,TE} = V_{TE}^2 (R_{load} + R_{TE}) \qquad \text{(Eq. 1-4)}$$

$$\eta_{TE} = \frac{W_{elec,TE}}{Q_H - Q_C} \qquad \text{(Eq. 1-5)}$$

TEG applications are limited due to their relatively η_{TE}. According to Rowe, the Seebeck coefficients of modern semiconductor materials are about hundreds of microvolts per degree C, which can lead to module efficiencies approaching 20% [7]. However, such high efficiencies are not achievable in working devices due to heat losses and current materials limitations. Material selection for a given TEG

application is directed by structural limitations of TE materials and contact materials joined to semiconductor layers. As shown in Figure 1-1, the thermocouple legs are mounted on an electric insulator through a contact material which introduces a contact resistance (R_C) between the TE and contact materials. Excessive thermal heat flux at the TE couples' joining point can cause a structural deformation which increases R_C and lowers η_{TE}.

The most common TE material, bismuth telluride (Bi_2Te_3), has a low operating temperature range of 300 to 500 K, and has been implemented in mW power applications such as biomedical sensors or environmental simulations. Other TE convertors such as lead telluride (PbTe) materials, with operating temperatures ranging from 570 to 950 K, are being developed for waste heat recovery purposes in light or heavy trucks and fuel-efficient cars which must meet the low emission standards [7]. Other thermoelectric materials, including some precipitate percentages have recently been developed and tested for better material properties, reliability and to widen the range of operating temperatures. P-type PbTe produce approximately 800 $W.m^{-1}$ [7]. The conversion efficiency of PbTe semiconductor materials operating around these temperatures, range about 8-11% [1].

Yu and Chau [9] and Crane [10] have studied TEG technology as a way to recover waste heat in vehicles to charge automotive batteries. In Yu and Chau's experimental study, the waste heat recovery system of the internal combustion engine of an automobile is prototyped using six Bi_2Te_3 thermoelectric modules; which are then sandwiched by a water-cooled copper radiator as the TE cold side and another copper plate as the heat source. Their results showed that the power generated by the

TEs quickly match the battery power demand. The experimental results from the prototyped assembly also showed a significant improvement of about 14.5% in its electrical efficiency when the heat source was kept constant at 373 K. This study however does not consider the effect of temperature change along the length of the TEs are not considered and the hot conjunction of TE experience a constant amount of heat flux which in reality of the combustor engines this assumption cannot be hold.

Qiu and Hayden [11] studied a combustion-driven TE power generation system, where the TE modules are integrated into a gas-fired furnace. Due to high operating temperature range of the furnace, PbSnTe TE material was chosen for the experimentations and mathematical modeling of the system. A one dimensional mathematical model has been developed in order to evaluate the amount of electrical power production and the efficiency of the system under different steady state conditions.

An overall TE module efficiency for a waste heat recovery application is defined by the product of the waste heat fraction passed through the TE, η_{ht}, and the electrical conversion efficiency of TE module, η_{TE}. Qui and Hayden modeled this efficiency with simplistic assumptions such as the burner surface and the combustion products being at the same temperature of $T_{h,}$ also in contact with hot side of the TE module [11]. Their results showed an increase of electrical efficiency of about 7.5% starting from 670 upto 1273 K and from 1273 K to 1473 K under TE integrated conditions; which also showed a 1.5% improvement in efficiency of the combustor by this modular integration. Further, the power output of the system was showed to increate from 100W at 670 K to about 550W at 1473 K at which point the system

seems to have reached its equilibrium condition. The validation experiments showed that PbSnTe modules on each side of the combustor produced over 1 kW at approximately 5% system efficiency for a residential heating system.

Chen et al. [12] studied the impact of implementing TEG for waste heat recovery in CHP systems by modeling TEG modules between hot and cold fluid streams in a cross-flow heat exchanger. The relatively simple model suggested that the electrical efficiency of the CHP system was improved by 0.3 while the waste heat recovery efficiency was reduced by 0.25%. This method is used in estimating the efficiency of other waste heat locations within the CHP system that are under different operating temperatures. In general, the overall CHP system efficiency was discovered to improve in a range of 0.25 to 0.35% depending on the range of operating temperature with TE conversion efficiency of around 15%. However, the TE conversion efficiency of 15% achieved in this model seems very high and not plausible in real systems where the TE's maximum conversion efficiency is determined to be around 5-6%.

Chen et al. [13] also investigated the effect of TE module integration into a exhaust recovery of a low-temperature proton exchange membrane fuel cell (PEMFC). For that study, results from a more comprehensive 3D CFD model of the TEG in Fluent™ are compared with measurements of temperatures and power outputs of TE modules installed on the surface of an exhaust pipe. Due to low operating temperatures of the PEMFC (430 to 450 K), Bi_2Te_3 TEs were chosen for this system and the model assumed T_H and T_C of the module at 423 and 303 K

respectively. The effect of TE integration on the overall system efficiency was not discussed.

Crane and Jackson [14] also investigated TEG from combustor waste heat using heated combustor cooling water exchanging heat with ambient air in a radiator in a counter flow system with ambient air flow channels with fins for enhanced cooling heat transfer. Cooling water was used to keep the temperatures low, for commercially available Bi_2Te_3 modules. The numerical model developed is based on a single tube with hot fluid flow, surrounding TE modules and external cooling air flow over extended heat transfer surfaces. Experimental results were compared with the simulation under different hot and cold fluid flow rates and R_{load}. The results showed that heat recovery with low-temperature Bi_2Te_3 TE is very sensitive to cooling flow rates.

Due to limited implementation in commercial applications, high temperature TE models have not been studied much for waste heat recovery of systems with high operating temperatures. Most of the studies performed have mostly been focused on low temperature Bi_2Te_3 which have lower thermal efficiencies [7]. However, as the development of high temperature TE modules progresses, recent studies have focused on high-temperature TEG, including a recent study in TEG in a hybrid SOFC combined heat and power CHP system [15]. The main goal of that effort was to assess how TEs could increase the electrical efficiency of the fuel cell system within the micro-CHP (<5 kWe) unit by 4-5% using high-temperature TEG modules. The proposed TE material for this study is Zn_4Sb_3. The researchers were unable to demonstrate the stated goal of improving the CHP system efficiency by 4 to 5 %

The development of high-temperature TEG for recovering electric power from fuel cell exhaust combustion may prove to be a cost effective application due to the fact that it might replace expensive batteries or the need for larger fuel cell stacks. TEGs do not increase emissions, noise, or moving parts and as such would not cause the fuel cell system to lose any of its nascent advantages. One of the main goals of this research is to perform a detailed modeling study of the TEG integrated catalytic combustor component in both a modular level as well as in a system level.

1.3 Fuel cell anode exhaust combustors

Many fuel cell systems require combustion of the excess fuel in an anode exhaust combustor. This section reviews some of the issues and development of these combustors including the use of catalytic combustors for such applications. Because of the focus of this thesis on small SOFC systems, the discussion will center around combustor integration with SOFCs.

SOFCs can operate on hydrocarbon fuels with minimal or no upstream fuel processing at very high efficiency [2]. SOFCs operating at temperatures above 873 K can do some internal reforming of smaller hydrocarbons to produce syngas in porous anode support layers, which have catalytic materials to support steam reforming of hydrocarbons and water-gas-shift reactions to make H_2. In SOFCs, the H_2 is readily electrochemically oxidized by O^{2-} ions from the electrolyte in the anode functional layer as shown in Figure 1.2 and detailed in Reaction 1.1

$$H_2(g,\text{anode}) + O^{2-}(\text{elec},\text{anode}) \Leftrightarrow H_2O(g,\text{anode}) + 2e^-(\text{anode})$$

(R.1.1)

Although not as rapid [10, 18] CO can also be electrochemically oxidized in the anode functional layer according to Reaction 1.2

$$\mathrm{CO(g,anode)} + \mathrm{O^{2-}(elec,anode)} \Leftrightarrow \mathrm{CO_2(g,anode)} + \mathrm{2e^{-}(anode)}$$

(R.1.2)

The O^{2-} ions from the electrolyte are provided by the oxygen reduction on the cathode side according to Reaction 1.3

$$\mathrm{0.5\,O_2(g,cathode)} + \mathrm{2e^{-}(cathode)} \Leftrightarrow \mathrm{O^{2-}(elec,cathode)}$$

(R.1.3)

The difference in O_2 chemical potential between the anode and the cathode produces a cell voltage, V_{cell}, which when combined with the external electron flows out of the anode and into the cathode produces power. A graphical configuration of SOFC chemical and electrochemical processes is shown in Figure 1-2. SOFC electric work is the product of electric current density i and operating voltage V_{cell}, integrated over the active functional layer area. Also, the energy input to the system can be defined as the amount of heat release associated with full oxidation of the fuel stream($\dot{m}_{fuel,in}\Delta h_{fuel,in}$).

$$\varepsilon = \frac{W_e}{Q_{in}} = \frac{\int i\, E_{cell} dA}{\dot{m}_{fuel,in}\Delta h_{fuel,in}}$$

(eq. 1-6)

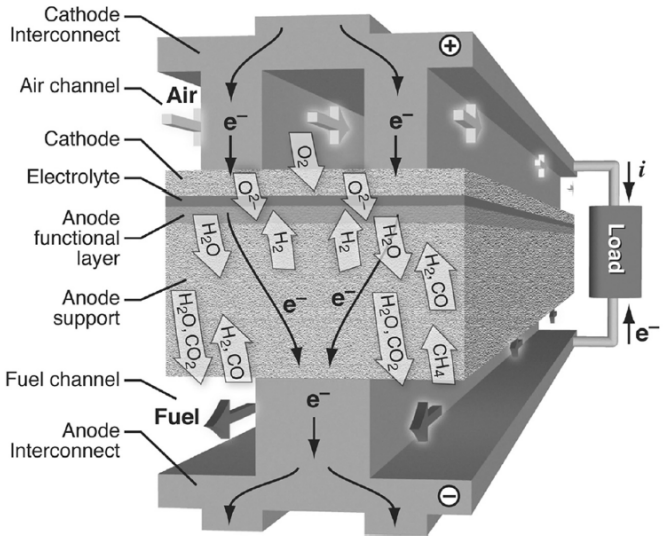

Figure 1-2: SOFC membrane-electrode assembly, illustrating chemical and electrochemical processes taken from Kee et al. [2]

Fuel utilization is a key factor in determining fuel cell efficiency. As the fuel concentration decreases along the anode channel the current density drops due to lower chemical potential driving forces and reduced kinetic rates. As shown by Zhu and Kee this limits fuel utilization to approximately 85% leaving at a minimum 15% of the fuel energy for an exhaust combustor. Typically internal or upstream pre-processing will convert this fuel into syngas, an H_2/CO mixture with additional spccies (notably product H_2O and CO_2), that must be burned in the anode exhaust combustor [2].

During start up heating of the SOFC power system, the amount of fuel utilization is very minimal. The fuel energy must be burned in a combustor (preferably the same as the anode exhaust) and the thermal energy release must be used to heat the combustor. The amount of fuel concentration entering the combustor

during the start up time of the system may be high depending on the rate of heating desired/allowed.

Because H_2 and CO both can be readily oxidized over metallic catalysts, many anode exhaust combustor designs have involved catalytic combustors [14] Catalytic combustors provide increased ranges of operation and lower emissions than more conventional flame combustors [14] and thus maintain fuel cell benefits of low emission and good operability. The combustion reaction occurring at this point in the catalytic combustor, would release some heat depending on the type of the fuel, the fuel to air ratio, and the flow temperature. Another way to speed up the starting up process is to heat up the incoming air flow into the cathode inlet. As a matter of fact implementing a waste heat recuperator that could recover the heat released during the initial combustion process period would be a great way of heating up cathode inlet air flow as well as expediting the start up period of the SOFC power system.

The process explained above can further assist the system performance after it reached the optimal operating condition, by oxidizing the remainder 15% of the fuel exiting the anode exhaust as well as reducing the anode exhaust temperature which at this point ranges about 800-900°C. This process would not only cause the thermal efficiency of the system to increase, but also would allow the system to reach the environmentally standard states of low temperature clean exhaust.

Figure 1-3 presents a graphical representation of the SOFC power system operation with the potential integration of TE modules at the catalytic combustor

surface. In this Figure syngas is considered as the working fuel, containing premixed composition of H_2, CO and H_2O species,

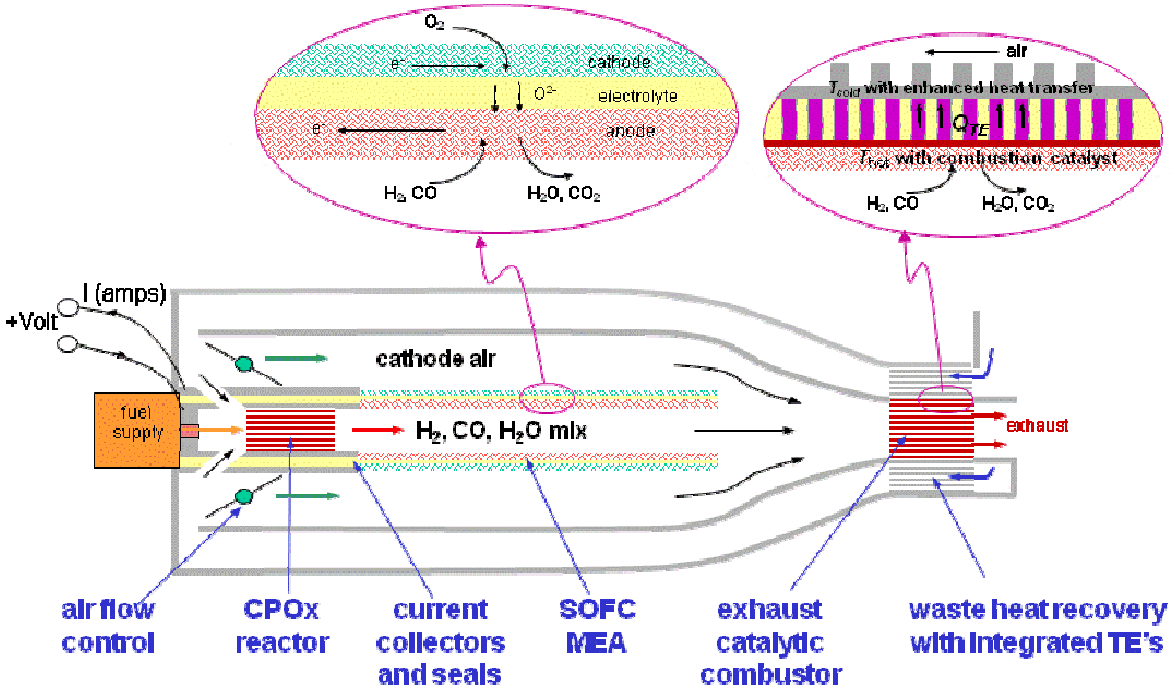

Figure 1-3: Prototypical small scale SOFC power system with catalytic partial oxidation pre-reformer and TE-integrated catalytic combustor.

which are flown into the anode channel of the fuel cell through a catalytic partial oxidation reactor, CPOx. H_2 and CO are oxidized in the anode according to Reactions 1.1 and 1.2, but in order to maintain good cell performance some fuel remains at the exhaust. Thus, the anode exhaust stream mixing with the cathode exhaust, air, will be mixed at the combustor inlet. The combustor flow inlet would contain H_2, CO, H_2O, CO_2, O_2 and N_2 where both streams would be close to fuel cell temperature, between 1000 and 1200 K.

Since 15% or more of the fuel has still passes through the anode to the combustor, further oxidation of the fuel in a downstream combustor/heat exchanger is used to heat up the incoming air stream for stable operation of the SOFC and CPOx reactor. Catalytic combustion is ideally suited for this application since it is amenable to burning streams with reduced heating value. High surface area Pt-coated washcoats in relatively narrow passages provides a means for effective oxidation of the remaining H_2 and CO in the anode stream (after it is mixed with oxidant, in this case the cathode exhaust. Adsorbed fuel species react with adsorbed oxygen on the Pt surface to form H_2O and CO_2 which desorbs back into the gas phase. The catalytic combustion causes most of the heat release to be deposited into the solid washcoat support and adjacent materials. As such, it provides an ideal hot source for pumping heat into the hot side of TE modules for the waste heat recovery process.

1.3.1 Integration of catalytic combustor with TEs

The value of providing a mean of waste heat recovery module and its influence on the performance and efficiency of the overall SOFC power system can be discussed further in this section. As shown in Figure 1-3, the cathode air supply enters the system in a counter-flow configuration with the catalytic combustor fuel/air mixture. Counter-flow heat exchange can accommodate optimal thermal heat recovery from the combustor and expediting the fuel cell heating up process by preheating the incoming cathode air flow. Preheating the cathode channel air flow through convection heat transfer provided by the heat exchanger membrane will cause the air to react with the cathode surface at a higher temperature; which in result will result in heating up the fuel cell at a faster time span than when the air flow inlet

is at room temperature. The process of thermal heat recovery of the combustor through preheating the air will cause the fuel cell to reach its optimal condition faster which would in result cause the fuel cell to generate electricity faster and thus utilizing fuel at the anode surface more efficiently reducing the waste of fuel consumption and requirement in the system.

During the start up period of the fuel cell while the cell and/or reformer is heating up to operating temperatures during which electrical power requirements for the balance of plant components such as air fan, pumps and power electronics are generally provided by batteries. Integrating TE modules into the catalytic combustor/heat exchanger between the walls section of the SOFC power system, as illustrated in Figure 1.3, may allow form some small amount of electric power generation with the hot combustor during the fuel cell system heat-up process. For the purpose of this study, planar thermoelectric modules that are widely available in the market are considered. The power generated by the TEG can then be served to charge batteries or directly fed to the system to provide electric power of the equipments.

Small SOFC power systems, depending on their operating cell voltage and working fuel, attain operating temperature ranges up to approximately 1200 K. Thus, the flows entering the anode exhaust combustor will require high-temperature TE materials for integration with the exhaust combustor. Considering the operating condition limitations of SOFC system, the advancement and availability of TEG modules in the market as well as their common applicability, PbTe was considered as

the best option for this system integration. The details of the material characteristics of PbTe TE would be given further in later sections.

1.4 Thesis outline and objectives

The available source of heat at the anode exhaust combustor component of high temperature fuel cell systems, and the relatively low efficiency of the small scale portable fuel cell systems due to balance of plant makes it worthwhile study the potential for TE modules as a means for converting fuel cell system waste heat into additional electric power. The main objectives of this study can be summarized as following:

- study the effect of TE integration into an anode exhaust catalytic combustor of on small SOFC fuel cell systems,
- investigate with steady state models how the TE/combustor integration impacts the SOFC system efficiency and performance,
- use transient detailed combustor models to assess how TE combustor operation can reduce start-up battery requirements of the system during system preheating.

This thesis is organized as follows. Chapter 2 presents a general simplified numerical model of the SOFC/TE integrated combustor that was initially developed in order to understand and test the validity, feasibility and physics of this modular integration under steady state conditions. In this section, the mathematical approach used to develop this model, the model's geometrical configuration will be explained. Three case studies chosen to perform analytical simulations using the developed

model would then be introduced and the results and their impact on the system performance, efficiency, TE power generation and TE integration feasibility will be discussed.

Chapter 3 discusses the methods and results of the detailed transient model of the TE integrated catalytic combustor model with a porous catalytic washcoat layer and finned air cooling passages as illustrated in Figure 1.4. Transient model results for different operating conditions and design parameters will be presented to show the impact of TE integration on air preheating, TE power generation and fuel consumption

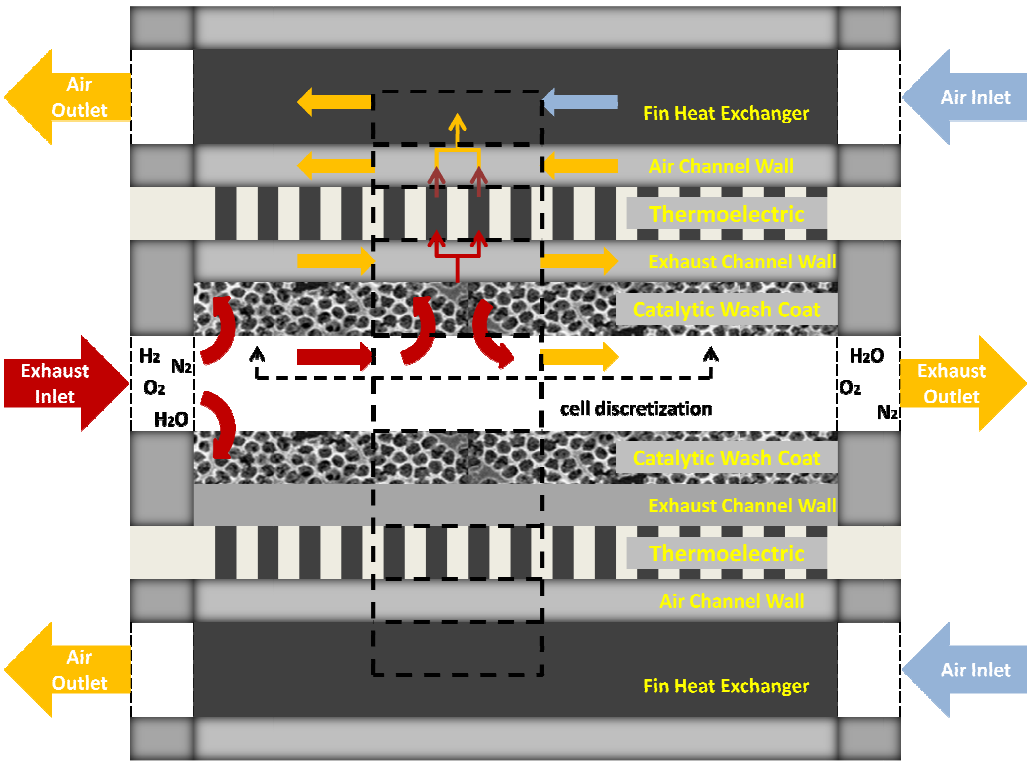

Figure 1-4: Integrated TE/catalytic combustor system with porous catalyst layer and fin heat exchanger

2 System modeling of SOFC TE/Catalytic Combustor

2.1 Introduction

The potential for thermoelectric integration into anode exhaust catalytic combustor to improve overall efficiency of small SOFC systems must be studied within the context of an integrated system. Because the fuel and temperatures to the combustor will be closely linked to the performance of the SOFC, the effectiveness of waste heat recovery through TE modules integrated into the combustor will be tied to the SOFC behavior. Previous modeling of the SOFC system, as illustrated previously in Figure 1-3, has indicated that a catalytic anode exhaust combustor can be effectively integrated with cathode air preheating to provide stable SOFC and combustor performance [1]. The combustor burns the anode and cathode exhaust mixed together while heating the incoming airflow stream through counter-flow heat exchanger passages integrated into the combustor. SOFC operating conditions such

as temperature, flow rates and cell voltage will affect the inlet conditions of the combustor and thus the potential for TE modules to be used to extract power.

This chapter presents an extension of the steady-state SOFC system model of Maxey et al. [16] that incorporates TE modules into an anode exhaust catalytic combustor. While the TEs may be used for electric power generation during the transient system start-up, this initial steady-state system model only focused on how waste-heat recovery through the TE modules may improve system efficiency during steady-state operation. The previous numerical model was initially developed to estimate the power generation of one tubular SOFC model with CPOx reactor and catalytic combustor with waste heat recuperator. The adaptation of TEs into the catalytic combustor and the modeling of their impact on heat transfer and net power produced are explained. The additional governing equations and relevant TE physical properties are also discussed as part of the whole system.

2.2 Model description

The system model was developed in Microsoft Excel using macros to solve the coupled non-linear conservation equations that govern the system. The model incorporates all of the individual components in the system: the catalytic partial oxidatiodation(CPOx) reactor, the SOFC, the anode exhaust combustor/air heat exchanger as shown in the schematic in Figure 1-3. The actual geometry used in the current study is shown in the Figure 2-1, which shows both the system geometry and how the system flows are passed between the components. The mass and energy balances are solved for finite volume discretizations in the components and at their

interfaces. Axial discretizations along each flow path are in the flow (x) direction but discretization in the transverse direction (r or y direction) are needed to capture temperature in walls and temperature and species in porous media such as in the fuel cell electrodes. The model solves the non-linear mass and energy conservation equations through an iterative process established in an Excel macro.

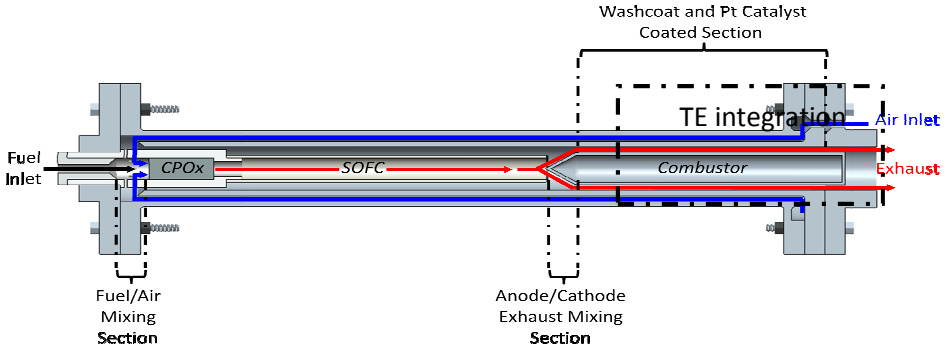

Figure 2-1: Cross-sectional view of the TE integrated SOFC/combustor model configuration taken from [16].

The system includes a single-cell tubular SOFC fed by a CPOx reactor and followed by a downstream catalytic combustor which also serves as a heat recovery device for the incoming air flow. TEs are integrated into the combustor to utilize waste-heat recovery to generate electrical power

2.2.1 CPOx reactor model

The first component of the model is a catalytic partial oxidation reactor. In the current study, the CPOx reactor upstream of the SOFC anode inlet is fed by n-butane and converts the fule mixed with air at a fixed carbon to oxygen (C/O) ratio. The exothermic self-sustaining reaction occur over a porous catalytic ceramic foam, as described in the work of Reihani and Jackson [17], produces H_2 and CO for

feeding the SOFC anode. All the model studies in this study use a C/O value of 1.0 and assume complete conversion of the butane to H_2 and CO. Temperatures of the reactor and surrounding walls are solved with an energy balance based on the exothermic heat release and conduction in the solid matrix and convection into the gas phase flows. The CPOx reactor housing is directly coupled to the SOFC allowing conduction from the CPOx reactor walls into the SOFC. The CPOx model along with all other component is cylindrical with tubular walls in order to facilitate integration with the tubular SOFC design study here as illustrated in Figure 2-1. Table 2-1 provides geometrical detail of the CPOx reactor modeled in this study.

Table 2-1: CPOx reactor geometric parameters

Geometric Property (units)	**Value**
CPOx Length including mixing regions (mm)	22
Axial discretization	5
Length of reactor section (mm)	7
Outer diameter of reactor section (mm)	5
Cathode inlet flow inner diameter (mm)	6
Cathode inlet flow inner diameter (mm)	8
Outer air flow inner diameter (mm)	9
Outer air flow outer diameter (mm)	9
Outer wall thickness (mm)	1

2.2.2 SOFC model

The SOFC model uses a tubular cell geometry and is based on a solution methodology developed from a detailed membrane electrode assembly (MEA) model presented in previous reference [20] as described in Maxey et al. [1]. Details of the SOFC geometery and material structures are described in the previous reference. The tubular SOFC has a 9.0 mm internal diameter and consists of a porous Ni/YSZ anode

(920 μm thick in the radial direction with the outer 50 μm serving as a less porous functional layer where the electrochemical oxidation reactors take place). A dense thin (~ 12 μm) YSZ electrolyte and a thin (~ 70μm) porous LSM/YSZ cathode are on the outer diameter of the tubular SOFC which has an outer diameter of 11.0 mm..

The governing equations applied through the MEA are a system of differential algebraic equations which are set to reach steady state conditions through an iterative process. The model is run in an isothermal mode where the temperature along a given axial slice remains uniform. The governing equations used to model the physical phenomena through the MEA structure include: 1) convective-diffusive transport from the channel flow to the fuel cell, 2) gas-phase diffusion through the porous electrodes, as described by the Dusty Gas Model, 3) reversible surface reactions including charge-transfer reactions and 4) transport of O^{2-} ions through the YSZ and electrons through the Ni and LSM [1].

In the MEA model, detailed microkinetics are adopted from DeCaluwe et al. [18] with additional CO chemistry being added from Habibzadeh [19]. The microkinetics includes H_2 and CO oxidation via charge transfer reactions on the anode side. The detailed charge transfer kinetics are used to calculate current density *i*, base on the activation voltage loss or overpotential at the electrocatalyst/electrolyte interface, η_{act} [1]. In addition, the fuel cell experienced other voltage losses and overpotentials through the MEA membrane due to concentration drops, η_{conc}, which drive the diffusion of reactants into the products out of both electrodes (Equations 2-1 and 2-2). P_k^{int} and P_k^{ch}represent the partial pressures at the electrode/electrolute

interface and in the channel flow, respectively.

$$\eta_{conc,an} = \frac{\bar{R}T}{2F}\ln\left(\frac{P_{H_2}^{ch}\,P_{H_2O}^{int}}{P_{H_2}^{int}\,P_{H_2O}^{ch}}\right) \quad \text{(Eq. 2-1)}$$

$$\eta_{conc,cath} = \frac{\bar{R}T}{4F}\ln\left(\frac{P_{O_2}^{ch}}{P_{O_2}^{int}}\right)$$

(Eq. 2-2)

Voltage losses due to Ohmic resistance to ionic and electronic transport within the electrolyte and both electrodes are determined by Ohm's law as presented in equation 2-3.

$$\eta_{ohm} = i\,(R_{elec,an} + R_{elec,cath} + R_{ion,electrolyte})$$

(Eq. 2-3)

As a matter of fact, the overall cell voltage, as described previously, can be reached through the following equation 2-4.

$$V_{cell} = V_{OCV} - \eta_{act,cath} - \eta_{conc,cath} - \eta_{act,an} - \eta_{conc,an} - \eta_{ohm}$$

(Eq. 2-4)

The model assumes that resistances along the current collector of the tublar cell are small enough such that V_{cell} along the length of the fuel cell. The Excel model solves for i at each discretized slice; which at this point the Butler-Volmer kinetic model will be used to determine the species composition along the cathode and anode channel. These values are also coupled through an energy balance along the axial direction to

solve for the temperature variations at the SOFC as well as the air flow streams (as indicated in Figure 2-1). The summation of the current densities, *i*, at each slice provides the total current produced by the SOFC; and the product of this current with the defined cell voltage provides the total power production of the cell which is used to determine the thermal efficiency of the cell as was presented in Figure 2-2. Geometric parameters for the SOFC are listed in Table 2.2 and were held constant throughout this current study.

Table 2-2: SOFC geometric parameters

Geometric Property (units)	**Value**
SOFC length (mm)	100
Axial Discritization	9
Anode inner diameter (mm)	5
Cathode outer diameter (mm)	6
Cathode flow outer diameter (mm)	8
Outer air flow inner diameter (mm)	9
Outer airflow outer diameter (mm)	9
Outer wall thickness	1
Anode, cathode three-phase-boundary length per unit volume electrode (m-2)	$3*10^{13}$
Functional layer thickness (μm)	20
Thickness of charge transfer reqion (μm)	10
Anode, Cathode porosity	0.57, 0.45
Active catalyst area per unit volume electrode (m^{-1})	$1*10^{7}$

2.2.3 Simplified catalytic combustor/TE model

The system model accommodates waste heat recovery by modeling the combustor wall as a corrugated high surface-area wall heat exchanger which transfers heat from the flow of anode and cathode exhaust to the outer counter-flow of incoming air, as shown in Figure 2-1 [1]. For this study, the combustor/heat exchanger model was modified to incorporate TEs between the hot and cold flow

walls. The updated model splits the heat exchanging wall into two hot side and cold side walls. The hot side wall, in contact with combustor stream serves as the TE hot junction and the cold side wall, in contact with incoming air stream functions, as the TE cold junction as illustrated in Figure 2-2.

In the TE module, n-type and p-type TE elements are electrically connected in series to form a TE couple and are separated with an equal surface area as their cross sectional area. Thus, the TE couple contact area to the hot side and the cold side wall can be defined as the cross sectional area occupied by n-type and p-type TE elements plus two spacing areas between the TE elements and the neighboring TE couple. The number of thermoelectric couples residing in each cell division is then estimated as following, equation 2-5, where $r_{comb,wall}$ is the combustor wall's outer radius, dx_j is the length of the jth cell and $A_{c,TE}$ is the TE couple's contact area.

$$n_{TE,j} = \frac{r_{comb,wall} dx_j}{A_{c,TE}}$$

(Eq. 2-5)

Based on commercially available TE modules, the TE element height was set to be 2 mm with a cross sectional area for each leg of each couple being 0.01 mm^2. Further dimensions of the TE module are given in Table 2-3.

In the model, the length of the combustor channel is divided into 7 discretizations in the axial direction along the flow. Because of symmetry, one side of the combustor that includes half of the combustor channel's height, one TE module and half of the air channel's height is considered for the simulations over each cell. The red dashed rectangle in Figure 2-3 represents one axial discretization where

energy conservation equations are applied in both horizontal (x) and vertical (y) directions. The energy balance equations are applied separately to individual sub-elements within the discretizations, i.e. the combustor flow, combustor wall, air wall, air flow and outer air flow.

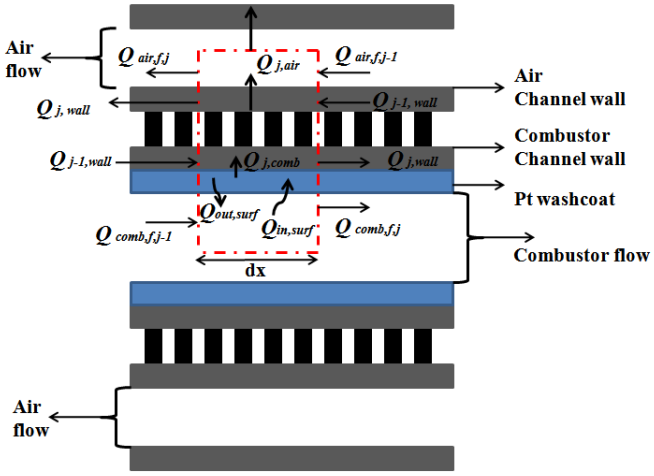

Figure 2-2: A schematic of a single axial discretization of a TE-integrated catalytic combustor.

Figure 2-2 shows the mass and heat transfer through each elemental layer within the axial discretization. Species mass balances within the combustor channel flow provide the basis for determining gas composition and properties along the length of the combustor. Energy balances in the combustor channel and in the walls, TE elements, and cooling air flow solve for temperatures when coupled with the combustor species balances. The coupled equations are solved through an iterative process such that the energy balances are converged to within 0.001 mW.

The combustor channel walls are covered with Pt-impegnated porous Al_2O_3 washcoat to provide rapid oxidation of H_2 and CO with the excess O_2 provided by the cathode exhaust flow. Although detailed surface chemistry models for CO and H_2

oxidation on Pt catalyst exist [20], for relatively rapid solution of the entire system, the combustor model here assumes reaction rates occur at a fixed fraction of mass transfer-limited conditions as determined by the diffusion rates from the flow to the porous washcoat of the fuel species. This approximation was deemed reasonable due to high temperatures in the combustor and the high reactivity of the Pt surface to both H_2 and CO at these temperatures. The mass transfer limits use Sherwood number correlations to predict mass transfer to/from the catalytic surface along the length of the combustor/waste heat recovery heat exchanger [1].

Convective heat transfer in the combustor channel between the flow and the combustor wall is calculated using Nusselt number correlations. Thermal conductivity of the combustor fluid, $k_{comb,f}$, is the product sum of the species thermal conductivity with species mole fraction. The heat transfer coefficient, $h_{T,comb}$, of the combustor wall is then gained from the Nusselt number of the flow according to equation 2-6.

$$h_{T,comb} = K_{comb,f}\, Nu/d_{hydr}$$

(Eq. 2-6)

Due to circular geometry of the combustor channel in this model, *Nu* is estimated using a Graetz number correlation as shown in equation 2-7; where Nu_{inf}, a_1, a_2 and a_3 are the geometrical constants for circular tubes, *dx* presents the length of discretdiscretization along the flow path, Re is Reynolds numbers, and Pr represents Prandtl number.

$$Nu = Nu_{inf} + a_1 \left(1000 \frac{dx}{d_{hydr}\,Re\,Pr}\right)^{a_2} e^{\left(\frac{a_3 dx}{d_{hydr}\,Re\,Pr}\right)}$$

(Eq. 2-7)

where the parameters for Nu in equation 2.7 are taken for annular flow from Groppi et al. [22]. Reynolds number is based on the cross sectional area of the combustor channel, $A_{comb,ch}$, times the dynamic viscosity of the flow. Thus, the enthalpy change of the j^{th} division along the combustor channel flow and the respective heat transfer terms through the flow and the wall is defined as follow:

$$\dot{Q}_{flow,x,j} = \dot{m}_{flow,x,j}\, h_{flow,j}$$

(Eq. 2-8)

where $\dot{m}_{comb,f,j}$ and $h_{comb,f,j}$ represent the axial mass flow rate and enthalpy of the combustor flow respectively. Convective heat transfer to the washcoat wall is calculated by equation 2-9:

$$\dot{Q}_{conv,y,j} = h_{T,comb,j}\, \Delta z_{comb}\, dx_j \left[\left(T_{comb,f,j} + T_{comb,f,j-1} \right) - \left(T_{comb,wall,j} + T_{comb,wall,j-1} \right) \right]$$

(Eq. 2-9)

Finally the exchange of enthalpy $\dot{Q}_{diff,y,j}$ due to the diffusion of different species into and out of the washcoat is given by equation 2-10.

$$\dot{Q}_{diff,y,j} = \sum_k \dot{m}_{k,y,j}\, h_{k,j}$$

(Eq. 2-10)

where $\dot{m}_{k,y,j}$ is the mass flux of species k in the transverse direction with positive $\dot{m}_{k,y,j}$ implying diffusion of species k out of the channel flow for cell *j* and $h_{k,j}$ is the enthalpy per unit mass at the flow temperature of each species.

At steady state, the energy balance for a discretization as indicated by Equation2-11 must be solved iteratively.

$$0 = \dot{Q}_{flow,x,j-1} - \dot{Q}_{flow,x,j} - \dot{Q}_{conv,y,j} - \dot{Q}_{diff,y,j} \quad \text{(Eq. 2-11)}$$

The combustor flow temperatures will be solved through an iterative process that satrisfies the species mass balance and equation 2.11 for each axial discretization. The geometric parameters for the cylindrical combustor model are provided in Table 2.3.

Table 2-3: Integrated TE combustor/heat exchanger geometric parameters

Geometric Property (units)	**Value**
Combustor channel length (mm)	50
Axial Discritization including upstream premixing	7
Combustor catalytic wall average diameter (mm)	7
Combustor channel hydraulic diameter (mm)	5.4
Thermoelectric thickness (mm)	2
TE element cross sectional area (mm^2)	0.01
TE element spacing area (mm^2)	0.01
TE couple contact area ($mm^{2)}$	0.05
Number of TE couple per discretization	12
Outer air flow inner diameter (mm)	9
Outer airflow outer diameter (mm)	11
Air Cannel hydraulic diameter (mm)	8
Outer wall thickness (mm)	2

The temperature of the combustor wall is coupled to the flow and evaluated similarly with energy balances which is determined by summing the conductive and

convective heat fluxes into and through the wall with the thermal energy release due to catalytic combustion in the porous washcoat. The energy release by the catalytic reaction is assumed to be initially taken in by the porous washcoat structure which is assumed to be in thermal equilibrium with the solid combustor channel walls . The heat released due to chemical reaction at the wall surface to the combustor flow, $\dot{Q}_{reac,j}$, is

$$\dot{Q}_{reac,j} = V_{wash,j} a_{cat} \sum_k \left(\dot{s}_{k,j} W_k\right)$$

(Eq. 2-12)

where $V_{\text{wash,j}}$ and $\dot{s}_{k,j}$ are the volume of the washcoat and the surface reaction rate per unit area (gmol·cm^{-2}·s^{-1}) of catalyst in the washcoat, a_{cat} is the catalyst surface area per unit volume in the washcoat. Under the assumptions that the catalytic reaction rates are proportional to the mass diffusion rates of fuel into the washcoat, $\dot{s}_{k,j}$ will be proportion to $\dot{m}_{k,y,j}$ for the fuel

$\dot{Q}_{wall,x,j-1}$ and $\dot{Q}_{wall,x,j}$ as it can be seen on Figure 2-5 are the conductive heat transfer which are calculated for the forward and backward conduction terms.

$$\dot{Q}_{,wall,x,j-1} = k_{wall} A_{comb,wall} \left(T_{comb,wall,j-1} - T_{comb,wall,j}\right)/0.5(dx_j + dx_{j-1})$$

(Eq. 2-13a)

$$\dot{Q}_{wall,x,j} = k_{wall} A_{comb,wall} \left(T_{comb,wall,j} - T_{comb,wall,j+1}\right)/0.5(dx_{j+1} + dx_j)$$

(Eq. 2-13b)

The heat flux from the combustor wall is then conducted towards the air channel wall at a lower temperature through thermoelectric couples at a rate of $\dot{Q}_{TE,j}$, where k_{TE} is the thermal conductivity of PbTe thermoelectric material.

$$\dot{Q}_{TE,j} = n_{TE}(2A_{TE})\, k_{TE}\, (T_{comb,wall,j} - T_{air,wall,j})/y_{TE}$$

(Eq. 2-14)

The sum of all of the heat and energy transfer terms into and out of the j^{th} discretzation will then be forced equal to zero to reach the combustor wall's temperature at steady state, equation 2-15.

$$0 = -\dot{Q}_{reac,j} + \dot{Q}_{diff,y,j} + \dot{Q}_{conv,y,k} + \dot{Q}_{,wall,x,j-1} - \dot{Q}_{wall,,x,j} - \dot{Q}_{TE,j}$$

(Eq. 2-15)

The heat conducted from the combustor wall to thermoelectric couples is then transferred to the air channel wall at lower temperature at a rate of $\dot{Q}_{TE,j}$. As air stream flowing through the air channel at room temperature picks up the heat from the wall through convective heat transfer at a rate of $\dot{Q}_{conv,air,y,j}$ where the convective heat transfer coefficient, $h_{T,air,j}$, is estimated the same method as of $h_{T,comb,j}$, assuming fully developed flows in the channels and heat transfer coefficient correlations over extended surfaces adapted from [14]. In addition, the conductive heat transfer is modeled along the cross sectional area of the air channel wall at a rate of $\dot{Q}_{wall,air,y,j}$, where thermal conductivity of the air channel wall, $k_{T,wall}$, is equal to that of the combustor wall equal to 16 W/mK, since both walls are modeled as Stainless Steel 304.

$$\dot{Q}_{conv,air,y,j} = h_{T,air,j}\,\Delta z_{air}\,dx_j\,\left[\left(T_{air,wall,j} + T_{air,wall,j-1}\right) - \left(T_{air,f,j} + T_{ir,f,j-1}\right)\right]$$

(Eq. 2-16)

$$\dot{Q}_{air,wall,x,j} = k_{T,wall}\,A_{cross,air,wall}\,(T_{air,wall,j} - T_{air,wall,j+1})/0.5(dx_{j+1} - dx_j)$$

(Eq. 2-17a)

$$\dot{Q}_{air,wall,x,j-1} = k_{T,wall}\,A_{cross,air,wall}\,(T_{wall,cs,j-1} - T_{wall,cs,j})/0.5(dx_j - dx_{j-1})$$

(Eq. 2-17b)

The sum of all the thermal heat flux going in and out of the air channel wall is set equal to the overall change of air wall's enthalpy, $\Delta h_{air,wall,j}$, set equal to zero in order to find the air wall's temperature at equilibrium condition.

The waste heat transferred to the relatively cool air walls \through thermoelectric modules, heats the air flow along the length of the channel in the cross-flow heat exchanger arrangement shown in Figure 2.2. Some of that heat is lost through the external wall at a rate of $\dot{Q}_{air,ext\_wall,j}$. This heat exchange between the system and the surrounding occurs through this wall and is modeled in such way that the system can either be fully insulated by multiplying the heat transfer coefficient with heat enhancement factor of 5 or can transfer heat to the surrounding when multiplied by a heat enhancement factor of 3 or lower.

$$\dot{Q}_{air,ext\_wall,j} = h_{T,ext,j}\, z_{air,f}\, dx_j \left[\left(T_{air,f,j+1} + T_{air,f,j} \right) - \left(T_{air,wall,j+1} + T_{air,wall,j} \right) \right]$$

The temperature of the air flow channel at the j^{th} cell is the calculated through iterative process of equaling the enthalpy change of air flow stream to zero.

$$0 = \dot{m}_{air,f,j-1}\, h_{air,f,j-1} - \dot{m}_{air,f,j}\, h_{air,f,j} + 0.5\dot{Q}_{air,surf,j} - 0.5\, \dot{Q}_{air,ext\_wall,j}$$

(Eq. 2-19)

The heat flux transferred from the combustor flow to the wall is conducted towards the air wall channel at a lower temperature through thermoelectric couples. The heat transfer creates temperature difference on each side of the TE couples, i.e. the combustor wall and the air channel wall, generating voltage at each couple. In reality the TE elements generate internal heat due to thermal heat conduction from the combustor wall to the air wall as well as the heat generated due to internal electrical resistances within the couples and the contacting areas. As a matter of fact, for simplicity of calculation in this model, the TE elements are not modeled as an individual discretized layer and thus the change in enthalpy, temperature and internal energy losses within the TE module are not calculated. The heat conduction term from combustor wall to the air wall, $\dot{Q}_{TE,j}$, is calculated through equation 2-14 where as it shown on Figure 2-2, would enter the TE element from combustor wall and enter air channel wall through length of TE.

Using the derived temperature values of combustor wall and air wall, the model calculates the TE power generation using the following definition, equation 2-27and28.

$$V_{TE,j} = \alpha_{TE}\left(T_{comb,wall,j} - T_{air,wall,j}\right)\ n_{TE,j}$$

(Eq. 2-27)

$$R_{TE,j} = \left(\left(\frac{2\,\rho_{TE} l_{TE}}{A_{TE,leg}}\right) + \left(\frac{4\,\rho_{c,TE}}{A_{TE,leg}}\right)\right)\ n_{TE,j}$$

(Eq. 2-28)

The voltage generated by the TE is calculated using Seebeck principle, equation 2-27, where $\alpha_{TE}$is the thermoelectric material's Seebeck coefficient, $T_{comb,wall,j}$ is the combustor wall temperature and $T_{air,wall,j}$ is the air wall temperature at the jth cell. In addition, the TE couple experience electrical resistance along the length of the elements as well as the local resistance due to contact resistance at the conjunction area. ρ_{TE} represents electrical resistivity of the TE material in (Ω·cm), l_{TE} is the TE element's height, A_{TE} is the TE n-type or p-type element's cross sectional area, $\rho_{c,TE}$ is the contact resistance of the TE material which is a constant value of $2.54 \cdot 10^{-6}$ (Ω·cm^2) (Ω·cm^2) for PbTe material [7]. Since the TE couples are electrically connected in series, the total voltage generated by the module is equal to sum of all voltages generated at each cell division. The overall power generated by the module is then calculated through the following equation 2-29.

$$W_{TE} = \left(\frac{\sum_{j=1}^{n} V_{TE,j}}{\sum_{j=1}^{n} R_{TE,j} + R_{load}}\right)^2 R_{load}$$

(Eq. 2-29)

In this model, the load resistance was set equal 1 Ω to reach maximum power output from the TE module.

Due to high anode and cathode exhaust temperature of the SOFC into the combustor, the material selection of the thermoelectric module as the heat exchanging module which can withstand this temperature range becomes an important factor of the system modeling. For the purpose of this study lead telluride (PbTe) TE material was an appropriate selection that fits system's operating conditions. The thermoelectric as well as the thermodynamic properties such as α_{TE}, , ρ_{TE} and k_{TE} of the PbTe material used in this model is taken from a previous study [21]. For the TE modeling of this section, the thermoelectric properties achieved for 6% Pb rich sample was chosen to replicate the TE module's behavior in the combustor component. Due to temperature dependances of these parameters, the respective material properties was measured within a certain testing temperature range. The fitted data from this study was then used to develop a numerical computation for these properties with respect to temperature. Figure 2-6 is the measured n-type and p-type $Pb_{1.06}Te$ Seebeck coefficient versus temperature measurement range of 80 to 900 K. According to Rowe the overall Seebeck coeffieicnt, α_{TE}, per couple is the difference between $\alpha_{TE,p}$ and $\alpha_{TE,n}$. Thus, the value of $\alpha_{TE,p,j}$ and $\alpha_{TE,n,j}$ is calucalted at each discretizations using the fitted curve functions where the known varriable is the TE temperature of the j^{th} cell, where the TE temprature is calcualted by averaging the combustor wall and air wall temperature.

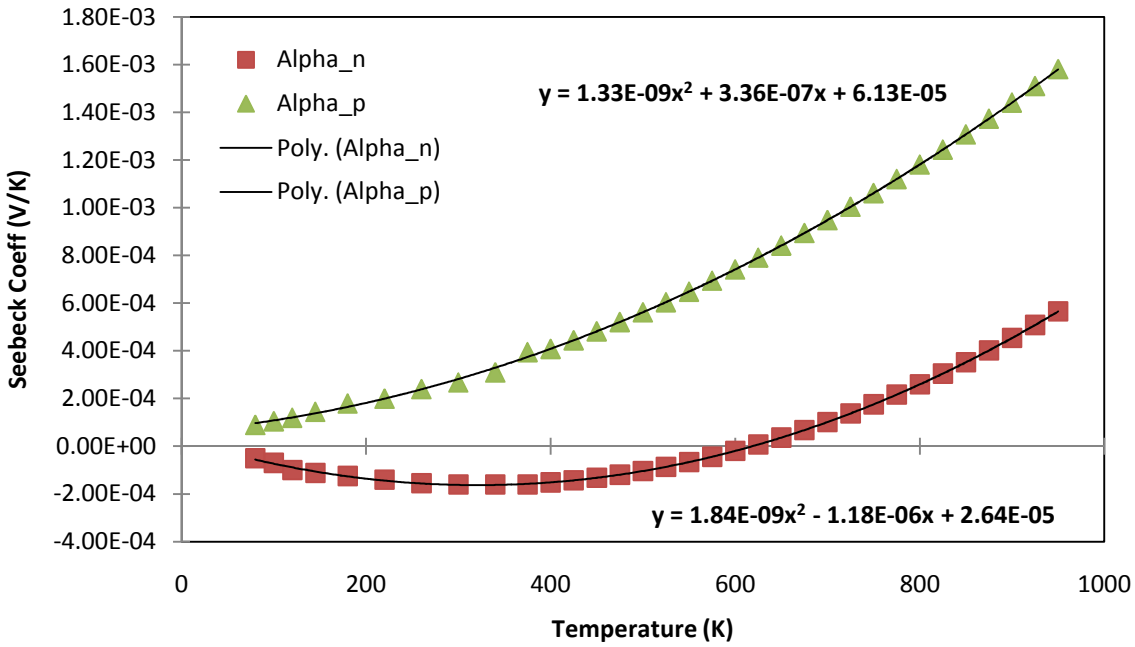

Figure 2-3: $Pb_{1.06}Te$ Seebeck coefficient versus temperature correlation

Figure 2-7 represents resistivity of both p-type and n-type $Pb_{1.06}Te$ material at temperature range of 80 to 900 K. The polynomial equations from the fitted curves are then used to calculate the n-type and p-type resistivity of a TE element at the j^{th} discretization the same way as Seebeck coefficient calculation is performed. However, the total resistivity of the TE couple is the sum of the n-type and p-type resistivity at each cell division [21].

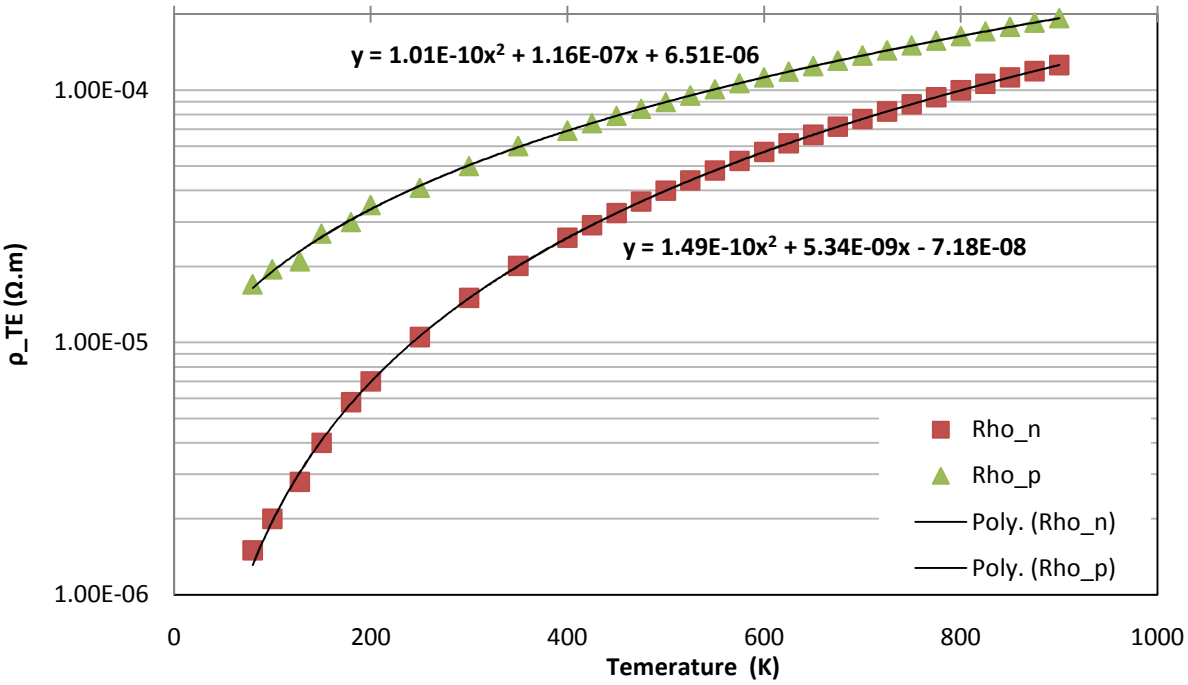

Figure 2-4: $Pb_{1.06}Te$ Electrical Resistivity versus Temperature correlation [21]

The thermal conductivity of the $Pb_{1.06}Te$ also changes with temperature. However, in the study performed by Heremans et al. [21], the thermal conductivity of the samples are assumed constant equal to 2.5 $W \cdot m^{-1} \cdot K^{-1}$ at the testing operating temperature of around 300 to 350 K.

To achieve a more precise thermal conductivity coefficient for the model the used for PbTe material with 6% Pb precipitation in Heremans study is consistent with the data provided by Rowe [7]. Based on the data provided, the thermal conductivity of PbTe at temperature range of 800 to 1100 K is in the range of 0.7 to 1.0 $W \cdot m^{-1} \cdot K^{-1}$ and since the range of combustor's channel temperature at steady state will vary within 800 to 900 K, for simplicity of the model, the thermoelectric thermal conductivity used is the averaged value of this range, 0.85 $W \cdot m^{-1} \cdot K^{-1}$.

In the modeling of the SOFC system with integrated TE catalytic combustor parameters

such as fuel and air inlet pressure is fixed equal to 1 atm where no pressure drop along the length of channels is assumed. As it was mentioned in the previous sections, the SOFC power generation and efficiency as well as the TE generation terms are achieved through simulating component temperatures at each component sub-layers that are discretized along the direction of the SOFC channel flow.

The mass transfer limited conversion of H_2 within a j^{th} discretized cell along the combustor channel flow is then modeled by multiplying the amount of conversion, calculated through Sherwood correlation, by a constant coefficient of 0.5. The amount of conversion for each fuel in each cell is calculated through the following equation:

$$\dot{m}_{y,k,j} = \varepsilon \dot{m}_x Y_k [1 - e^{(-k_{c,k,j}\, a_{wash} dx_j / \vartheta_{comb})}]$$

(Eq. 2-30)

where ε is the fraction of mass-transfer-limited converwion that occurs in each cell and is set to 0.5 in this study. $k_{c,k,j}$ is the mass transfer coefficient of species k ($m \cdot s^{-1}$) in j^{th} cell, a_{wash} is the exposed geometric surface area of the washcoat per unit length of the combustor channel cell, dx_j is the length of discretized cell and ϑ_{comb} is the velocity of the combustor flow (m/s). The $k_{c,k,j}$ is then correlated through equation 2-31, where Sh_k represents the Sherwood number of the species k, $k_{diff,k}$ is the diffusion coefficient of species k (m^2/s) over the hydraulic diameter of the combustor.

$$k_{c,k,j} = \frac{Sh_k k_{diff,k}}{d_{hydr,comb}}$$

(Eq. 2-31)

In addition, the Sherwood number and the diffusion coefficient of species are correlated through following equation 2-32, respectively.

$$Sh_k = Sh_{inf} + a_1 \left(\frac{1000\, z_{comb}}{d_{hydr,comb}\, Sc_k\, Re_{comb}} \right)^{a_2} e^{\left(\frac{a_3 \cdot d_{hydr,comb} \cdot z_{comb}}{Sc_k \cdot Re_{comb}} \right)} \quad \text{(Eq. 2-32)}$$

The Sherwood coefficients for a circular geometry are provided from a previous reference for a tubular geometry [22]; Sc_k represents the Schmidt numbers of species.

2.3 Modeling results

For this study, a baseline operating condition for SOFC power system was established at cell operating voltage V_{cell} = 0.75 V with an overall air to fuel stoichiometric ratio of 3.0 and tested along with V_{cell} of 0.7 and 0.8V conditions. The results driven from these simulations cell voltage of 0.7 V produces the highest amount of starting from 3.7A.m^{-2} to 0.77A.m^{-2} at the end of the fuel cell. The 0.8V cell voltage case has the lowest current density production with a sharp drop at the beginning of the cell. The 0.75 V cell voltage was found to have the steadiest current density generation generating about 3.3 7A.cm^{-2} to 0.57A.cm^{-2} along the length of the fuel cell.

In addition, the thermal efficiency as well as the amount of H_2 conversion at each case was also estimated, Figure 2-5. The thermal efficiency of the fuel cell operating at cell voltages V_{cell} = 0.7V is estimated about 33% versus 26% and 36%

for 0.8 and 0.75 V cases respectively. This model can then be implemented for multi cell systems whit relatively uniform operating conditions for all the cells.

Table 2-4: SOFC baseline operating conditions

Operating Conditions (units)	**Value**
Outlet Pressure (bar)	1.0
Ambient Temperature, inlet fuel and air temperatures (K)	300
Inlet fuel flow (g/s)	0.001
Overall air to fuel ratio	3
CPOx air to fuel equivalence ratio	5
Heat transfer coefficient through external walls (W/m^2K)	0.0

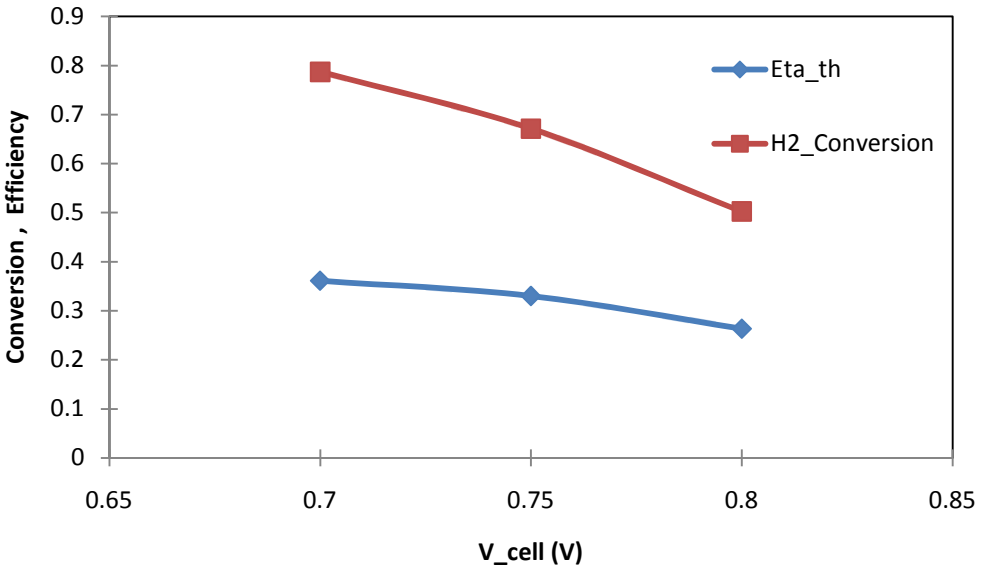

Figure 2-5: Thermal efficiency and H_2 conversion % of SOFC as a function of cell voltage.

Table 2-4 presents all the chosen baseline parameters for this model. The following sections present how the TEG was incorporated into the catalytic combustor model of this SOFC system. Then the results of the steady-state modeling show the

effectiveness of the TEG for increasing overall system efficiency for the SOFC system.

As it was mentioned earlier in the chapter, the SOFC system model without TE integration was used to simulate the system conditions at three different fuel cell voltages of 0.7, 0.75 and

0.8V, 0.75V being considered as the baseline case of the study. Accordingly, the upgraded version of this numerical simulator, with the integrated TE governing equations and thermoelectric properties, was also run under similar conditions to achieve a comparative case study of the original versus the TE integrated model. In this way, the effect of TE integration into SOFC anode exhaust catalytic combustor on the overall efficiency of the system can be studied.

All the three cases was run under similar inlet conditions of air to fuel ratio of 3, the mass limited conversion coefficient of 0.5, the air channel mass flow rate of 0.00454 g/s as well as the CPOx reactor inlet of $5.66*10^{-3}$ g/s as well as the air channel inlet temperature of 300K. The system was run integrating the heat transfer energy equations until the system reaches steady state, i.e. no change of enthalpy within the system. Figure 2-6 is the resulting flow temperature within the system starting from the CPOx reactor going into SOFC tube and through the catalytic combustor.

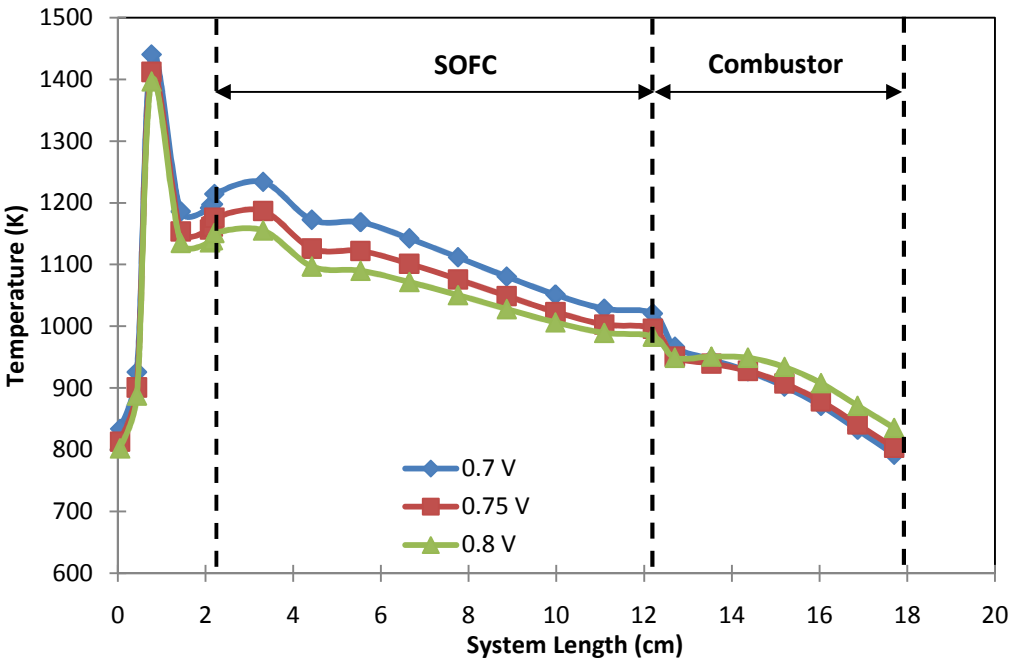

Figure 2-6: SOFC/TE integrated system temperature along the axial length of the channels with baseline operating conditions table 2-4.

In Figure 2-7, the amount of power generated by the TE at discretized cell along the length of the combustor channel is presented. Where the power generated in case of cell voltage of 0.8 V reaches 0.2 W very quickly and also decreases sharply going from 0.21 W to 0.03W in the last cell discretization. Whereas the other two cases generate power more steadily; however due to the large temperature difference at the last cell which is the exhaust point of the system versus the air inlet of the system, the TE power drops by order of 0.1 W.

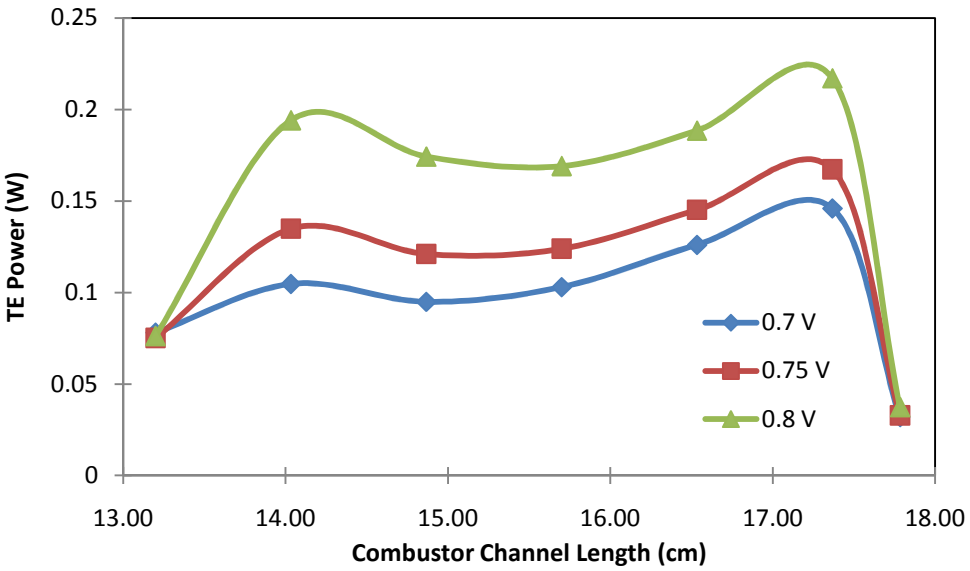

Figure 2-7: TE power generation along the length of combustor channel

Another important parameter in studying the functionality of the model is the ability of the catalytic combustor to consume the remaining fuel left in the SOFC anode exhaust. As a result the plot of the mass fraction of H_2 consumed along the length of the combustor for three different cell voltage cases is presented below in Figure 2-8. It should be noted that a mass limited conversion coefficient of 0.5 is applied for H_2 reaction in the combustor. Based on the results provided, the amount of H_2 composition entering the combustor with a cell voltage of 0.8V is higher and the amount of H_2 conversion is also higher than the other two cases. However, the system operating with a cell voltage of 0.7V consumes the majority of the fuel and the amount of H_2 exiting the combustor is about 0.0012.

One of the main goals of this research is to preheat the incoming airflow, entering the system at x = 18cm, by waste heat recovery of the combustor flow using

thermoelectric module. The combustor outlet air flow temperature on the cold junction of the TE, calculated at each case study, is presented bellow in Figure 2-9.

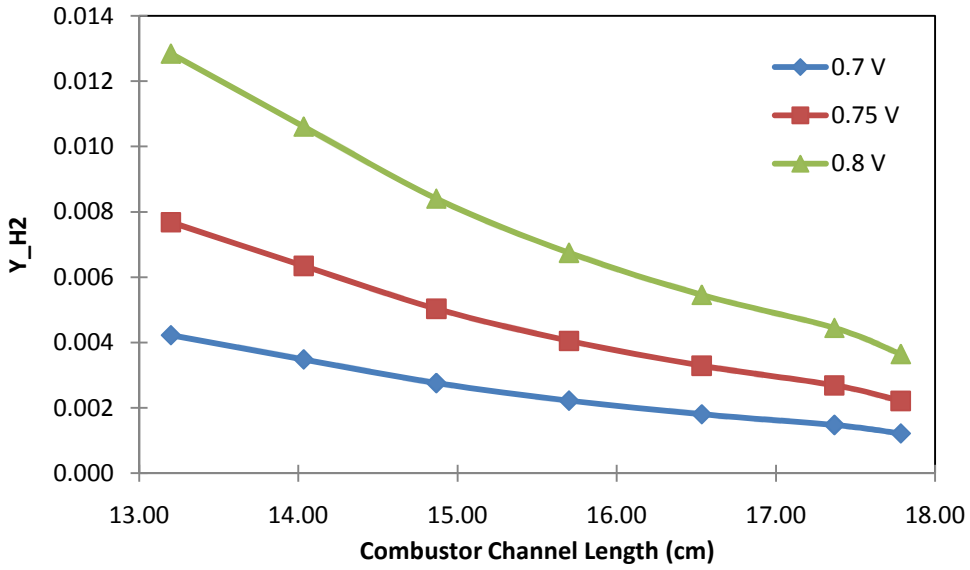

Figure 2-8: H_2 mass fraction along the combustor channel length

Figure 2-9 represents the total amount of power generated by TE during SOFC's steady state The TE module generates the maximum of power at 0.8 V cell voltage condition and the air flow temperature exiting the combustor chamber is preheated to 870K. The baseline condition of 0.75 V generated about 2.5 W of power and preheats the air to about 850 K.

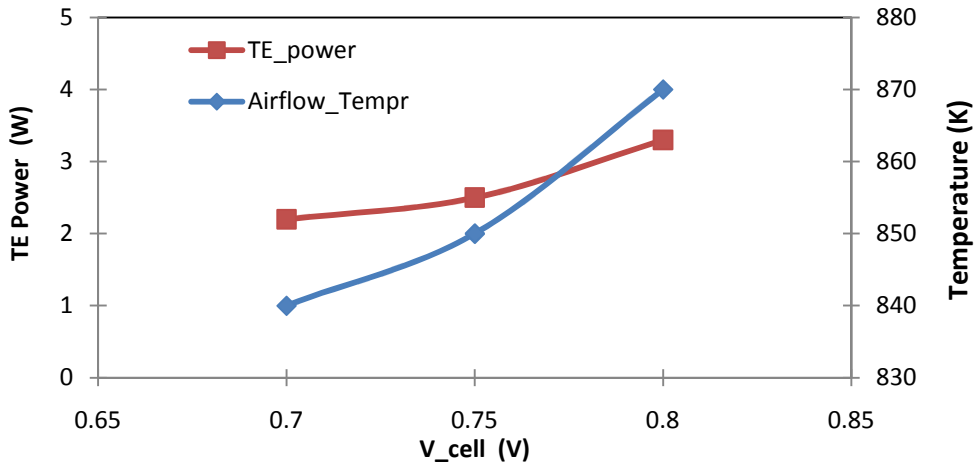

Figure 2-9: TE power generation and combustor outlet air flow temperature

Table 2-5 : Steady state system performance and power requirements

V_{cell} (V)	**0.7**	**0.75**	**0.8**
W_{SOFC} (W)	18.97	18.6	17.27
W_{TE} (W)	2.12	2.5	3.3
System H_2 conversion efficiency	0.907	0.83	0.71
η_{system}	0.464	0.464	0.448
Combustor air flow outlet temperature (K)	840	850	870
Power required for balance of plant (W)	2.36	2.06	1.26

In performing preliminary studies on the capacity of a TE integrated SOFC system to generate power in order to provide the power required for balancing the plant, the amount of power required from the plant is assumed to be about 0.1 of the total amount fuel or heat input to the system, in this case into SOFC. According to the above simulations, the amount of fuel's energy input to the system calculated to be 45.6 W which is constant for all the three cases. Thus, the power requirement to balance the plant for these set of operating conditions listed above, is about 4.5 W. Considering the amount of power generated by TE at each case, the amount of power

required to balance the plant at SOFC's steady state condition is 4.5 W minus W_{TE}, which is given in the above table.

The additional results gained from steady state simulations of these three cell voltage case studies are summarized in table 2-5. At the steady state condition SOFC has already achieved its optimal operating condition with appropriate amount of current production. However, another important goal of this research is to study the system performance under the start up condition and when the SOFC has not reached its ideal operating temperature.

Further, the system model was also tested with zero fuel conversion along the fuel cell and the combustor. It should be noted that since there is no fuel conversion along the SOFC channel, defining an operating cell voltage does not have an influence on system's operation since there is no reaction anywhere along the system and thus the start-up case study was only performed for V_{cell} of 0.75 V. Thus, this simulation would only provide system condition during SOFC star-up period when the fuel cell has not reached its optimal temperature and system produces very little power. The results gained from this study are provided below in table 2-6.

Table 2-6: TE integrated SOFC steady state system performance at start-up

W_{SOFC} (W)	0.002
W_{TE} (W)	0.016
H_2 conversion	0.0
η_{system}	$3.91*10^{-4}$
Fuel Heat input (W)	45.60
Power required for balance of plant (W)	4.54
Combustor air flow outlet temperature (K)	370

According to the results presented above, it can be seen that during start up condition of the system, the TE would need to generate about 5 W in order to provide enough power to balance the plant. Also, the combustor's air flow outlet temperature during start-up is at 370 K. Thus, in order for the combustor waste heat recovery component to serve its purpose, this temperature must be increased close to SOFC operating temperature of 800 K.

2.4 Discussion of results

In order to gain a better understanding of the affect of TE module implementation into

SOFC system, a comparative study of the system performance is necessary to be performed. Figures 2-10 to 2-12 represent the SOFC current density along the length of the SOFC tube at three different operating cell voltages where the blue data represent the TE integrated SOFC system and the red data represent the original SOFC system. According to the results provided, the TE integration into the anode exhaust of the SOFC combustor component has caused the current density generated by the fuel cell to decrease. At 0.7V cell voltage condition, the current density of the fuel cell has decreased about 0.5 to 1A/cm^2. On the other hand the rate of current density drop occur smoother in the system with integrated TE.

The H_2 conversion efficiency of both original system and the TE integrated system at different cell voltages is plotted and compared bellow in Figure 2-13. As it can be seen, the thermoelectric integrated system consists of higher H_2 conversion efficiency percentage than the original system. Both systems have the highest H_2

conversion efficiency with respect to other operating cell voltages, where the TE integrated system has achieved 90% H_2 conversion efficiency. In general, implementing TE for purpose of waste heat recovery through preheating the air has increased the H_2 conversion efficiency of the system about 15 to 20% in the cell voltage range of 0.7 to 0.8 V. This is due to the fact that the preheated air, crossing the combustor, results in heating up the fuel cell at a faster rate and thus the amount of fuel provided to the system will be more fully consumed than before where the fuel cell needed more fuel in order to reach the ideal condition.

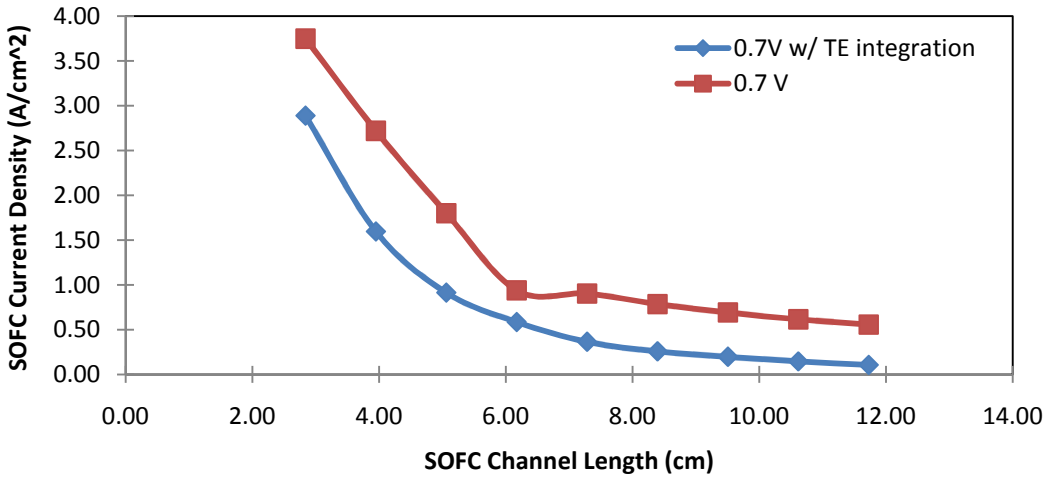

Figure 2-10: SOFC current density along the length of the length of SOFC tube at V_{cell} = 0.7V

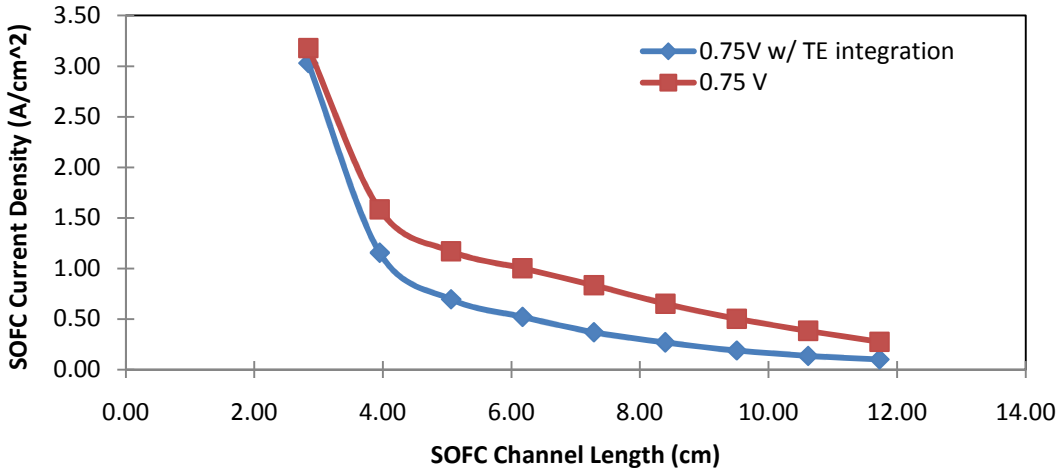

Figure 2-2 SOFC current density along the length of the length of SOFC tube at V_{cell} = 0.75V

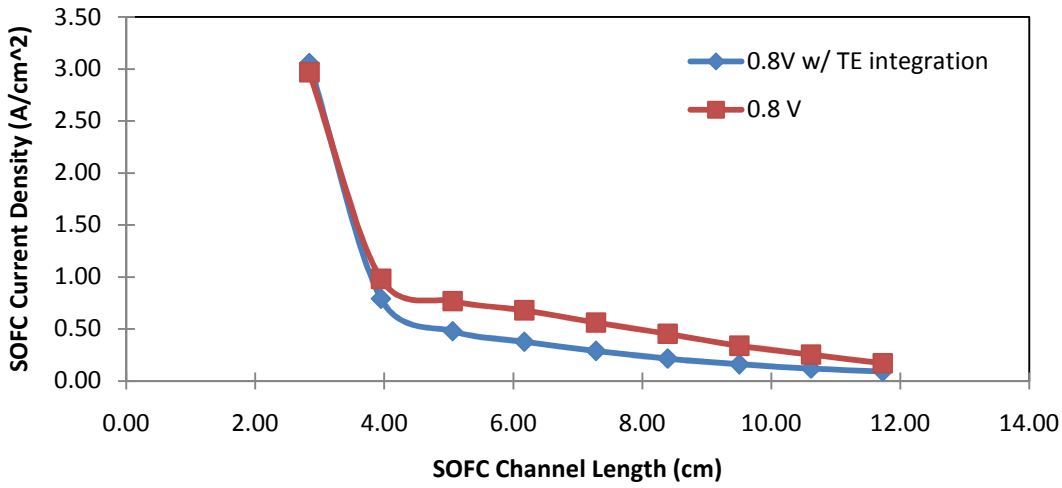

Figure 2-3 SOFC current density along the length of the length of SOFC tube at V_{cell} = 0.8V

Another important result driven by this model is the impact of TE module integration on the overall efficiency of the system. Figure 2-14 represents the comparative plot of original system efficiency versus the TE integrated efficiency at three cell voltage values. At cell voltage of 0.7V, the system efficiency with the TE integration has improved from 36 to 46% , at 0.75V from 33 to 46% and at 0.8 V

from 26% to 44%. It should be noted that the system efficiency is calculated as the ratio of the sum of the power generated from SOFC and TE over the amount of heat inputted into the system and the amount of power consumed by other equipments through a real SOFC power system is not provided.

The results presented in figure 2-2 and 2-3 show a drop of current within the SOFC and thus a net power loss through the fuel cell due to TE module integration. The 0.75 V case has a loss in an average current density production of 1 $A.cm^2$ and the 0.7 V case an average loss of 0.8 $A.cm^2$. In terms of net power, the operating cell voltage of 0.7 V experiences an average power loss of about 2.15 W from the fuel cell which it is regained through TE power production of 2.12 W. In case of 0.75 V cell operating voltage, the fuel cell losses a net power production of 2.9 W which some of it is recovered through 2.5 W of power generated by TE module. According to these results, it can be concluded that during steady state operating condition of the TE/SOFC system the module integration only increases the total efficiency of the system which assists in improving system's reliability and performance in the long run but does not assist in generating additional power for the system with the defined base line condition given above.

Comparing the numerical results achieved from these simulations with the original system performance, it can be concluded that the TE module integration improves the overall performance of the system through increasing its fuel consumption and thus producing a cleaner system exhaust as well as producing more power through TE which in result would cause the overall efficiency of the system to increase.

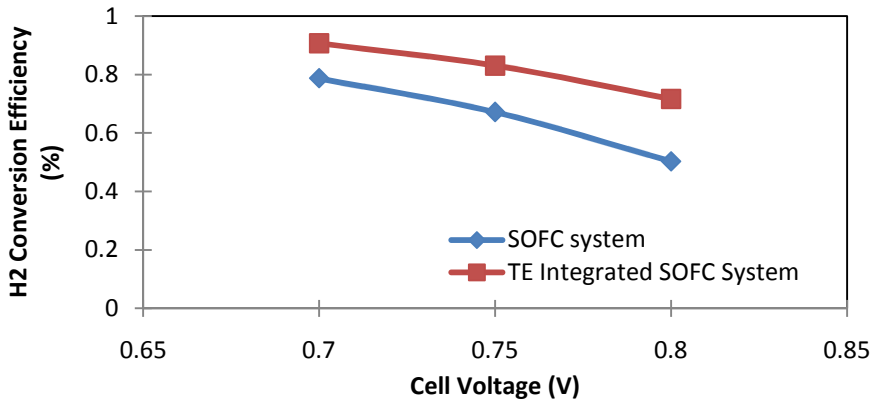

Figure 2-13: H2 conversion efficiency of the system at different cell voltages of 0.7, 0.75 and 0.8V

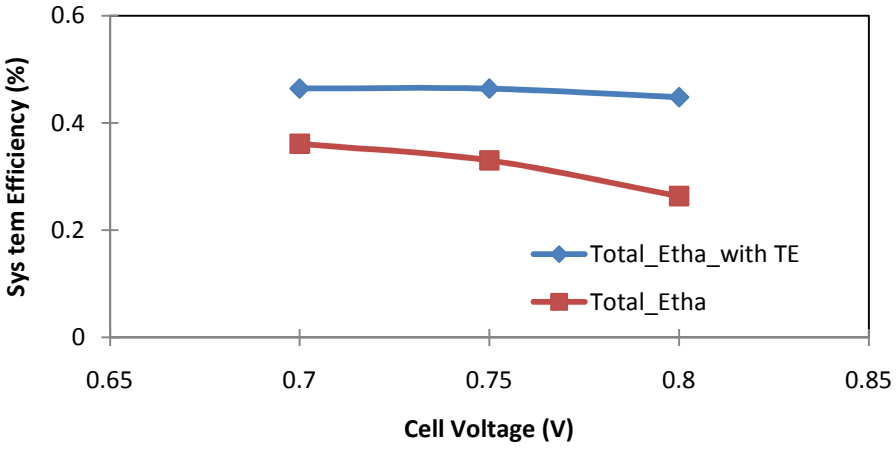

Figure 2-4: Overall system efficiency of original system versus TE integrated system at V_{cell} = 0.7, 0.75 and 0.8V

According to Maxey et al. the overall efficiency of a SOFC power system including the other relevant equipments is about 20-30%, where in the case of TE integration study and including the possible power consumption unit into system performance calculations, this number can be increased by 5-6% as it was expected in the motivation part of this study.

According to the results presented in Figure 2-13 and 2-14, it is shown that that during fuel cell's start up condition, the power generation through fuel cell channel and the TE module is very low. It can be observed that the system is very inefficient during this period. The overall system efficiency of the system was evaluated to be 0.0039 %. The simulations also resulted in SOFC temperature range of 400K which is well below its optimal operating conditions. Due to zero fuel conversion along the combustor, there is no heat transfer towards the air and thus one can evaluate the necessary amount of heat needed to be provided to the air in order to rise the fuel cell's temperature to its optimum condition. In this case, it is observed that the incoming air flow towards the cathode needs to be above at least 700K or higher, which is higher than the SOFC temperature, in order to provide preheating to the cell.

Most importantly, the steady state SOFC/TE system study shows that the TE module, with its respective geometrical structure defined in this model, can provide about 50 to 60 % of the required power for balancing the plant. As a matter of fact, providing a more precise analysis focusing on optimizing the heat transfer condition and studying other influential parameters on TE power generation can provide better solutions for the start-up condition of the SOFC system.

3 Integrated TE/Catalytic Combustor Model Development

3.1 Introduction

The previous chapter provides a general simplified mathematical study of the overall SOFC power system with the integrated TE into its catalytic combustor

channel. This chapter presents a more detailed numerical component model of a TE-integrated catalytic combustor for the fuel cell exhaust. The detailed model provides a more realistic evaluation of the thermochemical processes occurring in the TE integrated catalytic combustor and provides an assessment of how combustor/heat exchanger geometry impacts waste heat recovery, combustor operation, and TE power generation.

The model is developed in the Matlab environment using the Cantera toolbox for the thermochemistry and transport property calculations with detailed microkinetics based on the Pt-based C-H-O surface chemistry of Mhadeshwar & Vlachos in the catalyst layer. This chapter presents the numerical approach for the model in more detail. In addition, details on the combustor configuration and geometry will be discussed. Material properties used in modeling of the TE integrated catalytic combustor system in preparation for presenting model results in the following chapter.

3.2 Modeling thermoelectrics

Unlike the full cell system model presented in chapter 2, the transient model presented here calculates the internal temperature of the thermoelectric couples. The TE module has n-type and p-type elements connected at each end through thin conductor contacts creating TE couples electrically connected in series along the length of the exhaust/air channel as illustrated in Figure 3.1. In addition, the evolution with time of TE module temperatures and voltages are integrated by including the energy storage term in the governing equations for the TE modules.

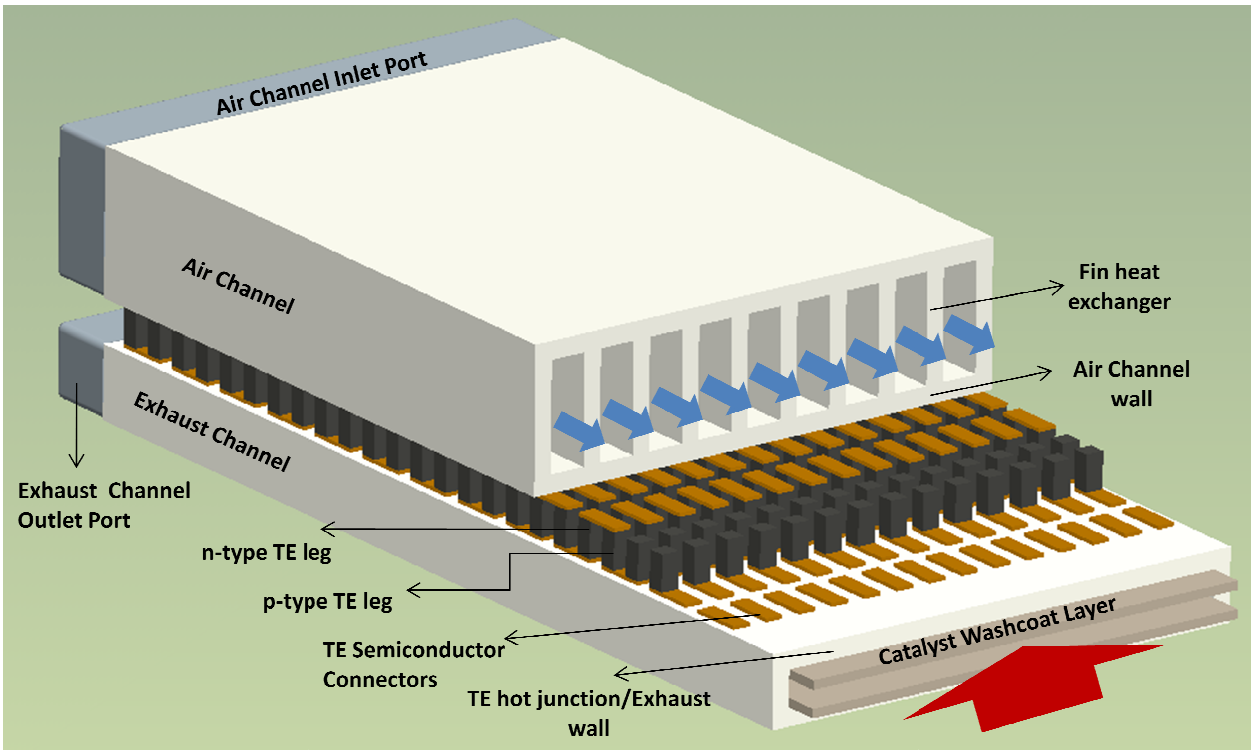

Figure 3-1: TE integrated Combustion waste heat recovery cut section configuration

The energy balance in the TE's includes the heat transferred through TE in the y direction from the catalytic channel walls to the cooling air passage walls. In the current model, the combustor is modeled with the washcoat and TE's on both side of the combustor channel. The TE temperature, T_{TE}, is required to capture the transient evolution of the TE modules during a combustor start-up process. The heat transfer into and out of the TE modules is given by the following equations.

(Eq. 3-1)

(Eq. 3-2)

where K_{TE} represents conductance of the TE couples as given by equation 3-3 where $k_{T,TE}$ is TE's thermal conductivity and $A_{TE,cond}$ is the conductance area of one TE couple.

$$K_{TE,j} = k_{T,TE,j}\, A_{TE,cond} 2/y_{TE}$$

(Eq. 3-3)

The number of TE couples per discretization $n_{TE,j}$ is given by equation 3-4.

$$n_{TE,j} = \frac{2n_{TE,z}\ dx_j}{x_{TE,couple}}$$

(Eq. 3-4)

In setting up the TE governing equations in this model, the set of TE couples at each cell division are assumed as one electric circuit where each couple are electrically connected in series. Thus, the total voltage of entire module across the combustor channel is the sum of individual voltages $V_{TE,j}$ generated by couples in each discretization based upon equation 3.7.

$$V_{TEj} = \alpha_{TE,j}\,(T_{comb,wall,j} - T_{air,wall,j})\, n_{TE,j}$$

(Eq. 3-7)

Since TE couples are connected in series, the current I_{TE} is constant across the module and total $R_{TE,j}$ for the couples in each discretization will be added up as presented in equation. 3.8, resulting in total voltage generated by TE module. The local resistance follows equation 3-8 where $\rho_{TE,j}$ is TE resistivity along the length of elements (Ω·m), $R_{TE,contact}$ is the contact resistance at 4 contacting areas between the

semiconductor connectors and TE elements per each couple, which is set equal to $5.08 \cdot 10^{-4}\ \Omega$ for PbTe TE material in contact with Cupper connectors [7].

$$R_{TE,j} = \left(2\frac{\rho_{TE,j}\ y_{TE}}{A_{TE,cond}} + R_{TE,contact}\right) n_{TE,j}$$

(Eq. 3-8)

The rate of resistive heat generation within the TE elements $\dot{Q}_{TE,elec}$ and the electric power produced by them $\dot{W}_{TE,elec}$ is also calculated for each discretized cell by equations 3-9 and 3-10.

$$\dot{Q}_{TE,elec,j} = 2\ n_{TE,j}\ I_{TE}^2 R_{TE,j}$$

(Eq. 3-9)

$$\dot{W}_{TE,elec,j} = 2\ n_{TE,j}\ I_{TE}\alpha_{TE,j}(T_{comb,wall,j} - T_{air,wall,j})$$

(Eq. 3-10)

Since the TE module is modeled with all of the couples wired in series, the current I_{TE} is constant through all of the couples.according to equation 3-11, where R_{load} is the specified load resistance connected to the TE module.

$$I_{TE} = \frac{\sum_{j=1}^{n} V_{TE,j}}{\sum_{j=1}^{n}(R_{TE,j} + R_{load})}$$

(Eq. 3-11)

The transient energy conservation equation for the TE couple is then solved through an integration process from t = 0 to t= t_{final} solving for TE's temperature and as a result, voltage and current generated by this module, equation 3-12.

$$\frac{dT_{TE,j}}{dt} = \frac{\dot{Q}_{y,TE,comb,j} - \dot{Q}_{y,TE,air,j} + \dot{Q}_{TE,elec,j} - \dot{W}_{TE,elec,j}}{m_{TE} C_{P,TE,j}}$$

(Eq. 3-12)

$m_{TE,j}$ is the product of the TE material density and volume of all the couples in discretization *j*, and $C_{p,TE,j}$ is the specific heat capacity of TE material. The model assumes that there is no convective heat exchange by the gases around the TE elements and also that radiation heat transfer between the hot and cold walls on each side of the TE couples in negligibly small .

3.3 Modeling catalytic combustor and cooling air channels

The transient catalytic combustor model also includes a porous catalyst layer model integrated with the combustor channel flow and a fin heat transfer model with the air cooling channel flow. The transient model incorporates the solid phase heat transfer into the solid matrices of the walls and the TE couples and thus provides a means for assessing the time scales for heating up combustor during a start-up condition.

The combustor channel consists of the exhaust flow, porous catalytic washcoat and exhaust wall. Figure 3-2 represents a structural schematic of TE-integrated catalytic combustor. Inlets and outlet ports are shown without any blockages to view the internal structure of both the catalytic combustor channel with its porous catalytic washcoat on each wall and the cooling air-passage with its fins. The integrated component is designed such that air passages and combustor channel

passages can be stacked in order to minimize heat loss to an external ambient. Fins in the air cooling passage are modeled to span the entire flow channel as illustrated in Figure 3.1.

The combustor exhaust channel consists of three sub-components of exhaust flow, porous catalytic washcoat and exhaust wall. The inlet flow species mass fractions ($Y_{\mathrm{k,com,port}}$), temperature ($T_{\mathrm{comb,f,port}}$), pressure ($P_{\mathrm{comb,f,port}}$), and mass flow rate ($\dot{m}_{\mathrm{comb},f,port}$) are specified for the combustor channel flow inlet port and in the current study these values are held constant during the transient integration. The combustor flow conditions are determined by mixing the oxidizer flow from the cathode/air supply and the anode/fuel supply and the system operation can be tested for fuel/air flows relative to the fuel cell's start-up condition or the for steady state conditions.

Inlet and outlet ports for the combustor are in contact with the surrounding as well as the system's inner walls and depending on the port's temperature the heat transfer is modeled to be conducted from surrounding (ambient condition) to the ports or vice versa and also from the ports to the neighboring walls.

Modeling of the porous catalytic washcoat layer follows a previous reference [17]. The porous washcoat layer is modeled with uniform porosity, $\varepsilon_{\mathrm{wash}}$, and thickness, δ_{wash} , assuming an inert Al_2O_3 support decorated with active Pt nanoparticle catalysts. The Pt catalyst loading gives a specified active catalyst surface area to washcoat volume ratio, a_{cat}, with a bounding wall on one side and open flow on the other side. The properties of the wachcoat catalytic layer are presented in the table below.

Table 3-1: Catalytic washcoat layer properties

$\varepsilon_{\text{wash}}$	0.5
a_{cat} ($cm_2 \cdot cm^{-3}$)	140200
Catalyst loading ($kg \cdot m^{-3}$ of washcoat)	10

Performance of the catalytic washcoat layer and the channel flow are highly influenced by the detailed surface chemistry mechanism. A Pt-H_2-CO-O_2 microkinetic surface model developed and validated against numerous experiments provided a basis for simulating catalytic combustion of both pure H_2 fuels and syngas H_2/CO fuels both for transient start-up and for steady-state conditions associated with burning anode exhaust from a syngas-fueled fuel cell [20].

Conservation of the gas phase mass and species fractions in the porous washcoat layer is solved in conjunction with the microkinetic surface chemistry model. Equation 3-13 provides the general mass conservation of all species combined.

$$V_{gas,j}\frac{d\rho_{gas,j}}{dt} = \dot{m}_{wash,j-1} - \dot{m}_{\text{wash},j} + \dot{m}_{y,j} + a_{\text{cat}}\sum_{k\_gas}\left(W_{k\_gas}\dot{s}_{k_{gas},j}\right)$$
(Eq. 3-13)

$\dot{m}_{y,j}$ is the gas species mass flowrate into the washoat, $\dot{s}_{k_{gas},j}$ is the molar production rate of gas species per unit surface area of the catalyst, and $W_{k-\text{gas}}$ is the molecular weight of the gas species. Axial mass flux along the length of the washcoat is negligibly small because of the thinness of the porous layer.

Assuming that the ideal gas law applies and the dimensionl equation 3.13 can be rewritten as follows where $Y_{k,gas}$ is the species mass fraction in the washcoat.

$$-V_{gas,j}\rho_{gas,j}\left(\frac{1}{T_j}\frac{dT_j}{dt}+\sum_{k\_gas}\frac{W_{gas}}{W_{k\_gas}}\frac{dY_{k,gas,j}}{dt}\right)=$$

$$\dot{m}_{y,j}+V_{gas,j}a_{\text{cat,j}}\sum_{k\_gas}\left(W_{k\_gas}\dot{s}_{k_{gas},j}\right)$$

(Eq. 3-14)

With the same assumptions for the total mass conservation equation, the gas species mass convervation equations can be written as follows are goverened by the following conservation equation 3-15:

$$V_{gas,j}\rho_{gas,j}\frac{dY_{k,gas,j}}{dt}=\dot{m}_{y,j}\left(Y_{k_{gas_{int}},j}-Y_{k,gas,j}\right)+A_{y,flow,j}\rho_{gas,j}YV_{y,k_{gas},j}+$$
$$V_{gas,j}a_{\text{cat,j}}W_{k\_gas}\dot{s}_{k_{gas},j}-Y_{k,gas,j}V_{gas,j}a_{\text{cat,j}}\sum_{k\_gas}\left(W_{k\_gas}\dot{s}_{k_{gas},j}\right)$$

(Eq. 3-15)

$YV_{y,k_{gas},j}$ represents the mass-weighted diffusion velocity of species k and its calculated through equation 3-15 where D_{km} represents the mixture-averaged diffusion coefficients and Sh_{k} is the species Sherwood number.

$$YV_{y,k_{gas},j}=\frac{D_{km,j}\,Sh_{k,j}}{d_{hyd,comb}W_{m,int,,j}}\left(W_{m,f,j}Y_{k,f}-W_{m,gas,j}\,Y_{k,gas,j}\right)$$

(Eq. 3-16)

where W_m is the average molar mass for a given flow condition.

JANAF standard tables from the Cantera data-based are used to calculate the gas-phase and surface-species thermodynamic properties with respect to temperature. The washcoat/exhaust flow involves significant dilution of reactants as a matter of fact, D_{km} is used for diffusion into and through the porous washcoat.

Surface species conservation for the active Pt catalyst in the washcoat is defined below where Γ_{surf} represents the surface site density of the catalyst and θ_{k_surf} is the surface site fraction of surface species k. The surface reaction at the catalytic washcoat surface is done by integration of reaction rates of species at the surface.

$$\Gamma_{surf} \frac{d\theta_{k\_surf}}{dt} = \dot{s}_{k\_surf} \qquad \text{(Eq. 3-17)}$$

The temperature of the combustor exhaust wall covered with washcoat is solved with the energy conservation equation of the porous media with the simplifying assumption that the catalyst, solid support, and gas-phase in the thin washcoat are in thermal equilibrium with each other in the transverse *y*-direction. Thus, in the washcoat and combustor wall only vary along the axial flow *x*-direction. The conduction between the washcoat and the supporting wall in the combustor is expected to keep the supporting wall and washcoat at the same temperature and thus the wall. $C_{P,wall}$ and $C_{P,wash}$ for the solid phases are varied with temperature and taken from properties for 99% pure Al_2O_3 . Al_2O_3 is also used for the combustor walls because an electronically insulating surface is needed on which to mount the TE couples. With novel Al_2O_3 processing as developed by Coorstek [23] and others, such detailed ceramic support structures are becoming available for catalytic reactors [24].

The energy conservation equation calculates how the total energy $E_{tot,wash}$ in the mult-phase computational cell changes with time. By making some assumptions regarding the various energy terms the washcoat internal energy, u_{l_solid}, can be

replaced with $C_{p,l\_solid}\, T_{comb,wall}$. The change of temperature with respect to time is as follow:

$$\frac{d(E_{tot,j})}{dt} = V_{gas}\frac{d\rho_{gas}}{dt}\sum_{k_{gas}}\left(u_{k_{gas},\mathrm{j}}Y_{k_{gas},\mathrm{j}}\right) + V_{gas}\rho_{gas}\sum_{k_{gas}}\left(u_{k_{gas},\mathrm{j}}\frac{dY_{k_{gas},\mathrm{j}}}{dt}\right) +$$

$$V_{gas}\rho_{gas}\sum_{k_{gas}}\left(C_{V,k_{gas},\mathrm{j}}Y_{k_{gas},\mathrm{j}}\right)\frac{dT_{wall,j}}{dt} + \sum_{l_{solid}}\left(V_{l_{solid}}\rho_{l_{solid}}C_{P,l_{solid}}\right)\frac{dT_{wall,j}}{dt} +$$

$$a_{\mathrm{cat}}\Gamma_{\mathrm{cat}}\sum_{k_{surf}}\left(\bar{u}_{k_{surf},\mathrm{j}}\frac{d\theta_{l_{surf},k_{surf},\mathrm{j}}}{dt}\right) + a_{\mathrm{cat}}\Gamma_{\mathrm{cat}}\sum_{k_{surf}}\left(\bar{C}_{P,k_{surf},\mathrm{j}}\theta_{l_{surf},k_{surf},\mathrm{j}}\right)\frac{dT_{wall,j}}{dt}$$

(Eq. 3-19)

The sum of the energy flux terms going in and out of the washcoat/exhaust wall is then defined as bellow which is then set equal to the right hand side of the above equation.

$$\frac{d(E_{tot,j})}{dt} = \dot{m}_{y,j}h_{k_{gas_{int}},j} + A_{y,flow}\rho_{gas}\sum_{k\_gas}\left(h_{k_{gas_{int}},j}YV_{y,k_{gas},j}\right) +$$

$$A_{y,flow}h_{T,flow}\left(T_{flow,j} - T_{wall,j}\right) + A_{x,cond}\frac{k_{T,x,eff}}{\mathrm{dx}}\left(T_{wall,j-1} - T_{wall,j}\right) -$$

$$A_{x,cond}\frac{k_{T,x,eff}}{\mathrm{dx}}\left(T_{\mathrm{wall,j}} - T_{wall,j+1}\right) - \dot{q}_{y,TE,comb,j}$$

(Eq. 3-20)

Equating both sides of the equation would result in equation 3-22 where the effective mass of the combustor wall is defined as sum of the gas phase mass in the washcoat, the mass of the bulk phase washcoat, mass of the surface site fraction species as well as the mass of the combutor wall support.

$$m_{Cp,eff,comb,wash} = V_{gas}\rho_{gas}\sum_{k_{gas}}\left(C_{V,k_{gas}}Y_{k_{gas}}\right) + \sum_{l_{solid}}\left(V_{l_{solid}}\rho_{l_{solid}}C_{P,l_{solid}}\right) +$$

$$a_{\mathrm{cat}}\Gamma_{\mathrm{cat}}\sum_{k_{surf}}\left(\bar{C}_{P,k_{surf}}\theta_{k_{surf}}\right) + \mathrm{m_{comb,wall}C_{V,comb,wall}}$$

(Eq. 3-21)

$$\left[m_{Cp,eff,comb,wash}\right]\frac{dT_{wall,j}}{dt} =$$

$$\dot{m}_{y,j}\left(h_{gas_{int},j} - u_{gas,j}\right) + A_{y,flow}\rho_{gas}\sum_{k\_gas}\left(h_{k_{gas_{int}},j}\, YV_{y,k_{gas},j}\right) +$$

$$A_{y,flow}h_{T,flow}\left(T_{flow,j} - T_{wall,j}\right) + A_{x,cond}\frac{k_{T,x,eff}}{\mathrm{dx_{avg,j-1}}}\left(T_{wall,j-1} - T_{wall,j}\right) -$$

$$A_{x,cond}\frac{k_{T,x,eff}}{\mathrm{dx_{avg,j-1}}}\left(T_{\mathrm{wall,j}} - T_{wall,j+1}\right) - \dot{q}_{y,TE,comb,j} -$$

$$u_{gas}a_{\mathrm{cat}}\sum_{k\_gas}\left(W_{k\_gas}\dot{s}_{l\_surf,k\_gas}\right) - a_{\mathrm{cat}}\sum_{k_{surf}}\left(\bar{u}_{k_{surf},\mathrm{j}}\dot{s}_{k_{gas},j}\right) -$$

$$V_{gas}\rho_{gas}\sum_{k_{gas}}\left(u_{k_{gas},\mathrm{j}}\frac{dY_{k_{gas},\mathrm{j}}}{dt}\right)$$

(Eq. 3-22)

The mass, species and energy conservation equations are also establish for the combustor channel flow. The change of mass flow rate at jth cell is found through the following linear differential conservation equation, 3-21. At the first cell division of the exhaust channel $\dot{m}_{comb,f,j-1}$ is set equal to the exhaust channel inlet port mass flow rate which is a known value.

$$\frac{dm_{flow,j}}{dt} = \dot{m}_{flow,j-1} - \dot{m}_{flow,j} - \dot{m}_{y,j}$$

(Eq. 3-23)

The combustor exhaust flow species mass fraction ($Y_{\mathrm{k,comb}}$) composition is then solved through integrating the following species conservation equation at the j^{th} cell division.

$$m_{comb}\ \frac{dY_{k,comb,j}}{dt} = \dot{m}_{x,j-1}\left(Y_{k,comb,j-1} - Y_{k,comb,j}\right) - \dot{m}_{y,j}\left(Y_{k_{gas_{int}},j} - Y_{k,gas,j}\right) -$$

$$A_{wash,x}\rho_{gas,j}YV_{y,k_{gas},j} \quad \text{(Eq. 3-24)}$$

For the non-adiabatic flow, the combustor flow temperature (T_{flow}) is then found by including the energy conservation equation the discretized channel flow of the combustor exhaust.

$$m_{flow}\, C_{V,flow} \frac{dT_{flow,j}}{dt} = \dot{m}_{flow,j-1}\left(h_{flow,j-1} - u_{flow,j}\right) - \dot{m}_{flow}\left(h_{flow,j} - u_{flow,j}\right) - \dot{m}_{y,j}\left(h_{gas_{int},j} - u_{flow,j}\right) - A_{y,flow} h_{T,flow}\left(T_{flow,j} - T_{wall,j}\right) - A_{y,flow}\rho_{gas} \sum_{\text{k\_gas}}\left(YV_{y,k_{gas,j}} h_{k_{gas},int,j}\right) - m_{flow,j} \sum_{\text{k\_flow}}\left(u_{\text{k,flow,j}} \dot{Y}_{\text{k,flow,j}}\right) \quad \text{(Eq. 3-25)}$$

The air cooling channel includes fin extended surfaces for heat transfer enhancement across the flow path. The fins stretched across the entire channel height of the flow and thus extended to both walls of the air channel as indicated in Figure 3-1. This parallel fin configuration with adiabatic tips is presented in Fundamental of Heat and Mass transfer by Incorpera et al. [25]. For this configuration, the effective height of the fin equals half of the original height, the fin properties and heat transfer are modeled as following equations. m_{fin} represents fin's m number which is the square root of the ratio of convective heat transfer coefficient ($h_{T,air}$) over the conductive heat transfer coefficient ($K_{T,wall}$). A_{fin} is the total fin area in contact with the base wall and the total available area for heat conduction through the fins, η_{fin} represents the fin effectiveness.

$$m_{fin} = \sqrt{\frac{2\, dx\, h_{T,air}}{K_{T,wall} z_{fin} dx}} \quad \text{(Eq. 3-26)}$$

$$A_{fin} = n_{fin,z}\left(z_{fin} + \left(y_{fin,eff} - z_{fin}\right)\right) dx \quad \text{(Eq. 3-27)}$$

$$A_{surf,fin} = 2\, y_{fin,eff}\, dx \qquad \text{(Eq. 3-28)}$$

$$\eta_{fin} = \tanh\left(\frac{m_{fin} y_{fin,eff}}{m_{fin} y_{fin,eff}}\right) \qquad \text{(Eq. 3-29)}$$

Air channel is modeled as a bulk piece including the fin extended surfaces as a whole structure. Based on the above fin properties, the air channel wall temperature, including fins, and air flow temperature can then be solved for by setting up energy conservation equation for a discretized wall and air flow cell. The heat is also modeled to be transferred along the length of the fins parallel to the direction of the air flow.

$$m_{fin\_wall}\, C_{V,fin\_wall} \frac{dT_{fin_{wall},j}}{dt} = A_{cross,fin} K_{T,fin_{wall}} \left(T_{fin_{wall},j-1} - T_{fin_{wall},j}\right) - A_{cross,fin} K_{T,fin_{wall}} \left(T_{fin_{wall},j} - T_{fin_{wall},j+1}\right) + \dot{q}_{y,TE,air,j} - h_{T,air}\left(A_{cond,fin,j} - n_{fin}\, A_{surf,fin}(1-\eta_{fin})\right)\left(T_{fin_{wall},j} - T_{air.j}\right)$$

(Eq. 3-30)

The exchange of heat between fin surfaces and the air flow causes the air flow temperature to rise as it flows down stream of the channel. The change of air flow temperature at a sliced division can be solved through the following energy conservation equation, equation 3-31.

$$m_{flow}\, C_{V,flow} \frac{dT_{flow}}{dt} = h_{T,air}\left(A_{cond,fin,j} - n_{fin}\, A_{surf,fin}\left(1-\eta_{fin}\right)\right)\left(T_{fin_{wall}} - T_{air}\right) - m_{flow} \sum_{\text{k\_flow}} \left(u_{\text{k,flow}} \dot{Y}_{\text{k,flow}}\right) + \dot{m}_{flow,j-1}\left(h_{flow,j-1} - u_{flow}\right) - \dot{m}_{flow}\left(h_{flow} - u_{flow}\right)$$

(Eq. 3-31)

Since there is no chemical reaction between the air flow and the fin walls, the species mass fraction and mass of the air flow is conserved according to the following equations 3-32 and 3-33.

$$\frac{\partial m_{air}}{\partial t} = \dot{m}_{air,j-1} - \dot{m}_{air}$$

(Eq. 3-32)

$$\frac{\partial Y_{k,air}}{\partial t} = \dot{m}_{air,j-1}(Y_{k,air,j-1} - Y_{k,air})$$

(Eq. 3-33)

The change of pressure throughout the length of the channel is calculated by the algebraic equation 3-35 based on the assumption that pressure equilibrates instantaneously with respect to the thermal and species transients.

$$0 = P_{flow,j-1} - P_{flow} - 0.5 f_{flow} \rho_{flow} v_{flow}^2 dx/d_{hydr}$$

(Eq. 3-34)

f_{flow} is the air flow's friction factor based on Reynold's number, v_{flow} represents the velocity of the flow times the length of the discretization over the hydraulic diameter of the channel. The same approach is also used to calculate the pressure change within the combustor exhaust channel.

All the presented governing equation are solved by dividing the length of the combustor system into equal discretized cells along the axial direction of the flow, first cell begins after the exhaust inlet port and the inlet conditions are set equal to the ports conditions. A set of linear and non-linear differential conservation equations are set for the exhaust channel flow and the porous catalytic washcoat species mass

fraction, temperature, mass flow rate and pressure at j^{th} cell division. The neighboring cell discretizations (j-1 and j+1) and the porous catalytic washcoat layer j^{th} solution properties are linked together through mass and heat transfer. Due to the chemical reactions at the channel flow/washcoat interface and the surface species adsorption and desorption, the overall mass and species mass fraction of the exhaust flow at the j^{th} cell is then determined based on the surface reactions.

3.4 Model configuration

Figure 3-1 represents the compact TE integrated combustor waste heat recovery configuration used in for modeling of the combustor waste heat recovery system. The structure of the combustor channel is a rectangular exhaust channel with one inlet port and an outlet port.

The combustor configuration used in the numerical modeling of this section is a double sided air channel combustor. In other words, the combustor system contains one main exhaust channel which is surrounded by two TE modules which each side of the exhaust wall is set as the hot junction TE wall and the two air cooling channels across the TE couples are set at the cold junction wall support of the TE. The side view of this system is shown in Figure 3-7.

3.4.1 Geometrical design

As it was discussed in the previous section, the overall combustor structure includes a rectangular configuration with flat plate shape TE housing in between exhaust and air channel. The geometrical parameters of this model are chosen to be

close to that of the TE integrated SOFC system in chapter 2. As it was mentioned earlier in this chapter one of the main key differences between this model and the TE integrated SOFC model is the addition of the TE physical and thermodynamic properties in modeling of the combustor system. As a matter of fact, the axial divisions applied along the flow path of channels would also consist of TE couples at each discretdiscretized cell. The total length (x) and the width (z) of both exhaust and air channels are set based on the number of TE couples along the respective direction. The TE geometry is laid out as shown in the following Figure. The lengths of n-type and p-type element sides are, TE length and width are equal to each other equal 1 mm, the height of TE (y_TE) is 2 mm and the spacing length between each element and the neighboring couple (x_space) is also 1 mm. In addition, height of contact is set equal to 0.2 mm based on measurements performed on a real module. The length of a couple, in either z or x direction, would be equal to 2*(x_TE + x_space) = 4 mm.

The base line case geometry of this model contains 20 couples in the x direction and 7 couples in the z direction. The total length and width of the exhaust channel is shown below Figure 3-5 and the respective values given in table 3-2. The exhaust channel wall surrounding has a thickness of 1 mm which makes the width of the flow and the height of flow equal to 26 and 1.9 mm respectively. The channels hydraulic diameter is estimated as following:

Table 3-2: Exhaust channel geometry parameters

Exhaust width (mm)	28
Exhaust length (mm)	80
Exhaust height (mm)	4
Channel hydraulic diameter (mm)	3.5
Wall_thickness(mm)	1
Washcoat_thickness(mm)	0.05

Since the total length of the combustor system including the air and exhaust channel are based on the number of TE couples, then in order for the solver to accurately capture the total thermal heat transfer and the chemical processes effect along the length of the channels and normal to the flow direction, the length of each discretized cell is also set based on the number of TE couples. For the baseline case the length of the discretization along the channel flow direction is equal to length of one TE couple or in other words there is only one TE couple in the x direction and 7 TE couples in z direction. The inlet and outlet ports of the channels are modeled in such way that the port wall thickness covers the attaching wall areas of the channel and the opening volume of the port contains the amount of flow entering the system. The wall of the ports is also set fixed to be 1mm.

The air channel geometrical configuration is presented in Figure 3-6. The detailed dimensions in Table 3-3 are chosen such that the combustor system can later be added to a small 30 W fuel cell system.

Table 3-3: Air channel geometry parameters

Air flow height (mm)	6
Air flow width (mm)	26
Channel hydraulic diameter (mm)	3
Fin thickness (mm)	3
Fin spacing (mm)	2
Fin effective height (mm)	3

The fins are extended all the way to the length of the channel and number of fins in the z direction at the baseline condition is set to be 9 which can be changed by

changing the fin's spacing length or thickness. The fin effective height is also approximated as half the height of the channel's air flow.

3.4.2 Modeling heat transfer and boundary conditions

The heat and mass transfer properties of the combustor system is solved by defining conservation equations for specified region of individual sub-layers of the combustor which are then integrated simultaneously to evaluate the properties of each cub-layer at the specified point along the channel. Discretized divisions along the axial direction of the channel which in this model includes one main combustor exhaust flow, two porous catalytic washcoat layers and wall support on each side, two TE module and two air cooling channels. The only source of heat input into the system is provided through the combustion reaction of the exhaust channel flow with the catalytic washcoat layer and itself. In defining the overall mass and thermal energy transfer throughout the combustor channels and system's sub-layers, this model assumes an equal distribution of mass and energy at the combustor exhaust channel. As a matter of fact the conservation equations are applied to one side of the combustor channel and the overall system property such as temperature and mass of the double system is captured by multiplying these conservation equation terms by two, in order to mirror the property of both sides of the system. The sketched dashed line in the center of the combustor exhaust channel, Figure 1-4, is where the model's layer division is applied.

Although the heat and mass transfer governing equations applied to the exhaust combustor channel was described in detailed in section 3.2 however, a set of

boundary condition should also be defined for individual sectional components of the combustor system in order to close the set of non-linear differential equations. The combustor channel and air channel inlet ports's condition provides the channel's inlet conditions. So that the point of intersect between the outlet of the inlet port and the inlet of the channel flow is set at x=0. Thus the following boundary conditions are set; at x= 0, $T_{port,x=0} = T_{flow,x=j}$, $X_{k,port,x=0} = X_{k,flow,x=j}$, $P_{port,x=0} = P_{flow,x=j}$ and $\dot{m}_{port,x=0} = \dot{m}_{flow,x=j}$. Furthermore the port's inlet wall temperatures are set such that if port's wall temperature is higher than ambient temperature and heat is conducted from the surrounding to the wall and reversely if the outlet port's wall temperatures are higher than the surrounding then the heat from the walls would be conducted to the surrounding

$$\dot{Q}_{amb,in} = h_{T,amb} A_{port,wall} (T_{amb} - T_{port,wall})$$

(Eq. 3.35)

$$m_{\text{poet,wall}} \frac{dT_{\text{port,wall}}}{dt} = \dot{Q}_{amb,in} - k_{\text{T,port,wall}} A_{port,wall} (T_{port,wall} - T_{wall})$$

(Eq. 3.36)

Some assumptions have been made throughout the sub-layers of the combustor exhaust channel in order to further simplify the governing equations applied to each layer. Some of the assumptions made for the exhaust gas flow and catalytic washcoat interface include isobaric conditions in the washcoat, equilibration between the solid and gas phase temperatures in each washcoat cell and no radiative heat transfer within or from the washcoat. Figure 3-1 depicts the combustor exhaust channel layers at a fixed point where y = 0. The model assumes the washcoat/exhaust

channel layer as one bulk phase where the temperature across the length and height of the wall discretization remains uniform.

1. $\delta_{channel} < y < \delta_{channel} + \delta_{wash} + \delta_{wall}$: $\frac{\partial T}{\partial y} = 0$ (Refer to Figure 3-1)

2. at $y = \delta_{channel} + \delta_{wash} + \delta_{wall}$: $\frac{\partial Y_k}{\partial y} = 0$

3. At $y = \delta_{flow}$: $T_{wash,surf} = T_{gas,wash}$

Number 2 refers to fact that there is no species mass transfer between the washcoat and exhaust wall support interface, and the third boundary condition refers to the assumption that the washcoat gas species are assumed to be at the same temperature as the washcoat layer/ exhaust channel walls.

3.4.3 Material and fluids properties

The material used in the combustor system modeling can be divided into five categories: the exhaust channel structure, air channel structure, catalytic washcoat layer, exhaust and air ports and TE elements. The material used in modeling of the TE material is PbTe (Lead Telluride) thermoelectric which was also used in the modeling of the TE integrated SOFC system presented in chapter 2. The Seebeck coefficient and the resistivity of the thermoelectric material estimation with respect to temperature is the same as presented in section 2.2.2. Due to simplicity of the previous model, the thermal conductivity was considered to be constant however, in this model the thermal conductivity estimation of PbTe material with respect to temperature is performed using the fitted approximation presented in Figure 2-8. Since the heat transfer through the TE elements are also being modeled, other

properties of PbTe thermoelectric material is also considered which is provided in the table below [7].

Table 3-4: PbTe Thermal properties

Density (kg/m^3)	1.159
Specific heat capacity (J/kg.K)	155
Contact Resistivity (Ω.m^2)	2.54*10^{-10}

The material chosen for both the exhaust and air channel ports, the surrounding walls as well as the catalytic washcoat layer of the exhaust is Alumina (Al_2O_3). The material properties of Al_2O_3 grade 1-4 with respect to temperature are taken from NIST cryogenics database [26]. The density of the Al_2O_3 is 3825 Kg/m^3.

$$C_p\,(T) = -1679 + 431.66 \log (T)$$

(Eq. 3-39)

$$K_T\,(T) = 5.5 + 34.5\, e^{-0.0033(T-273.15)}$$

(Eq. 3-40)

This system model is modeled in such way that each sub-component of the system, for example air channel or exhaust channel walls, are treated as separate but yet connected components and their respective material property can be changed individually. For this matter, the model also contains the properties of other materials such as Copper and Stainless Steel-304 using the NIST data base as well as Bismuth Telluride thermoelectric properties. The air channel walls including the fins can then be modeled with Cu and the channel ports can be modeled using SS-304 and for a low temperature system operation condition, Bi_2Te_3 can be used as a low termperature TE material.

The combustor exhaust inlet of the model, as mentioned before, contains a mixture of anode and cathode exhaust and thus the fluid entering the combustor is a mix of moist H_2 composition from anode as the fuel with dried air from cathode as the oxidizer. The base line case of this system is modeled to have pure dried fuel input of $X_{H2} = 1$, mixed with dried cathode containing $X_{O2} = 0.2139$ and $X_{N2} = 0.27861$, where the amount of fuel to air ratio is controlled by defining equivalence ratio, Φ. An equivalence ratio of 0.5 was found suitable for the operation of the system. Thus, the amount of anode mass flow rate inlet to the system is estimated as following, where $\dot{m}_{cathode,in} = 7.86*10^{-5}$ (kg/s).

$$\dot{m}_{anode,in} = \dot{m}_{cathode,in}\Phi/(4.76 * W_{air}/W_{comb})$$

(Eq. 3-41)

The moist anode exhaust contains, H_2O, N_2 and H_2 species and the dried cathode exhaust only contains O_2 and N_2. In addition, the air flow entering the cooling air channel is also set separately. For this fluid, dried air with fixed species composition of $X_{O2} = 0.21$, $X_{N2} = 0.79$, inlet pressure of 1 bar and the ambient temperature of 303 K is used and the other thermal and physical properties are imported from Cantera database. Table below presents the air flow properties.

The same definitions are then applied for the exhaust stream. One of the study cases applied to this model is based on the results achieved from the TE/SOFC model with a cell operating voltage of 0.75 V with zero H_2 conversion along the system. The anode and cathode exhaust fluid compositions and temperature are driven from the outlet of the SOFC model. Based on this study, the anode exhaust composition is as follow: $X_{H2,in} = 0.5504$, $X_{N2,in} = 0.4494$ and $X_{H2O,in} = 0.0002$ at $T_{flow,in} = 430$ K and the

cathode exhaust contains $X_{O2} = 0.2139$, $X_{N2} = 0.7861$ and T = 400K. Having these set these condition into this combustor model, the exhaust channel inlet condition and other thermal properties are then defined as follow:

3.5 Numerical Methods

The two dimensional detailed combustor model developed in this section is a numerical

solver which integrates a system of nonlinear differential equations at a vector specified time span. This model is setup in Matlab environment using ode15s solver, a variable-order solver based on numerical differentiation formulas, which is a stiff ordinary differential equation solver. Stiff ODEs are usually used for systems which their transient region has a different scale than that of its surrounding. For example systems involving chemical reaction rates use these solvers since they typically converge to a final solution quite rapidly. As a matter of fact using ode15s solver is a great tool for modeling this component since it involves chemical reaction processes within the combustor channel as well as the combustor catalytic surface.

In addition, this solver has the ability of solving differential algebraic equations when consistent initial values are set through defining a singular mass matrix. A singular mass matrix is a diagonal matrix of ones that indicate the respective differential algebraic equations with a previously defined initial condition. Although if the initial value is not consistent, the solver perceives it as an initial guess and solves the equation respectively. Another factor within ode15s solver which is very beneficial for the solver's reliability and efficiency is its ability of defining j-pattern

for the set of differential equations. J-pattern property is set to a sparse matrix of form JP(i,j) = 1, if any k variable of (i,k) component of the mass matrix (M(t,y)) depends on component j of y and if the variables are not dependent it would automatically be set to zero. The solver uses this sparsity pattern to generate a sparse Jacobian matrix numerically, where a large and sparse jacobian matrix can greatly accelerate execution time of the model. For example, the combustor's wall temperature depends on the species composition in the catalyst washcoat, the combustor flow temperature as well as the TE temperature and so the sparse matrix for these variables is set to be 1. Furthermore, there are certain user defined options available for this solver that results in a more accurate and reliable integration process of finding solutions. These options include error control properties, step-size properties and etc.

The error control properties of the solver is in such way that it estimates the local error, e, in the i^{th} component of the solution. This error then must be less than or equal to the acceptable error which is a function of the specified relative tolerance and the specified absolute tolerance. Relative tolerance is a measure of the error relative to the size of each solution component and absolute tolerance is defined as the threshold below which the value of the i^{th} component is unimportant and determines the accuracy when the solution approaches zero. For ordinary problems the solver usually delivers rough accuracy equivalent to the requested accuracy. However, for problems running on longer time intervals it delivers less accuracy and thus would need tighter tolerances. In addition, for the absolute error tolerance the scaling of the solution component y is very important and if this scaled solution component be somewhat smaller than the absolute tolerance, then the solver is constrained to obtain any

correct digits in y. For example, in combustion modeling solution components such as temperature, mass flow rate, pressure and mass are scaled by dividing each respective component with 1000, 0.001, 1(atm) and 1respectively. The relative tolerance should be in correct digits for all the components except those smaller than the absolute tolerance; which in that case the AbsTol(i) should be set small enough that would get correct digits in y(i) in order to compute the solution components more accurately. In running process of this model, it was noted that the relative tolerance and the absolute tolerance values have a great impact on the system convergence towards the solutions and that both absolute and relative tolerances need to be set relative to the defined initial conditions. In this model the appropriate range of relative tolerance was found to be about $5*10^{-5}$ and the absolute tolerance was found in the range of $5*10^{-9}$.

Step size properties of the solver includes the initial step size which helps the model recognize the scale of the problem as well as setting bounds on the sizes for subsequent time steps. The initial time step is usually based on the initial slope of the solution, so if the solution attains a zero slope initially then the initial time step might be too large. Thus specifying this value would assist the solver for a faster execution. In this model, the initial time step is set to be 10^{-12} s which is regardless of the set integration time step. Another option provided by this solver is the usage of a timestep control tool, referred to as MaxStep in Matlab, which confronts the solver to take large inaccurate timestep irrelevant to the scale of the problem as well as preventing it to take small timesteps which would slow down the integration. This values is suggested to be a fraction of the defined time period. During the testing process of the model, it was noted that system faces some instabilities due to

integration of the surface reaction terms which occur in short periods of time. Thus, the system would be set to run for 5 to 6 minutes with maximum time step intervals as small as 1/100 of a second and as soon as system reaches a stable condition, the system is then set to be run for longer periods of time with larger timesteps of 1/10 to 1/4 depending on the total time interval set for the system.

4 Integrated TE/Catalytic Combustor Model Results

4.1 Performed modeling studies

Development of the detailed TE integrated catalytic combustor system, described in previous chapter, enables users to study the performance of the catalytic combustor channel, TE module and the air cooling channel as individual components as well as part of a whole system. One can study the influence of a particular sub-component, e.g. TE module, on the entire system by changing a particular parameter of that sub-component.

As it was mentioned earlier, one of the main goals of this research is to study the effect of TE module integration on the SOFC power system performance and efficiency during system's start-up period when the SOFC anode is not consuming much fuel and not generating enough power. The case studies performed in this chapter are mainly focused on modeling conditions similar to that of the SOFC system's start-up condition. The performance characteristics of the TE integrated catalytic combustor model is then tested under different state property conditions, sub-component geometries, channel flow conditions in order to achieve the optimized start-up operating condition for the system.

This chapter will first introduce a base line case study (section 4.2) of the combustor system. The system model performance results under steady state and transient conditions, such as temperature distribution, fuel consumption and TE power generation along the length of the channel will then be discussed. Using this case as the baseline, the parametric study of the system is then performed by holding some of the baseline values constant and studying the system performance under a different condition. Before performing additional system analysis, the model's results' precision is tested by performing a grid study on the model by increasing the length of the integration cell region dx.

The parametric case studies performed includes the study of TE and combustor exhaust channel geometrical affect's on overall system's operating temperature, fuel consumption, TE power generation and the combustor efficiency. For the combustor exhaust's geometrical study, the model was run with a doubled channel length which would add to the number of TE couples along the length of the channel. The thermoelectric geometry case study was performed by doubling the height of the TE couples from the one in the base line case and keeping the rest of the parameters constant. In another case, air channel heat transfer enhancement study is performed by decreasing the number of fins along the width of the air channel and study its impact on air flow preheating.

This model further explores the effect of different inlet flow conditions of channels on combustor system performance. In another study, exhaust inlet flow condition was kept the same however, the anode mass flow rate was estimated using a different approximation which results in higher H_2 species mole fraction composition.

The effect inlet flow on system performance is also explored by increasing the air channel's inlet flow rate by a factor of 2.

Lastly, the influence of TE module integration on SOFC power system performance and efficiency is evaluated by applying anode and cathode exhaust state conditions, achieved from TE/SOFC system model in chapter 2, as the exhaust inlet conditions of the TE/catalytic combustor model. The TE power generation and waste heat recovery accumulated through this model will then be applied to the SOFC system to achieve a system performance analysis such as efficiency, waste heat recovery and power production.

4.2 Results for high-temperature PbTe thermoelectric

In order to study the TE integrated combustor model performance under fuel cell's exhaust start up condition, a set of inlet conditions close to the start-up state property conditions was defined and simulated to develop a base line case. The model was tested to run at its optimal performance with the defined base line conditions and the rest of the parametric study of the model will be based upon this base line.

The combustor system model base line case is selected as a PbTe TE module with porous catalytic Pt covered washcoat layer and fin heat exchangers within the air channel. The baseline geometry of the exhaust channel, air channel geometry, and washcoat layer properties are already presented in table's 3-1, 3-2 and section 3.3.3 respectively. The base line channel discretization's length of integration (dx) along the length of the combustor is set equal to the length of one TE couple, 4 mm, which is 20 cell divisions along the channel. The base line inlet flow properties was set in

such way to imitate the fuel-cell start up conditions where no or very few amount of fuel has been consumed. The anode and cathode exhaust species composition is set with pure Hydrogen and air feedings with stoichiometric ratio of 2 to 1 and at low inlet temperature of 250°C where the fuel cell has not been heated yet. The cathode mass flow rate at the combustor inlet port is set equal to the air channel's mass flow rate equal to $7.86*10^{-5}$ kg.s^{-1}. The anode mass flow rate into the system is then approximated through equation 3-5 with an equivalalnce ratio of 0.5 and equal to $5.72*10^{-7}$ kg.s^{-1}. The combustor inlet condition can then be summarized as follow in table 4-1.

Table 4-1: Combustor's exhaust flow base line conditions

X_H_2	0.094
X_O_2	0.19
X_N_2	0.71
Temperature (K)	523.15
Mass flow rate (kg.s^{-1})	$7.92*10^{-5}$

The air channel inlet condition was set as dry air, entering the system at ambient condition. The model was then run for 11minutes of simulation time in order to reach steady state condition and the conservation equations were integrated at 0.05 s time intervals.

Figure 4-1 below is the TE integrated combustor channel temperature distribution at each sub-layer section of the system along the length of the channel at steady state condition. Since the combustor system configuration is modeled as a cross flow heat exchanger, the air channel inlet temperature and condition is located at the opposite end from the exhaust inlet port. On the following figures the air

channel inlet properties is at channel length of 8 cm and the air channel outlet port is located at 0^{th} length.

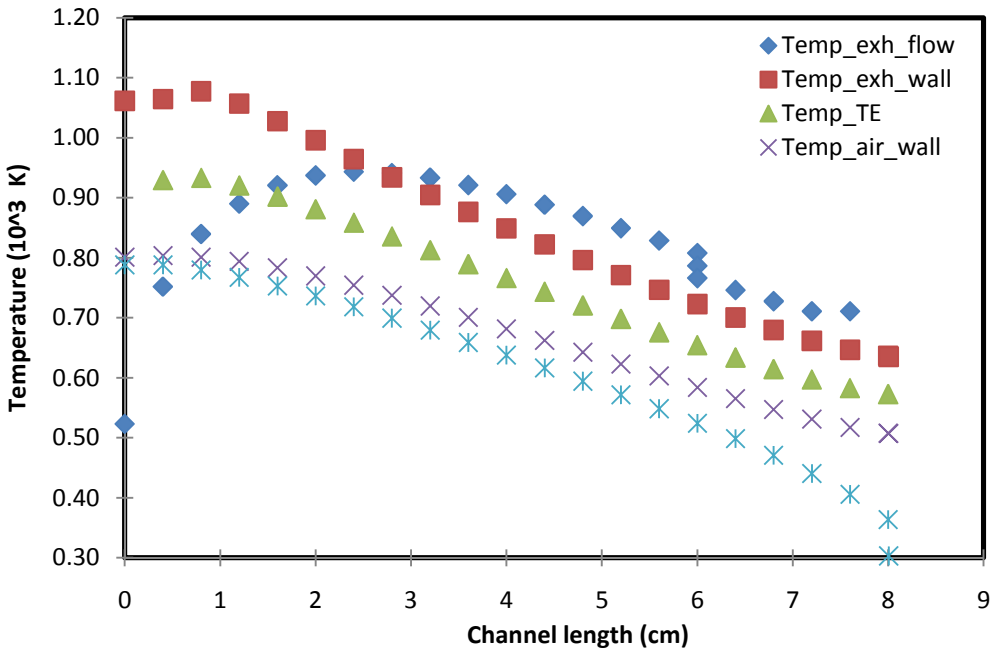

Figure 4-1: Baseline case combustor channel temperature distribution

Figure 4-2 represents exhaust channel flow species mass fraction along the length of the combustor channel. H_2 and H_2O mass fractions are on the primary axis and O_2 mass fraction is plotted on the secondary axis on the left hand side. Figure 4-3 represents the washcoat layer species mass fraction. As shown on this figure the washcoat layer is covered with H_2 at the first cell division, reacting with the catalyst surface, increases the the washcoat layer temperature, which is also the same as the exhaust wall temperature, to 1100 K and the remainder of the washcoat layer will only be covered with O_2 and H_2O.

The catalytic surface site fractions, $\theta_{lsurf,ksurf}$, is also calculated and plotted along the length of the combustor channel, figure 4-4. As it can be seen, as the Pt

active site fractions decreases the amount of O species coverage on the surface increases.

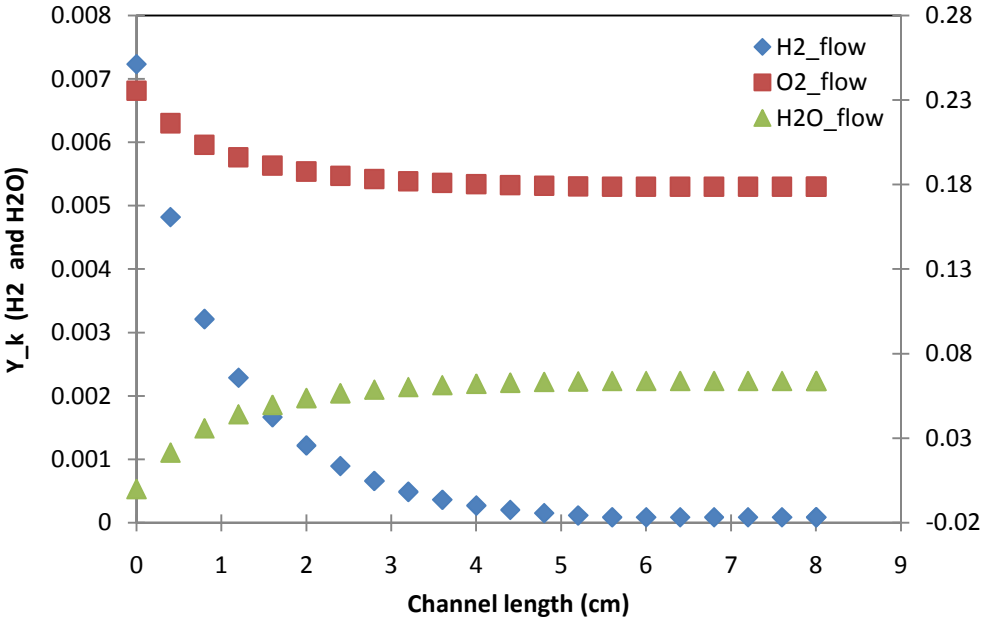

Figure 4-2: Exhaust channel flow species mass fraction

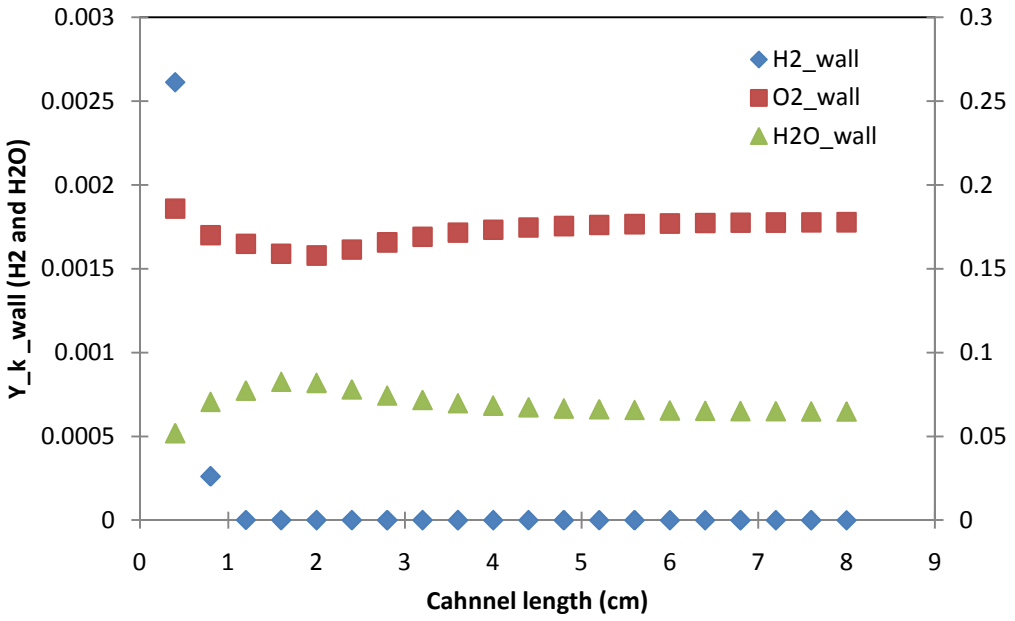

Figure 4-3: Washcoat layer species mass fraction

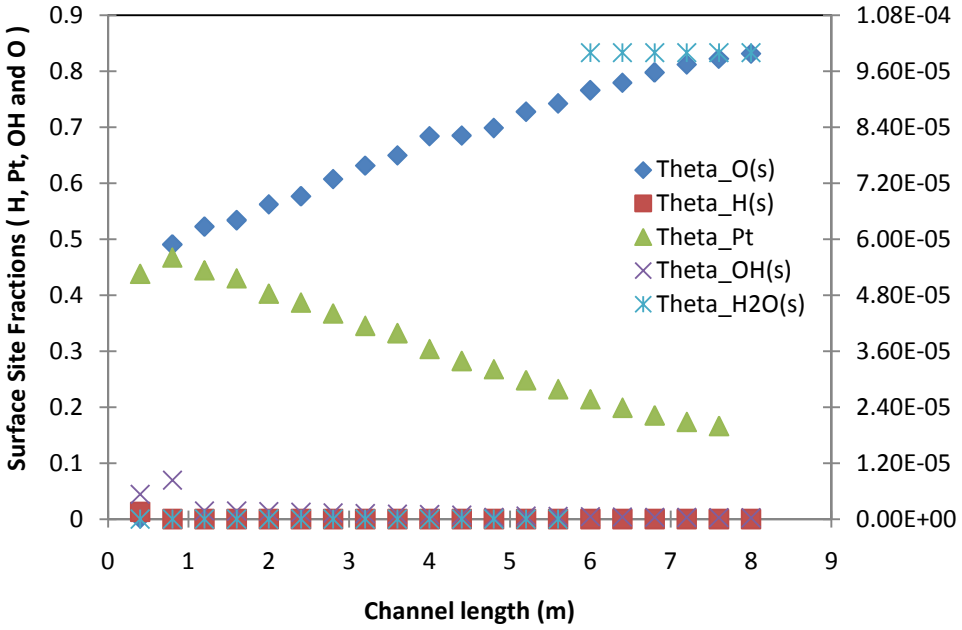

Figure 4-4: Surface species site fractions

The TE current and power generation under transient condition was also calculated and plotted in figure 4-5, along with the measure TE couple's temperate in the combustor channel's mid cell division at length of 4 cm. The total current and power measurements of TE module is uniform along the length of channel and the load resistance used to measure the power was set at 1Ω.As it can be seen on this figure, at the initial time, the system generates 0.6 A of current and 3.8 W of power, however due to the fast surface reaction processes and combustion light within the exhaust channel, the temperature of the exhaust wall and the channel will drop for the first few seconds and then starts to increase very quickly after the light off. Thus, the power generated first decreases exponentially until after the system reaches its equilibrium condition at which point the system generates a steady power of 1 W.

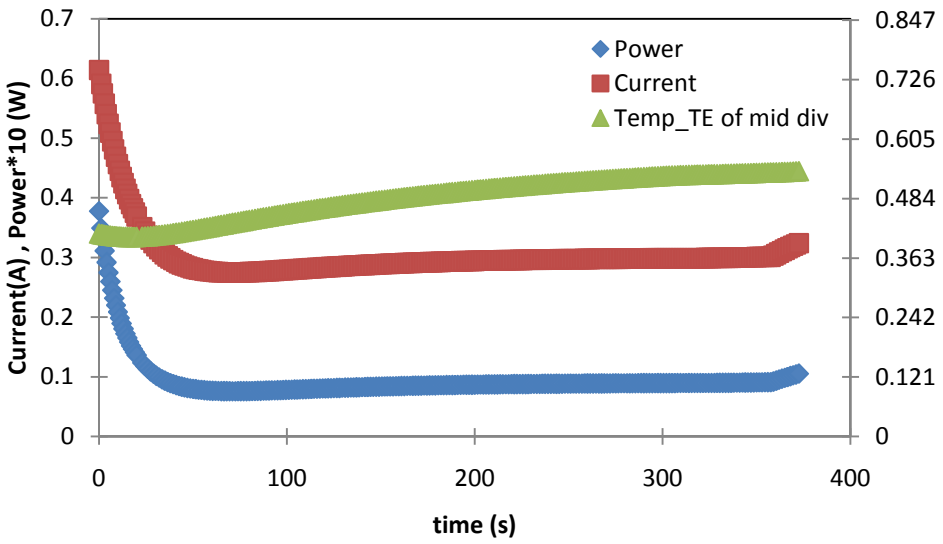

Figure 4-5: Base line TE power generation transient study

Figure 4-6 is the summary of the overall combustor system performance from a power generation and thermal heat recovery and fuel consumption stand point. At channel length of about 4 cm downstream from the combustor channel inlet, all the H_2 within the channel flow is consumed and exhaust flow stream exiting the system only contains 0.002 mass fraction of H_2O and 0.18 mass fraction of O_2. In addition, the air flow temperature entering the system at room temperature will reach a temperature of 800K after 11 minutes of simulation.

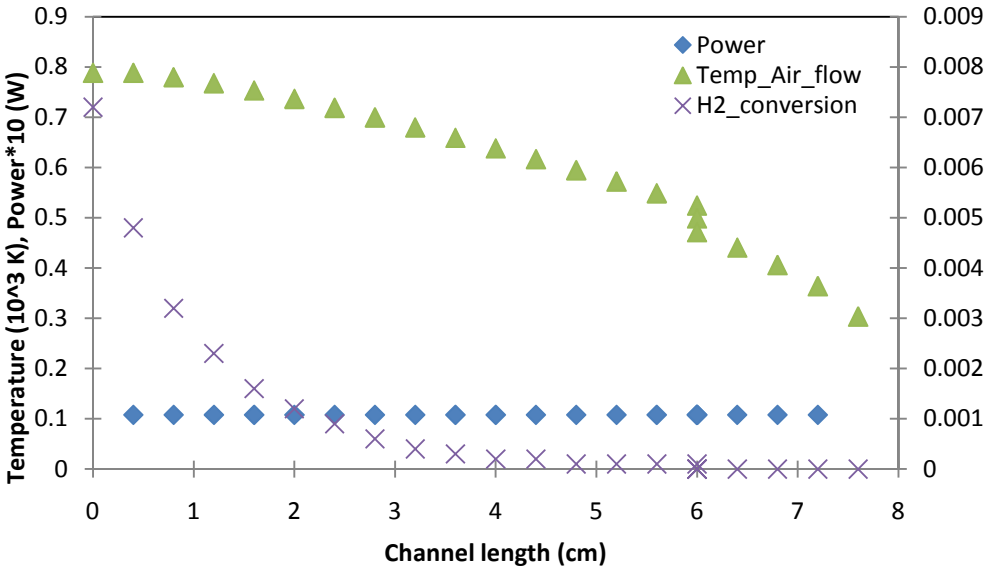

Figure 4-6: Base line case system performance

In the grid case study all the system inlet properties and the geometrical characteristics of the combustor is kept the same as of the baseline condition, however the length of the discretized integration divisions are increased by a factor of two which is proportional to having two couples per each discretized cell.

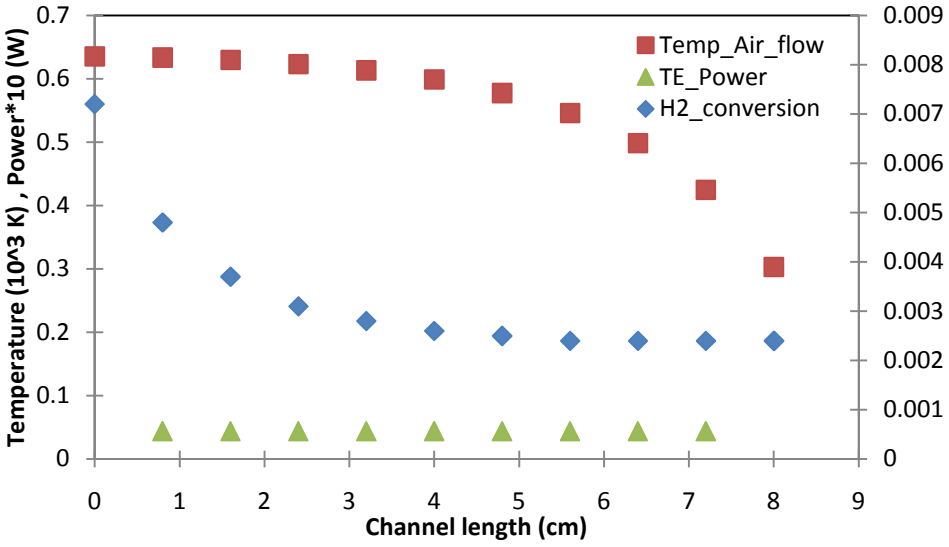

Figure 4-7: Grid study system performance analysis

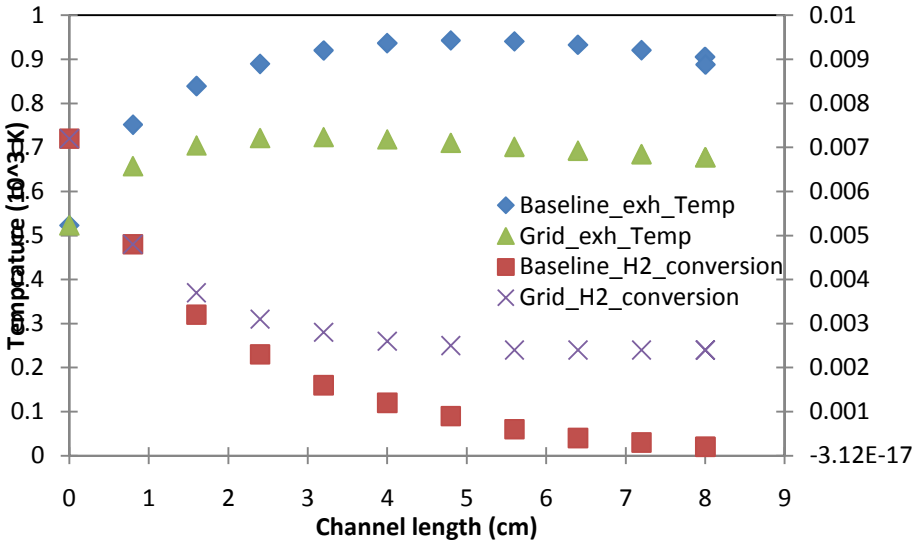

Figure 4-8: Baseline versus grid comparative system performance study

Figure 4-7 represents the plot of the system performance under increased grid size condition. According to these results, the system will produce a total power of 0.04 W under the exact samy operating conditions as of the base line when the discretized cell are as long as two TE couple per division. In addition, figure 4-8 represents a comparative study between the two cases. Only about 70% of the H_2 mass fraction of the exhaust channel flow is consumed in the grid case study where the baseline condition with smaller cell discretization shows a full H_2 along the length of the channel.

The remaining parametric case studies performed on the TE integrated catalytic combustor system are based off of the baseline case presented above and the discretizations long the channel are kept constant as of the baseline throughout the simulations.

4.2.1 Effect of TE geometry and combustor geometry

TE couple geometry parametric study:

In the following case, all the exhaust and air channel inlet conditions are the same as of the base line condition with equivalence ratio of 0.5 and exhaust inlet temperature of 523K and same mass flow rates. In this case study the effect of TE geometry on TE performance is studies by increasing the height of TE couples at a base line value of 2 mm by a factor of 2.

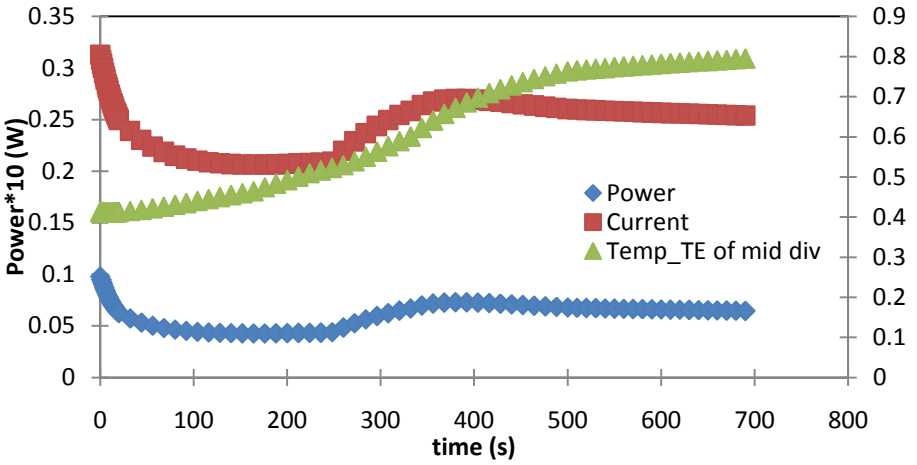

Figure 4-9: Transient TE power generation study at y_{TE} = 4 mm

According to the results achieved from this geometry case simulation, it is observed that longer TE couples reduce the heat transfer from the exhaust channel to the air channel, figure 4-10. Also, due to the longer length the couples experience more resistivity along its length and thus the amount of power produced by TE module when system reaches equilibrium is reduced to 0. 47 W comparing to 1 W of power generated at the base line condition. Figure 4-11 presents the overall combustor

system performance where the amount of H_2 conversion along the length of the channel is the same as the baseline, however the longer TE length causes the air flow temperature to decrease to 735 K and thus reducing the air preheating by almost 70 K comparing to the base line scenario.

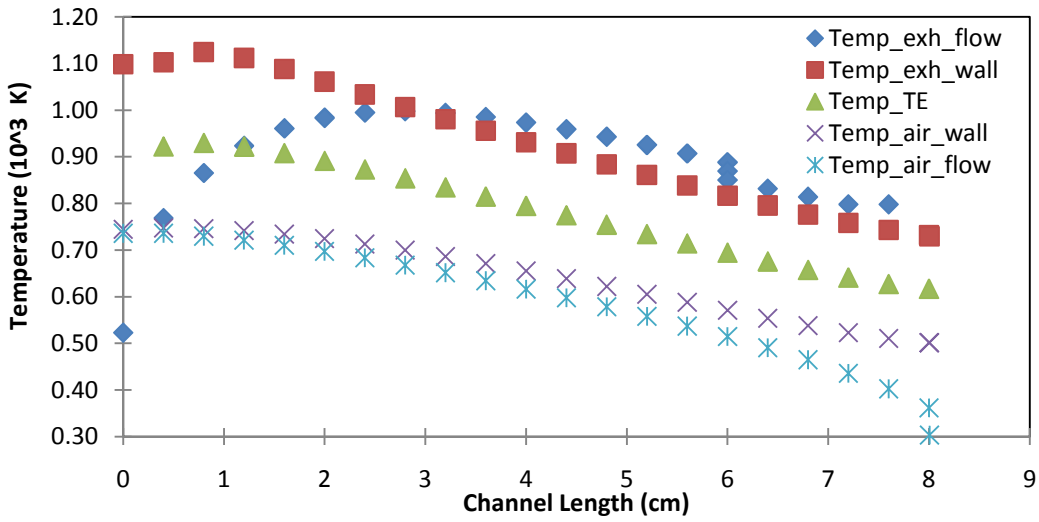

Figure 4-10: Combustor system temperature distribution along the channel length at y_{TE} = 4 mm

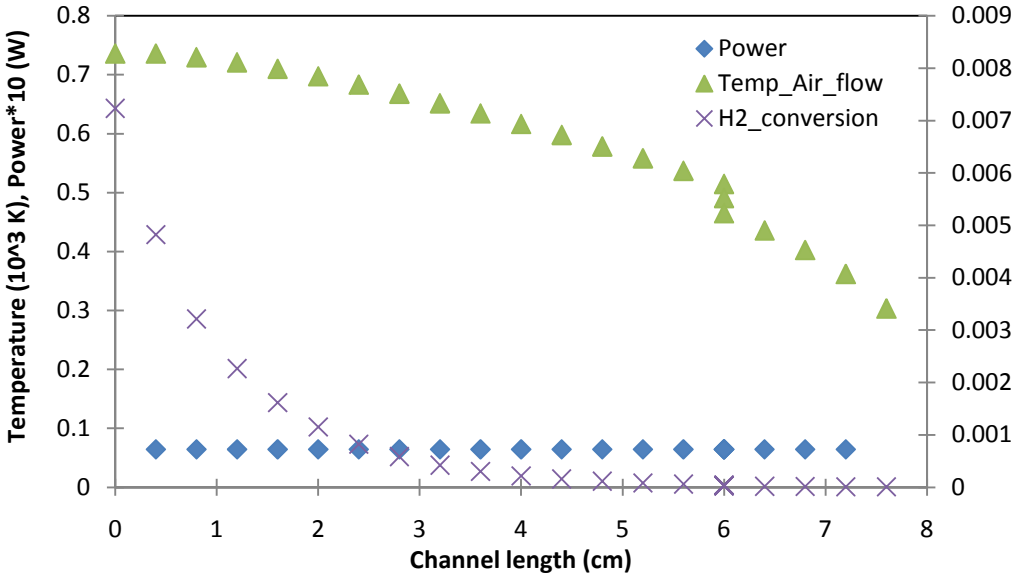

Figure 4-11: System performance analysis at y_{TE} = 4 mm

Combustor channel length parametric study:

In this case study the effect of length of the combustor system on the overall fuel consumption, power generation and performance of the system is calculated and analyzed. The total length of the system is increased from 8 cm of baseline length by a factor of 2 to 16 cm.

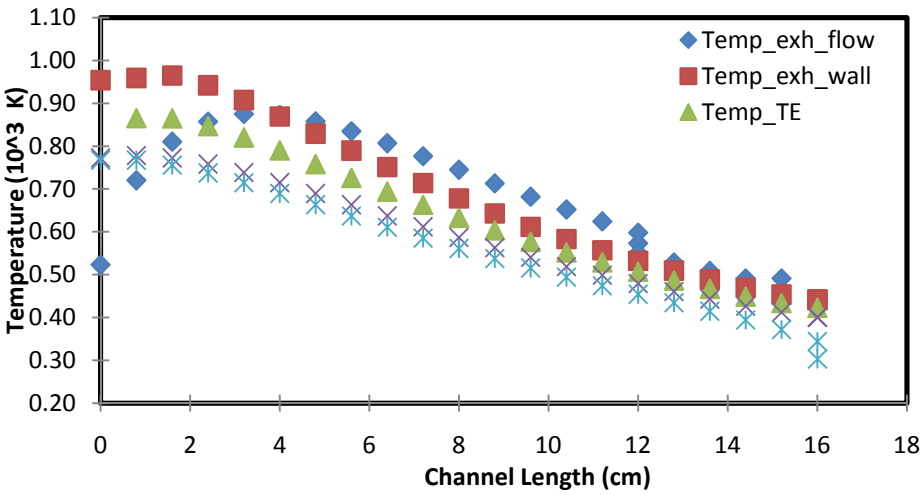

Figure 4-12: Combustor system temperature distribution at x_{comb} = 16 cm

Elongation of the system length by a factor of 2 has reduced the operation temperature range of the system. The exhaust wall temperature for example only reaches up to 950 K whereas in the base line condition is as high as 1100K. However, the heat transfer flux through the sub-layers of the system is high and causes low temperature difference along the channel at each layer. The effect of this factor can be seen in figure 4-13 which causes the total power generation by the TE to decrease to 0.04 W. However, the temperature of the air flow exiting the system is very close to that of the baseline condition and the length of combustor does not influence this factor by much. Since the length of the channel is longer the amount of

fuel consumption along the length of the channel occurs further downstream of the channel at x = 8 cm.

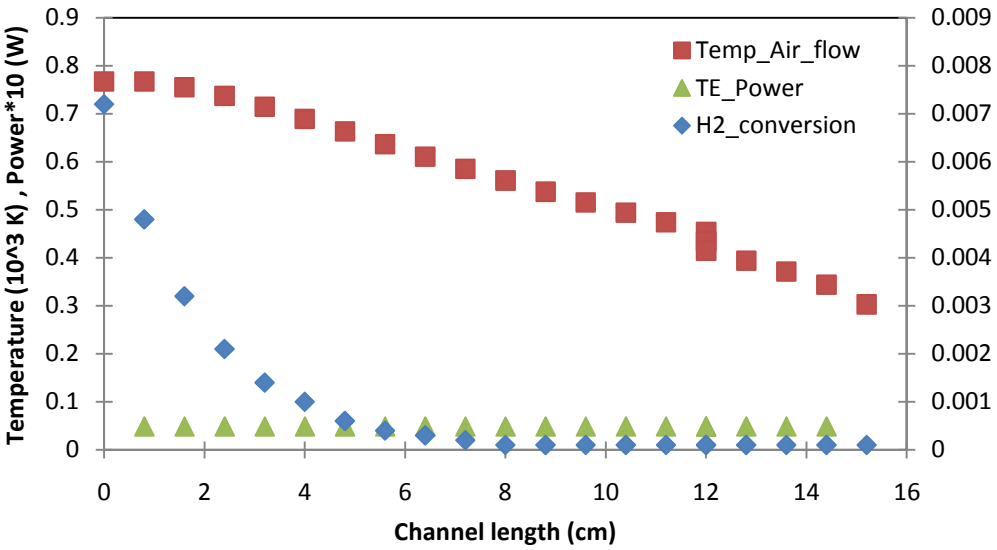

Figure 4-13: System performance analysis with x_{comb} = 16 cm

One interesting observation made through this case study is the effect of channel length on washcoat species mass fraction. Due to the longer channel length the washcoat contains more H_2 species along the length of the channel in comparison to the baseline case where the all the H_2 is burned and reacted within the 1 cm downstream of the inlet.

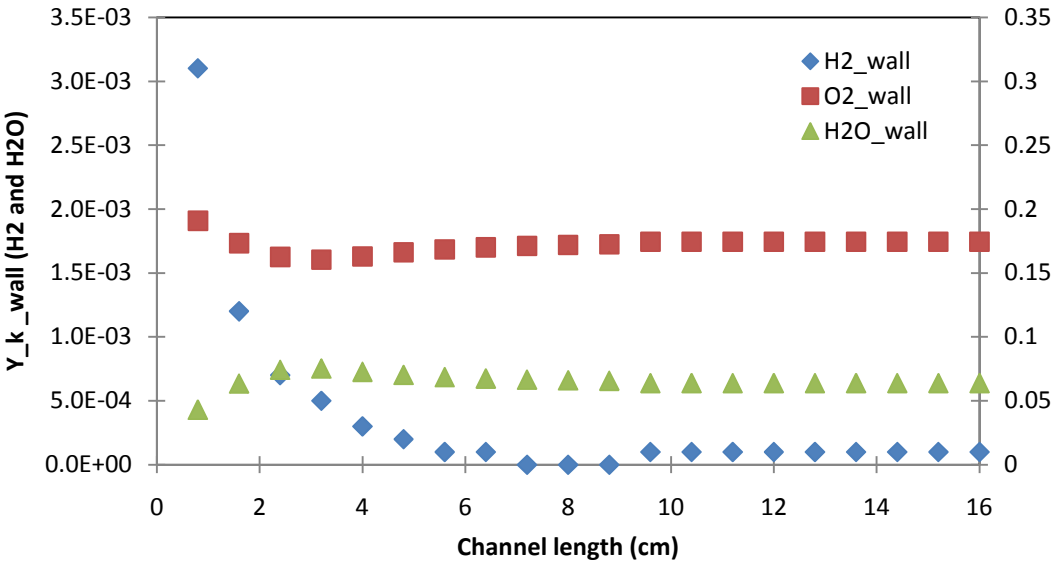

Figure 4-14: Washcoat species mass fraction along the channel length with xcomb = 16 cm

Fin number parametric study

In this study the effect of fins on waste heat recovery and preheating the air flow stream is examined by reducing the number of fins from the baseline case of 9 fins to 4 fins along the width of the air channel and parallel to the flow stream. In this study, the fin thickness and height remained the same as presented in section 3.3.1 and only the spacing between the fins was increased from 2 mm to 5 mm, keeping the width of the channel at constant value of 26 mm.

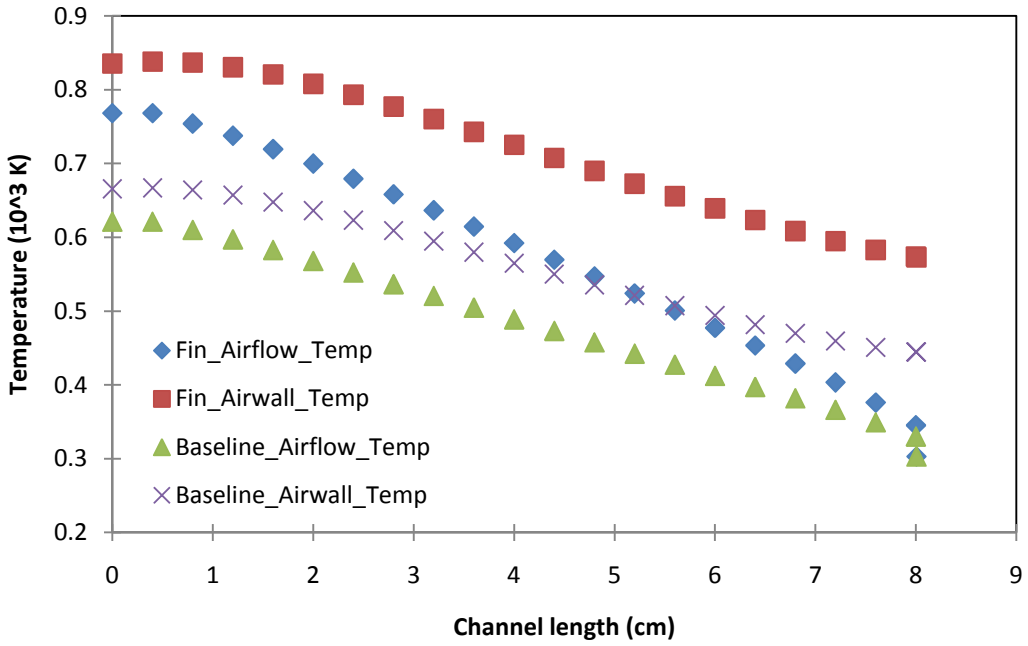

Figure 4-15: Baseline versus fin study air channel temperature gradients

According to the simulations, it is observed that the decreasing the number of fins within the air channel only influences the air channel wall and flow temperature. Figure 4-15 is a comparative analysis on the effect of fin number parameter versus the baseline case on air channel temperature. Based on these results the air and flow temperatures are slightly decreased by an order of 100K in the case with 4 fins at the inlet of the air channel. However, the outlet flow temperature on both cases would reach a temperature very close to the baseline condition.

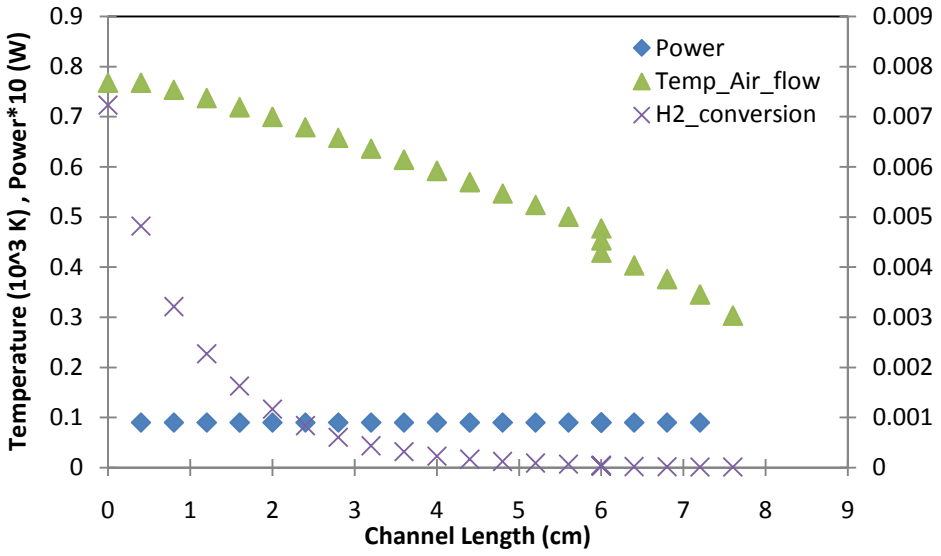

Figure 4-16: System performance analysis with reduced number of fins

4.2.2 Flow conditions effect on performance

Besides the parametric studies performed in the previous section to investigate the effect of system geometry on its performance, the TE integrated catalytic combustor system is also tested under different exhaust and air channel inlet conditions.

Anode mass flow rate approximation:

This case will first explore the effect of anode mass flow rate approximation on the overall performance of the system. It should be noted that the exhaust channel fuel composition stoichiometry and equivalence ratio are all equal to the baseline condition and the only difference is the anode mass flow rate approximation performed as following versus the baseline condition performed in equation 3-5.

$$\dot{m}_{anode,in} = \frac{\Phi\, \dot{m}_{cathode,in} \sum(MW_{k,anode} \dot{x}_{k,anode})}{(\mathrm{MW_{k,cathode}} \dot{x}_{k,cathode})(2\dot{x}_{H2,anode})(\dot{x}_{H2,cathode})}$$

(Eq. 4-1)

The inlet catalytic combustor inlet condition due to the above approximation is then evaluated as following in table 4-2.

Table 4-2: Combustor channel inlet condition

X_H_2	0.173
X_O_2	0.173
X_N_2	0.653
Temperature (K)	523.15
Mass flow rate ($kg.s^{-1}$)	$1.153*10^{-6}$

The simulated results achieved based on the above approximation can be found in the following figures. The inlet fuel composition with equivalence ratio of 0.5 has H_2 mass fraction of 0.014 and 0.21 O_2. Figure 4-17, shows a complete fuel consumption along the length of the combustor channel.

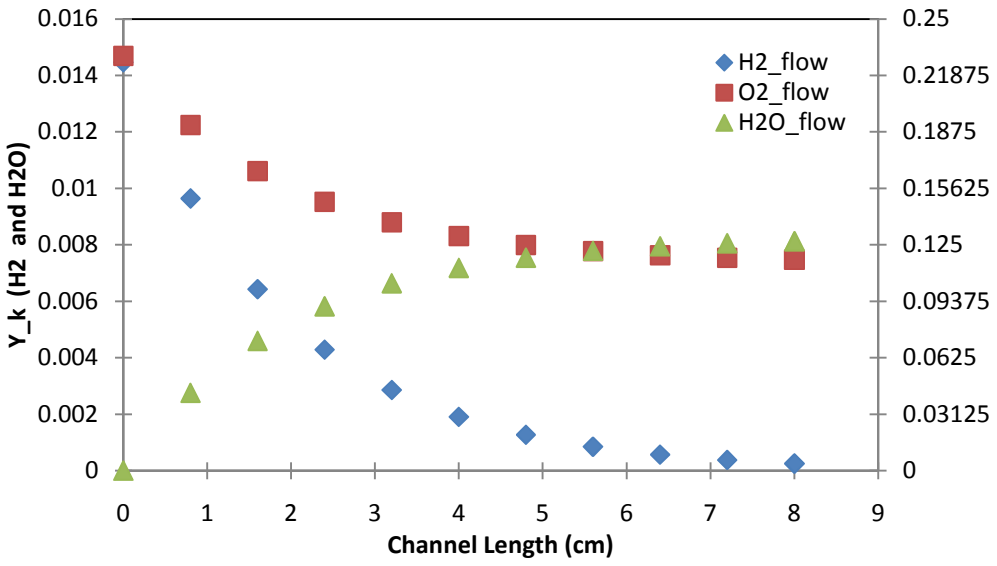

Figure 4-17: Combustor channel flow species mass fraction

The system's temperature distribution along the length of the channel is also plotted in figure 4-18. Due to the high H_2 composition at the combustor's inlet, the combustor provides more energy input to the system and thus the combustion temperature is increased. The wachcoat/exhaust wall support temperature in this case has reached a value of about 1400K and the fuel stream will exit the combustor system at a high value of 800K which exceeds the standard system exhaust conditions. Also, the air flow is preheated to 1100 K which for waste heat recovery purposes and SOFC initial preheating, exceeds the system's operating temperature range.

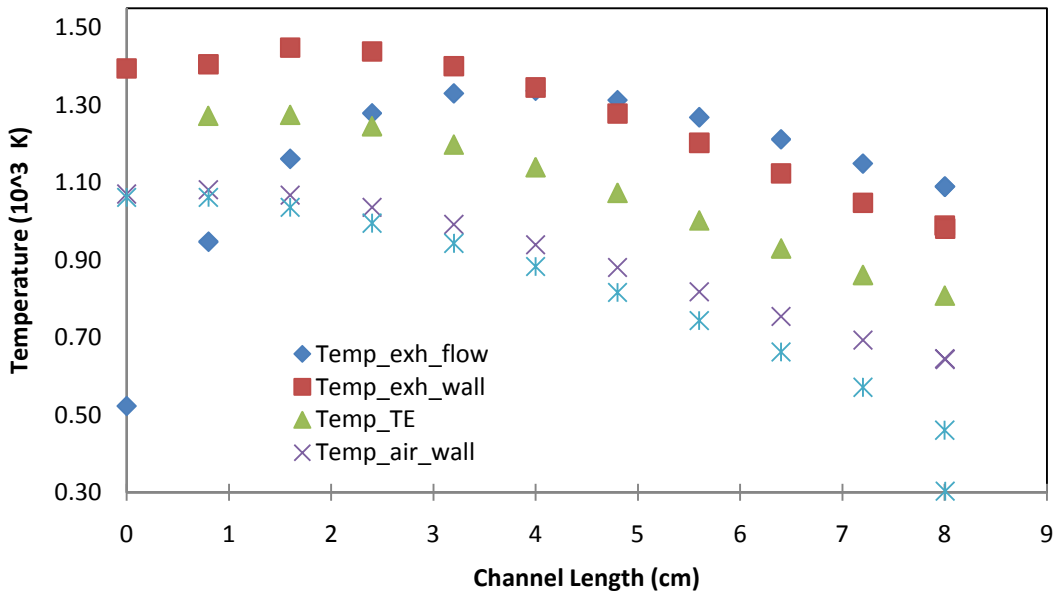

Figure 4-18: Combustor system temperature distribution

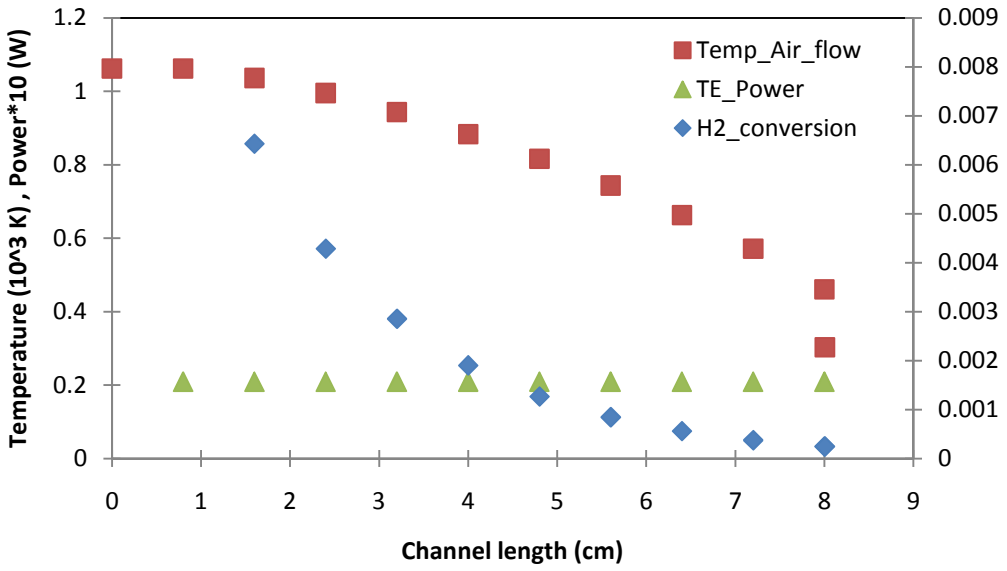

Figure 4-19: System performance analysis with new anode mass flow rate analysis

The effect of this approximation on the overall system performance is shown in figure 4-19. It can be seen that since the system's operating temperature has increased, the TE module experiences higher heat transfer flux through it couple and thus generating two times more power than the base line condition equal to 2 W.

Air flow rate case study:

In this case, the mass flow rate of the air channel stream was increased by a factor equaling $1.57*10^{-4}$ $kg.s^{-1}$. Figure 4-20 summarized the effect of this change on important system parameters. As it can be seen the air flow temperature exiting the combustor system is at 610K whereas in baseline case the air flow reaches higher temperature of about 800K in simulation time duration of 11 minutes. On another note, the following results also show an improvement in TE power generation in the system. By increasing the air channel's mass flow rate the power generated by the TE module is increased by 0.6 W, generating a total power of 1.6 W.

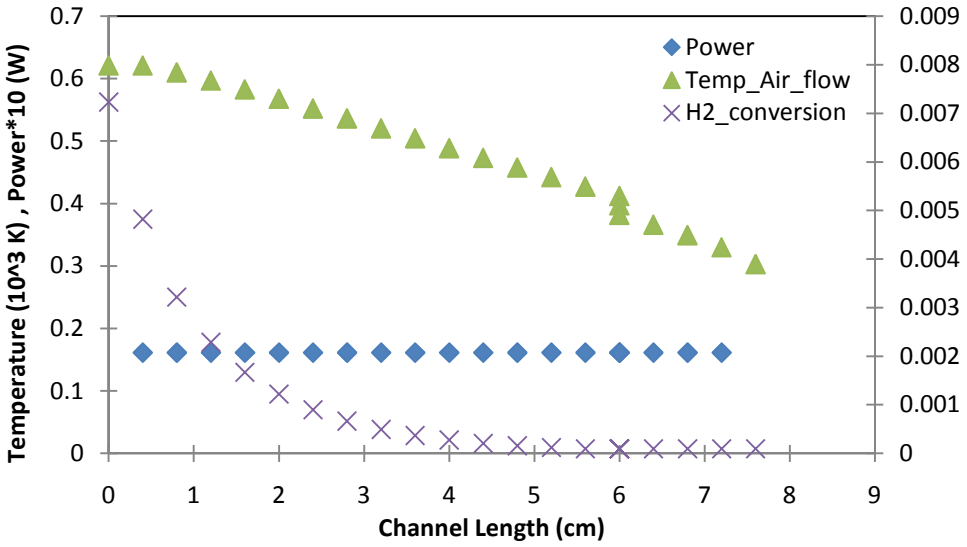

Figure 4-20: System performance analysis with doubled air flow mass flowrate

The result of the transient study performed on this case can be found in figure 4-21. As it can be seen TE module generates about 4 W at the star-up state of the system and very quickly drops to about 1.2 W at when it remains constant for about 5 minutes, and then starts increasing and reaching an equilibrium value of 1.6W.

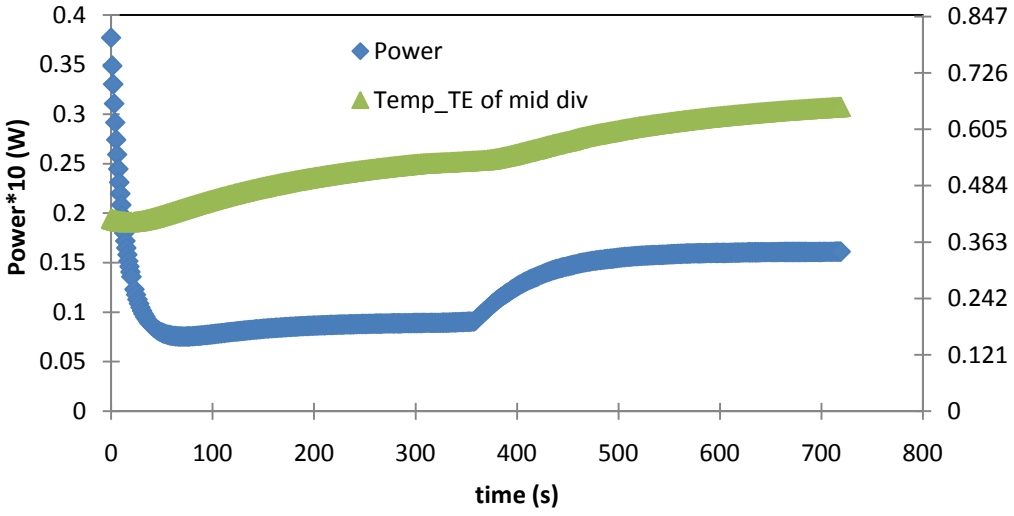

Figure 4-21: System power generation transient study

This phenomenon can be explained somewhat through the following figure. Figure 4-22 represents the transient results from a discretization at the combustor's mid cell division about half way downstream of the inlet. Based on this results, the exhaust flow and wall temperatures are increasing with time when they reach about 600K after about 400 seconds, the temperatures has a sudden increase of value at which point where the Pt site fraction becomes activated and OH species on the surface will go to zero and Pt and O site fractions become active at the surface.

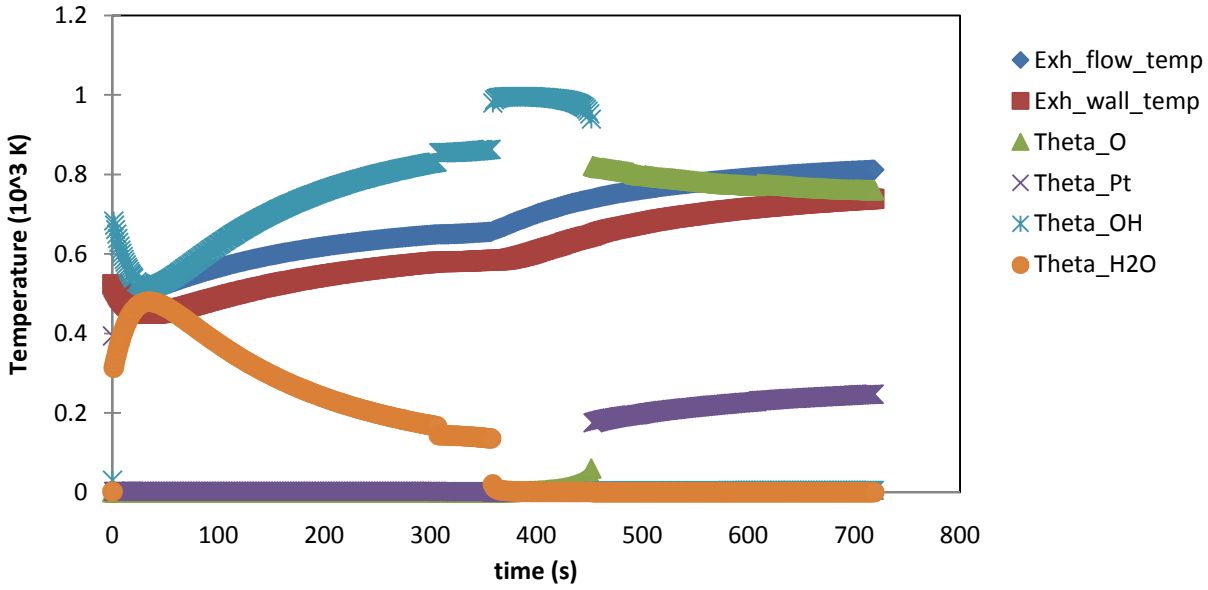

Figure 4-22: Surface site fraction and temperature transient study

4.2.3 Fuel cell integration relevant conditions

The case studies presented above including the baseline case presented in section 4.2, and the respective channel flows' inlet conditions were designed to capture cases similar to anode/cathode exhaust condition of a SOFC system during its start-up period. The results taken from TE integrated SOFC system model explained in chapter 2 was used as inlet conditions of the TE integrated catalytic combustor

model in order to combine the respective results of the TE integrated combustor model with SOFC system model data and analyzing the effect of TE implementation of SOFC system performance and efficiency. The combustor channel's inlet condition driven from SOFC start-up condition analysis from chapter 2 is given in table 4-3. Using these conditions, the amount of fuel energy input to the combustor system can be derived using equation 4-2 to 4-4 which it will be the same as an SOFC/combustor system during its start-up period with no fuel conversion along fuel cell. Where H_2 lower heat of combustion, $h_{H2,lowerheating}$, is $2.423*10^5$ kJ.kgmol^{-1}.

Combustor heat input calculations and fuel cell's efficiency calculations:

$$\dot{m}_{exh,in} = \dot{m}_{cathode} + \dot{m}_{anode}$$
(Eq. 4-2)

$$MW_{tot} = \sum_{k,species}(x_k\, MW_k)$$
(Eq. 4-3)

$$\dot{Q}_{fuel,in} = h_{H2,lowerheating}\left(\frac{\dot{m}_{exh,in}}{X_{H2,in}MW_{H2,in}}\right)$$
(Eq. 4-4)

Table 4-3: SOFC inlet conditions during start-up period

SOFC inlets	Inlet
X_H_2	0.096
X_O_2	0.19
X_H2O	0.0002
X_N_2	0.71
MW_{tot} (kg.kgmol^{-1})	26.3916
Temperature (K)	423.15
$\dot{m}_{exh,in}$ (kg.s^{-1})	$6.6*10^{-6}$

The TE integrated catalytic combustor system characteristics achieved using the above inlet conditions came out as following. The total amount of power

generated by TE module came out to be about 0.5 W after 11 minutes of operation. The H_2 turns out to be fully utilized along the channel as expected and the air flow was heated reaching outlet temperature of 1000K.

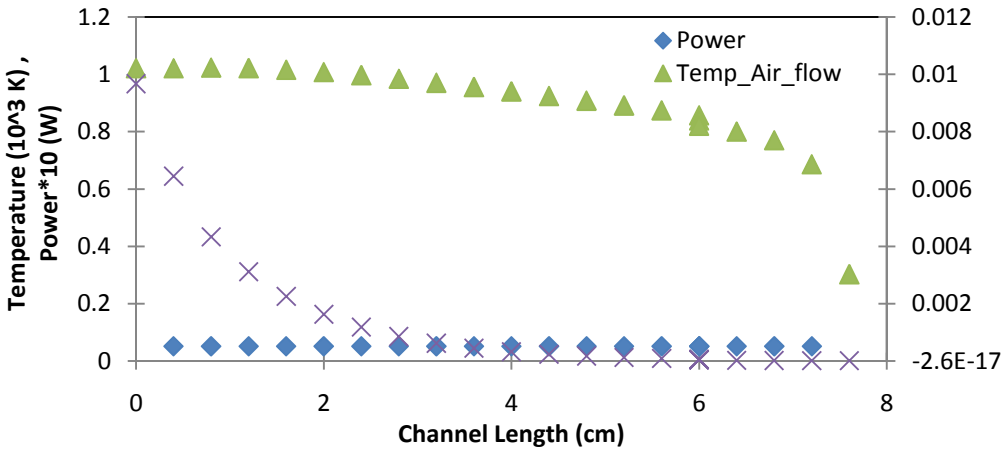

Figure 4-23: Combustor system performance with SOFC exhaust condition

Using the results gained from this simulation and combining it with the SOFC system performance gained in section 2.3 (W_{SOFC} = 0.002 W) the SOFC system can be recalculated using equation 4-5, results in a new system efficiency of 0.012.

$$\eta_{SOFC} = \frac{W_{SOFC}+W_{TE}}{\dot{Q}_{fuel,in}}$$

(Eq. 4-5)

Table 4-4: TE integrated SOFC system efficiency at start-up

$\dot{Q}_{fuel,in}$ (W)	45.6
W_{TE} (W)	0.5
W_{SOFC} (W)	0.0002
η_{system}	0.012

Furthermore, the results gained from TE/catalytic combustor model can also be used to estimate the ability of a TE integrated waste heat recovery system in providing enough power to the SOFC system to balance the plant and reduce the size of the battery within the system during start-up condition. For this matter, the assumption made for the required power for balance of the plant made in section 2.3 can also be applied for this section in order to gain a better understanding of the effect of TE integration into catalytic combustor of a SOFC system during start up condition. Based on analysis performed above, the combustor with the defined inlet conditions driven from SOFC model can generate 0.5 W at the 11^{th} minutes of operation. Thus, if the power required for balance of plants is about 0.1 of the amount of fuel energy input to the system (~5W), according to the above estimates, the TE module needs to generate 4.5 W more power in order to balance the system.

According to these results gained from the TE integrated catalytic combustor model and the results driven from the SOFC model, the amount of heat input provided into the SOFC system was estimated to be about 45.57 W, and the power produced by the fuel cell, W_{SOFC}, is as low as 0.002 W. Thus, combining the SOFC results during its start-up period and the results gained from the base line case of TE/catalytic combustor model with TE power generation of 1.1W; it is found that the SOFC system with an integrated TE catalytic combustor component the above modeling characteristics, can have an efficiency of 2.4% during its start-up and producing a total power of 1.12 W.

4.3 Discussion of results

According to the results achieved from the TE geometry case study presented in figure 4-9 and 4-10, it is observed that increasing the length of TE couple by a factor of 2 will result is a total power production of 0. 47 W which is almost the half of the amount produced in the baseline case. This is due to the fact that the heat conduction throughout the TE couple is reduced and thus the couple experienced. From the fin parametric study, one can conclude that number of fins does not have a major impact on the overall performance of the system and thus it is not an important factor in system performance optimization.

In the parametric study of combustor channel length, a total power reduction

The anode mass flow rate approximation, resulted in higher H_2 / O_2 mass fraction composition within the system increasing the overall temperature range of the system to about an average value of 1100 K and generated two times as much power than the baseline condition. Althrough the double power generation factor is an improvement within the system, however in reality the PbTe modules can't withstand such high range of temperature and the module will face deformation and melting the joint connectors as described in chapter 1.

The air flowrate study showed an improvement in TE power generation by increasing the temperature difference between the hot and cold junctions of the TE couple, however the preheating process in this case does not reach the SOFC operating temperature and would not affect the start-up time of the fuel cell system majorly. However, by creating a condition with higher fuel concentration in the

exhaust flow stream that could provide more energy input to the system as well as keeping the air mass flow rate at this level might provide ideal condition for more TE power generation through the combustor channel.

Furthermore, performing transient analytical studied on air flow rate case, showed that both exhaust channel temperatures and TE power generation with respect to time experience some instabilities, figures 4-21 and 4-22, where both temperatures and power will initially decrease and then slowly increase with time. Plotting the surface site fractions and studying the surface reactions with time, figure 4-22, it was noted that the catalytic surface experience instabilities due to fast reaction rate between Pt coated washcoat and fuel stream. These instabilities might be due to integration processes of the solver and being able to handle the fast reaction rates at the surface. However, the catalytic surface seems to gain its equilibrium and reach a stable condition after 5 minutes of simulation time and system would operate towards reaching equilibrium after another 6 minutes of simulation time period.

In section 4.2.3 the relevant SOFC exhaust condition, used in the TE integrated catalytic combustor model, in order to gain a general understanding of the SOFC system performance when a more realistic combustor model is used. The baseline case inlet condition was carefully approximated to match the SOFC outlet conditions during its start-up period. Combining the two models and using the SOFC heat input calculations and the TE power production from the combustor model, showed a 2.4% improvement in efficiency. This calculation can also be applied for other conditions studies above. For example, the anode mass flow rate and air mass flow case studies, where the air channel flow rate was increased by a factor of 2 and anode mass flow

rate was approximated using equation 4-1, showed the maximum amount of TE power generations of 2 and 1.6 W. As a matter of fact, applying these outputs into equation 4-5 will result in SOFC system efficiency 3.5 and 4.3 %.

As it was discussed in previous section, the results gained from the TE/catalytic combustor system analysis can be used to determine the impact of TE integration on providing enough power to balance the SOFC system's plant power requirements. The analysis made above can then also be applied to one the baseline condition or one of the parametric studies. In this case the air channel mass flow rate case study is chosen to apply the combined TE integrated catalytic combustor/SOFC system performance study. Combustor's inlet conditions, which is also set to generate conditions close to SOFC's start-up conditions, is as follow:

Table 4-5: Air flow case study inlet conditions

Combustor's inlets	Inlet
X_H_2	0.096
X_O_2	0.19
X_H2O	0.00
X_N_2	0.71
MW_{tot} (kg.kgmol^{-1})	26.39
Temperature (K)	523.15
$\dot{m}_{exh,in}$ (kg.s^{-1})	7.91*10^{-5}

The amount of fuel energy input to the system, including SOFC power generation during start up, the following results is achieved.

Table 4-6: TE integrated catalytic combustor power generation calculations

Combustor's inlets	Inlet
$\dot{Q}_{fuel,in}$ (W)	100.1
W_{TE} (W)	2

W_{SOFC} (W)	0.0002
η_{system}	0.019
Power required to balance the plant (W)	10

5 Conclusion

5.1 Summary

The main goal of this research is to evaluate the effect of TE module integration into the anode exhaust catalytic combustor of fuel cell system and study its impact on the overall system thermal and electrical efficiency, fuel consumption and system reliability during start-up period of small scale fuel cell system. This evaluation was performed through development of a 2-D steady state TE/SOFC system model as well as a 2-D transient TE integrated catalytic combustor model. The results driven from each model was then combined in order to achieve a conclusion regarding the impact of this module integration in both the sub-component level and the overall system level.

The results achieved from the SOFC/TE system model indicated an improvement in system efficiency by about 1% at the baseline condition of V_{cell} = 0.75V during system's steady state condition and when the fuel cell has reached its optimal operating conditions. In addition, the TE module produced a total average power of 0.15 W during this condition, figure 2-9, and the air flow outlet from the combustor was heated to 820 K, figure 2-11. The system model was also evaluated for the same baseline condition with zero fuel conversion along the system to achieve

a similar evaluation of fuel cell's start-up condition. The result showed an overall TE power generation of 0.016W and air flow outlet temperature of 400K.

This research successfully developed a transient 2-D simulation tool in order to model the TE integrated catalytic combustor system with detailed catalytic surface reaction calculations. This model was tested under for an inlet baseline condition based upon fuel cell's exhaust outlet condition at its start up point. The effect of TE integration and power generation of the module was tested under different parametric study cases. The baseline case showed a total TE power generation of 1.1 W with air outlet temperature reaching 780K in 11 minutes of simulation time with fuel to air stoichiometric ratio of 2 for pure H_2 fuel composition.

The fuel cell exhaust condition evaluated through TE/SOFC system model at its start-up condition was then used as the TE/catalytic combustor model's inlet condition to evaluate the effect of TE integration on the overall SOFC system performance. According to these results, the TE module will produce about 1.1 W of power after 11 minutes of simulation time, during which the system's air outlet temperature has reached 780 K. Implementing these results into SOFC system efficiency calculations, it was shown that the efficiency is improved from $3.9*10^{-5}$ to 0.024 within 11 minutes when the combustor has reached equilibrium. In Maxey et al.'s study [1] it was mentioned that the small scale SOFC (< 100 W) power systems have start-up periods of about 15 to 20 minutes for the fuel cell to reach its optimal temperature. As a matter of fact, the modeling result shows that heating the air to up to 780 K after 11 minutes will create an ideal fuel cell preheating condition and fuel

cell can reach its optimal operating conditions at a faster rate of about 5 to 10 minutes.

In addition, observing the transient results of species site fractions on porous catalytic washcoat surface in figure 4-22, it is observed that after combustor reaches stable conditions both Pt and O species site fractions are active, which indicates that H_2 reacts with the surface as soon as it hits the catalytic washcoat which shows mass limited conversion behavior. As matter of fact, the mass limited conversion assumption made for TE/SOFC system model was a valid assumption.

In conclusion, the modeling results achieved both from TE/SOFC system and TE/catalytic combustor system showed improvements in thermal and electrical efficiency of the overall system during fuel cell's start-up condition. In addition, the study on catalytic combustor showed a full fuel utilization along the length of combustor where the exhaust of the channel would only contain O_2, N_2 and H_2O species at the outlet and also the exhaust flow temperature is reduced to about 400 K upon exit of the system.

Based on the transient analysis performed in sections 4.2 and 4.3 on impact of TE integration into catalytic combustor and combining it with SOFC system, it is shown that this modular integration with the current system design and inlet conditions can provide about 2 to 3% of the SOFC system's plants power requirements during the start up period of the SOFC. This can simply indicate that TE integration into the combustor exhaust of fuel cell systems can provide some initial power at the start up of the fuel cell operation which results in reducing the battery

requirement of the system. Also, this performance can be further improved by designing bigger combustors with different materials to enhance or reduce heat transfer through out the system.

5.2 Recommendations for future work

SOFC systems are usually operated on hydrocarbon based fuels such as n-butane. Considering the fact that he catalytic combustor model is capable of performing detail surface reaction calculations, one of the most important steps for achieving more realistic fuel cell system operation evaluation is to also use hydrocarbon fuel compositions as the combustor exhaust flow and study the combustion processes and TE integration effect under this operating conditions.

During the development and testing of the TE/catalytic combustor model, it was noted that the model has very low tolerances towards particular inlet conditions and the simulations would fail during the integration process. This occurrence is mainly due to stiff nature of the solver and the relative and absolute tolerances defined for the system. As a result, one of the important steps for future improvements of the model is to study the possibility of using other solvers provided in Matlab toolbox, or to detect the solution variable with steep slopes which cause instabilities during the integration process at the initial time step period.

Although the modeling studies showed improvements in fuel cell system performance and efficiency and TE module power generation using PbTe thermoelectric material. However, with the recent advancement in thermoelectric material development another interesting consideration for the future work can be the

implementation of other TE material with higher Seebeck coefficients, lower thermal conductivities with temperature operating ranges which would match the system's operating conditions.

References

[1] Maxey, C. J., G. S. Jackson, A. Seyed Reihani & S. Decaluwe. 2008a. Integration of catalytic combustion and hear recovery with meso-scale solid oxide fuel cell system. In *imece*, 1-8. Boston, Massachusetts, USA: ASME.

[2] Kee, R. J., H. Y. Zhu, A. M. Sukeshini & G. S. Jackson (2008) Solid oxide fuel cells: Operating principles, current challenges, and the role of syngas. *Combustion Science and Technology,* 180**,** 1207-1244.

[3] Zhu, H. Y. & R. J. Kee (2006) Thermodynamics of SOFC efficiency and fuel utilization as functions of fuel mixtures and operating conditions. *Journal of Power Sources,* 161**,** 957-964.

[4] Kattke, K. J. & R. J. Braun (2011) Characterization of a novel, highly integrated tubular solid oxide fuel cell system using high-fidelity simulation tools. *Journal of Power Sources,* 196**,** 6347-6355.

[5] www.delphi.com/manufacturers/auto/fuelcells/

[8] www.protonex.com

[7] Rowe, D. M. 2006. CRC Handbook of Thermoelectrics. Boca Raton: CRC/Taylor & Francis.

[8] Fleurial, J. P. (2009) Thermoelectric Power Generation Materials: Technology and Application Opportunities. *Jom,* 61**,** 79-85.

[9] Yu, C. & K. T. Chau (2009) Thermoelectric automotive waste heat energy recovery using maximum power point tracking. *Energy Conversion and Management,* 50**,** 1506-1512.

[10] Crane, D. T. 2003. Optimizing Thermoelectric waste heat recovery from an automotive cooling system. In *Mechanical Engineering*. College Park, MD: University of Maryland.

[11] Qiu, K. & A. C. S. Hayden (2008) Development of a thermoelectric self-powered residential heating system. *Journal of Power Sources,* 180**,** 884-889. (2009) A Natural-Gas-Fired Thermoelectric Power Generation System. *Journal of Electronic Materials,* 38**,** 1315-1319.

[12] Chen, M., H. Lund, L. A. Rosendahl & T. J. Condra (2010b) Energy efficiency analysis and impact evaluation of the application of thermoelectric power cycle to today's CHP systems. *Applied Energy,* 87**,** 1231-1238.

[13] Chen, M., S. J. Andreasen, L. Rosendahl, S. K. Kaer & T. Condra (2010a) System Modeling and Validation of a Thermoelectric Fluidic Power Source: Proton Exchange Membrane Fuel Cell and Thermoelectric Generator (PEMFC-TEG). *Journal of Electronic Materials,* 39**,** 1593-1600.

[14] Crane, D. T. & G. S. Jackson (2004) Optimization of cross flow heat exchangers for thermoelectric waste heat recovery. *Energy Conversion and Management,* 45**,** 1565-1582.

[15] Rosendahl, L. A., P. V. Mortensen & A. A. Enkeshafi (2011) Hybrid Solid Oxide Fuel Cell and Thermoelectric Generator for Maximum Power Output in Micro-CHP Systems. *Journal of Electronic Materials,* 40**,** 1111-1114.

[16] Maxey, C. 2010. Thermal integration of tubular solid oxide fuel cell with catalytic partial oxidation reactor and anode exhaust combustor for small power application. In *Mechanical Engineering*. College Park, MD: University of Maryland.

[17] Seyed-Reihani, S. A. & G. S. Jackson (2004) Effectiveness in catalytic washcoats with multi-step mechanisms for catalytic combustion of hydrogen. *Chemical Engineering Science,* 59**,** 5937-5948.

[18] DeCaluwe, S. C., H. Zhu, R. J. Kee & G. S. Jackson (2008) Importance of anode microstructure in modeling solid oxide fuel cells. *Journal of the Electrochemical Society,* 155**,** B538-B546.

[19] Habibzadeh, B. 2007. Understanding CO Oxidation in SOFC's Using Nickel Patterned Anode. In *Mechanical Engineering*. College Park, MD: University of Maryland.

[20] Mhadeshwar, A. B. & D. G. Vlachos (2007) A catalytic reaction mechanism for methane partial oxidation at short contact times, reforming, and combustion, and for oxygenate decomposition and oxidation on platinum. *Industrial & Engineering Chemistry Research,* 46**,** 5310-5324.

[21] Heremans, J. P., C. M. Thrush & D. T. Morelli (2005) Thermopower enhancement in PbTe with pb precipitates. *Journal of Applied Physics,* 98**,** 6.

[22] Groppi, G., A. Belloli, E. Tronconi & P. Forzatti (1995) A comparison of lumped and distributed models of monolith catalytic combustors. *Chemical Engineering Science,* 50**,** 2705-2715.

[25] Incropera, F. P., D. P. DeWitt & J. Wiley. 2007. Fundamentals of Heat Transfer. Hoboken, NJ: John Wiley, c2011.

[26] Angrist, S. W. 1982. Direct Energy Conversion. Boston: Allyn and Bacon, Inc.

[27] www.coorstek.com

[28] www.ferrotec.com/products/thermal/modules/highPower/